EXCITED MOLECULES IN GASEOUS FLOW SYSTEMS

Kinetics and Mechanisms of the Formation and Reactions of $O_2(^1\Delta_g)$ and $O_2(^1\Sigma_g^+)$

by

SARA JOAN ARNOLD

B.Sc., University of British Columbia, 1963

A THESIS SUBMITTED IN PARTIAL FULFILMENT OF

THE REQUIREMENTS FOR THE DEGREE OF

DOCTOR OF PHILOSOPHY

in the Department of

CHEMISTRY

We accept this thesis as conforming

to the required standard

THE UNIVERSITY OF BRITISH COLUMBIA

September, 1966

In presenting this thesis in partial fulfilment of the requirements for an advanced degree at the University of British Columbia, I agree that the Library shall make it freely available for reference and study. I further agree that permission for extensive copying of this thesis for scholarly purposes may be granted by the Head of my Department or by his representatives. It is understood that copying or publication of this thesis for financial gain shall not be allowed without my written permission.

Department of CHEMISTRY

The University of British Columbia
Vancouver 8, Canada

Date October 7, 1966

The University of British Columbia

FACULTY OF GRADUATE STUDIES

PROGRAMME OF THE

FINAL ORAL EXAMINATION

FOR THE DEGREE OF

DOCTOR OF PHILOSOPHY

of

SARA JOAN ARNOLD

B. Sc. (Hons.), The University of British Columbia

THURSDAY, OCTOBER 6, AT 3:30 P.M.

IN ROOM 261, CHEMISTRY BUILDING

COMMITTEE IN CHARGE

Chairman: I. McT. Cowan

N. Basco
A. V. Bree
D. P. Chong
F.W. Dalby
C. A. McDowell
N. Paddock
R. E. Pincock
G B. Porter

External Examiner: B. A. Thrush

Department of Physical Chemistry
University of Cambridge
Cambridge, England.

Research Supervisor: E. A. Ogryzlo

EXCITED MOLECULES IN GASEOUS FLOW SYSTEMS

ABSTRACT

When oxygen is passed through a microwave discharge, the oxygen atoms being destroyed by distilling mercury through the discharge, an excited molecule $O_2(^1\Delta_g)$ was observed to be the primary discharge product. This excited molecule was found to be immune to collisional deactivation by a wide range of added foreign gases, with the exception of certain substituted ethylenes which it oxidized. The principal mode of decay of $O_2(^1\Delta_g)$ was nonradiative decay, with $k_{nonrad.}$ equal to 0.178 $sec.^{-1}$.

The excited molecule $O_2(^1\Delta_g)$ however, was observed to undergo two novel energy pooling processes.

$$2\ O_2(^1\Delta_g) \longrightarrow \{O_2(^3\Sigma_g)\}_2 \quad (\text{or } 2\ O_2(^3\Sigma_g^-)) + h\nu\ (6340 \text{ and } 7030)$$

$$2\ O_2(^1\Delta_g) \longrightarrow O_2(^1\Sigma_g^+) + O_2(^3\Sigma_g^-)$$

The first of these energy pooling processes gave rise to two broad structureless bands at 6340 A and 7030 A which had not previously been observed in discharged oxygen. These bands, the intensity of which is proportional to the square of the $O_2(^1\Delta_g)$ concentration and independent of the total pressure in the system, are believed to result from a simultaneous electronic transition in two $O_2(^1\Delta_g)$ molecules with the emission of a single photon. The 6340 A band appears if both molecules undergo a (0-0) transition in the $a^1\Delta_g \longrightarrow X^3\Sigma_g^-$ system and the 7030 A. band if one molecule undergoes a (0-0) transition and the other a (0-1) transition.

The second of these energy pooling processes is a disproportionation reaction which leads to the formation of a second excited molecule $O_2(^1\Sigma_g^+)$. The rate constant for this reaction was found to be 1.3×10^3 $l.moles^{-1}sec.^{-1}$, in disagreement with the results of Young and Black by a factor of 10^4.

Both energy pooling processes are believed to have a common intermediate, $\{O_2(^1\Delta_g)\}_2$, which is either a metastable double molecule or a colliding pair of

molecules.

The principal mode of decay of $O_2(^1\Sigma_g^+)$ was nonradiative decay, with $k_{nonrad.}$ equal to 64.6 $sec.^{-1}$

Unlike $O_2(^1\Delta_g)$, $O_2(^1\Sigma_g^+)$ was found to be collisionally deactivated by a wide variety of added foreign gases, with the most effective deactivator tried being water. The rate constants for the reaction

$$O_2(^1\Sigma_g^+) + Q \longrightarrow O_2 + Q$$

were determined for fourteen different quenchers. A good correlation between quenching efficiency and the magnitude of the intermolecular potential between the quencher and $O_2(^1\Sigma_g^+)$ has been obtained.

Two additional energy pooling processes involving excited oxygen molecules and either molecular iodine or nitrogen dioxide were observed. Both resulted in the formation of an excited molecule, $I_2(^3\Pi_{ou}^+)$ or NO_2^*, which emitted in the visible.

GRADUATE STUDIES

Field of Study: Physical Chemistry

Topics in Physical Chemistry	A. V. Bree J. A. R. Coope
Spectroscopy and Molecular Structure	A. V. Bree C. Reid B. A. Dunell
Theoretical Chemistry	R. F. Snider
Chemical Kinetics	G. B. Porter D. J. L. James

Related Studies:

Linear Algebra	R. C. Thompson
Modern Physics	D. L. Williams
Topics in Organic Chemistry	J. P. Kutney D. E. Mcgreer F. McCapra
Topics in Inorganic Chemistry	N. Bartlett R. C. Thompson W. R. Cullen
Seminar	N. Bartlett

PUBLICATIONS

Arnold, S.J.; Ogryzlo, E.A.; Witzke, H.
Some New Emission Bands of Molecular Oxygen
J. Chem. Phys. 40 1769 (1964)

Arnold, S.J.; Browne, R.J.; Ogryzlo, E.A.
The Red Emission Bands of Molecular Oxygen
J. Photochem. Photobiol. 4 963 (1964)

Arnold, S.J.; Finlayson, N.; Ogryzlo, E.A.
Some Novel Energy Pooling Processes Involving
$O_2(^1\Delta_g)$ J.Chem. Physics 44 2529 (1966)

Arnold, S.J.; Ogryzlo, E.A.
The reaction $2\ O_2(^1\Delta_g) \longrightarrow O_2(^1\Sigma_g^+) + O_2(^3\Sigma_g^-)$
J. Geophys. Res. (submitted for publication)

Arnold, S.J.; Ogryzlo, E.A.
Gas Phase Quenching of $O_2(^1\Sigma_g^+)$
J. Chem. Phys. (submitted for publication)

SARA JOAN ARNOLD.

EXCITED MOLECULES IN GASEOUS FLOW SYSTEMS

Kinetics and Mechanisms of the Formation and Reactions of $O_2(^1\Delta_g)$ and $O_2(^1\Sigma_g^+)$

ABSTRACT

When oxygen is passed through a microwave discharge, the oxygen atoms being destroyed by distilling mercury through the discharge, an excited molecule $O_2(^1\Delta_g)$ was observed to be the primary discharge product. This excited molecule was found to be immune to collisional deactivation by a wide range of added foreign gases, with the exception of certain substituted ethylenes which it oxidized. The principal mode of decay of $O_2(^1\Delta_g)$ was nonradiative decay, with $k_{nonrad.}$ equal to 0.178 sec.$^{-1}$

The excited molecule $O_2(^1\Delta_g)$ however, was observed to undergo two novel energy pooling processes.

$$2\ O_2(^1\Delta_g) \rightarrow \{O_2(^3\Sigma_g^-)\}_2 \text{ (or } 2\ O_2(^3\Sigma_g^-)) + h\nu(6340 \text{ and } 7030)$$

$$2\ O_2(^1\Delta_g) \rightarrow O_2(^1\Sigma_g^+) + O_2(^3\Sigma_g^-)$$

The first of these energy pooling processes gave rise to two broad structureless bands at 6340 A and 7030 A which had not previously been observed in discharged oxygen. These bands, the intensity of which is proportional to the square of the $O_2(^1\Delta_g)$ concentration and independent of the total pressure in the system, are believed to result from a simultaneous electronic transition in two $O_2(^1\Delta_g)$ molecules with the emission of a single photon. The 6340 A band appears if both molecules undergo a (0-0) transition in the $a^1\Delta_g \rightarrow X^3\Sigma_g^-$ system and the 7030 A band if one molecule undergoes a (0-0) transition and the other a (0-1) transition.

The second of these energy pooling processes is a disproportionation reaction which leads to the formation of a second excited

molecule $O_2(^1\Sigma_g^+)$. The rate constant for this reaction was found to be 1.3×10^3 l.moles^{-1} sec.$^{-1}$, in disagreement with the results of Young and Black by a factor of 10^4.

Both energy pooling processes are believed to have a common intermediate, $\{O_2(^1\Delta_g)\}_2$, which is either a metastable double molecule or a colliding pair of molecules.

The principal mode of decay of $O_2(^1\Sigma_g^+)$ was nonradiative decay, with $k_{nonrad.}$ equal to 64.6 sec.$^{-1}$. Unlike $O_2(^1\Delta_g)$, $O_2(^1\Sigma_g^+)$ was found to be collisionally deactivated by a wide variety of added foreign gases, with the most effective deactivator tried being water. The rate constants for the reaction

$$O_2(^1\Sigma_g^+) + Q \rightarrow O_2 + Q$$

were determined for fourteen different quenchers. A good correlation between quenching efficiency and the magnitude of the intermolecular potential between the quencher and $O_2(^1\Sigma_g^+)$ has been obtained.

Two additional energy pooling processes involving excited oxygen molecules and either molecular iodine or nitrogen dioxide were observed. Both resulted in the formation of an excited molecule, $I_2(^3\Pi_{ou}^+)$ or NO_2^*, which emitted in the visible.

TABLE OF CONTENTS

	Page
Abstract	ii
List of Tables	vi
List of Illustrations	viii
Acknowledgements	x
INTRODUCTION	1
EXPERIMENTAL	
Materials	13
Flow System	14
Excited Molecule Production	17
Destruction of Oxygen Atoms	18
Spectroscopic Studies	19
Measurement of $O_2(^1\Sigma_g^+)$ and $O_2(^1\Delta_g)$ concentrations	20
RESULTS	
The emission bands	24
Relationship between 6340 A and 7030 A band intensities and $O_2(^1\Delta_g)$ concentration	29
Relationship between the $O_2(^1\Sigma_g^+)$ concentration and the $O_2(^1\Delta_g)$ concentration	32
Temperature dependence of the 6340 A band	37
Reactions of $O_2(^1\Delta_g)$	40
Reactions of $O_2(^1\Sigma_g^+)$	43
Energy pooling processes	60
DISCUSSION	
Spectroanalysis	68
Relationship between $O_2(^1\Sigma_g^+)$ and $O_2(^1\Delta_g)$ concentration	79
Decay of $O_2(^1\Delta_g)$	92
Species $\{O_2(^1\Delta_g)\}_2$	98
Reactions of $O_2(^1\Sigma_g^+)$	109
Energy pooling processes	122
$O_2(^1\Delta_g)$ and $O_2(^1\Sigma_g^+)$ in upper atmosphere	126
CONCLUSIONS	
Summary	132
Suggestions for further work	133
REFERENCES	135

LIST OF TABLES

Table		Page
I.	Principal band systems of oxygen.	4
II.	States of the oxygen molecule formed by recombination of $O(^3P)$, $O(^1D)$ and $O(^1S)$ atoms.	8
III.	Ratios of the intensities of the 6340 A band, the intensity of the 7030 A band and the $O_2(^1\Delta_g)$ concentrations.	30
IV.	Relationship between the intensity of the 6340 A band, the intensity of the 7030 A band and the $O_2(^1\Delta_g)$ concentration.	31
V.	Ratios of the intensities of the 7619 A band the $O_2(^1\Delta_g)$ concentration.	34
VI.	Relationship between the intensity of the 7619 A band and the $O_2(^1\Delta_g)$ concentration.	35
VII.	Steady State $O_2(^1\Sigma_g^+)$ concentration and $O_2(^1\Delta_g)$ concentration.	36
VIII.	Ratios of the decay rate, $d[O_2(^1\Delta_g)]/dt$, and the average $O_2(^1\Delta_g)$ concentration.	39
IX.	Intensity of the 6340 A band at four different temperatures.	41
	The effect of added gases on the $O_2(^1\Sigma_g^+)$ concentration.	
X.	Water as an added gas.	45
XI.	Deuterium oxide as an added gas.	46
XII.	N-heptane as an added gas.	47
XIII.	Methanol as an added gas.	48
XIV.	Ammonia as an added gas.	49
XV.	Dimethyl ether as an added gas.	50
XVI.	Hydrogen sulfide as an added gas.	51
XVII.	Carbon dioxide as an added gas.	52

LIST OF TABLES (CONTD)

Table		Page
XVIII.	Chloroform as an added gas.	53
XIX.	Hydrogen bromide as an added gas.	54
XX.	Methane as an added gas.	55
XXI.	Nitrogen as an added gas.	56
XXII.	Argon as an added gas.	57
XXIII.	Carbon monoxide as an added gas.	58
XXIV.	Helium as an added gas.	59
XXV.	Ratios of the intensities of the 6340 A band, the intensities of the 7619 A band and the intensities of the NO_2^* emission.	63
XXVI.	Methods used to measure the absolute concentration of $O_2(^1\Sigma_g^+)$ and $O_2(^1\Delta_g)$.	77
XXVII.	Rate Constants for the formation of $O_2(^1\Sigma_g^+)$ by mechanism A and mechanism B.	86
XXVIII.	Values of log(IT) and $IT^{3/2}$.	106
XXIX.	Rate constants for $O_2(^1\Sigma_g^+)$ quenching.	112
XXX.	Linear Combinations of Vibrational Modes of Quenchers Approximating 5238 cm^{-1} or 13120 cm^{-1}.	117
XXXI.	Values of e_{ij} the intermolecular potential between $O_2(^1\Sigma_g^+)$ and the quencher.	120

LIST OF ILLUSTRATIONS

Figure		Page
1.	Potential energy diagram for oxygen.	7
2.	Flow system.	15
3.	Diagram of detector circuit.	22
4.	Emission spectrum of electrically discharged oxygen afterglow.	25
5.	High resolution spectrum of 7619 A. band	26
6.	Microdensitometer trace of high resolution spectrum of 6340 A band	28
7.	The intensity of the 7619 A band as a function of distance along the reaction tube.	33
8.	$O_2(^1\Delta_g)$ concentration as a function of distance along the reaction tube.	38
9.	The effect of the addition of ethylene and its methylsubstituted derivatives on the $O_2(^1\Delta_g)$ concentration	42
10.	The effect of the addition of various amounts of water on the $O_2(^1\Sigma_g^+)$ concentration.	44
11.	Low resolution spectrum of NO_2^* emission.	61
12.	Microdensitometer tracing of high resolution spectrum of I_2^* emission.	65
13.	Log (I_1/I_2) against log $\{[O_2(^1\Delta_g)]_1/[O_2(^1\Delta_g)]_2\}$.	72
14.	Plot of the ratio $[O_2(^1\Delta_g)]^2/I$ against pressure	74
15.	Log $[I_1(7619)/I_2(7619)]$ against log $\{[O_2(^1\Delta_g)]_1 / [O_2(^1\Delta_g)]_2\}$	
16.	Plot of the ratio $[O_2(^1\Delta_g)]^2/I(7619)$ against pressure	
17.	Plot of $2.303 \dfrac{[O_2(^1\Sigma_g^+)]_{ss}}{[O_2(^1\Delta_g)]^2_{ss}}$ $\log \left\{[O_2(^1\Delta_g)]^2 - \dfrac{[O_2(^1\Delta_g)]^2_{ss}}{[O_2(^1\Sigma_g^+)]_{ss}} [O_2(^1\Sigma_g^+)]\right\}$ against time.	85

LIST OF ILLUSTRATIONS (CONTD)

Figure		Page
18.	Log (R_1/R_2) against log $\{[O_2(^1\Delta_g)]_1/[O_2(^1\Delta_g)]_2\}$	92
19.	The observed first order decay constant, k_{obs}, for $O_2(^1\Delta_g)$ against pressure.	94
20.	Log (IT) against temperature.	103
21.	Plot of I∘ (7619)/I(7619) against quencher concentration.	111
22.	Log $k_{quencher}$ against boiling point.	112
23.	Log $k_{quencher}$ against log $k_{third\ body}$.	115
24.	Log $k_{quencher}$ against e_{ij}/k.	
25.	Log $\{I_1(NO_2^*)/I_2(NO_2^*)\}$ against log $\{[O_2(^1\Delta_g)]_1/[O_2(^1\Delta_g)]_2\}$	123

ACKNOWLEDGEMENTS

To Dr. E. A. Ogryzlo, my research director, who suggested this study and to whom I am indebted for his help and support,

to Dr. D. P. Chong, for his many valuable suggestions and for reading the manuscript,

to Drs. G. B. Porter, N. Basco, A. V. Bree, W. Dalby and A. Douglas for helpful discussions and suggestions,

to the many members of the technical staff who assisted in the construction and maintenance of the equipment,

to Professor J. E. Smith, Dr. S. Nash and the Mathematics Department for an assistantship and to the Chemistry Department for an assistantship,

to Miss D. Symons for typing the manuscript and to Mr. J. Caldwell for help in preparing the illustrations.

INTRODUCTION

Although the reactions of oxygen atoms have been studied for many years (1), only recently have investigators looked at the reactions of electronically excited oxygen molecules. This is possibly because of the difficulty in obtaining an atom-free stream of excited molecules suitable for kinetic and spectroscopic studies.

However, in 1958 Ogryzlo (2) showed that the electrodeless microwave discharge which had been utilized so successfully in the production of oxygen atoms could also be used to produce electronically excited oxygen molecules. He observed that, upon distilling mercury through the discharge and thus destroying the oxygen atoms, one can obtain an energy-rich species O_2^* in suitable concentrations for kinetic studies.

The present work is concerned with an identification of the electronically excited molecules present in electrically discharged oxygen and with a study of some of their reactions.

Electronically Excited States of Oxygen†

What are the possible electronically excited states of oxygen?

The lowest electron configuration of O_2

$$KK(\sigma_g 2s)^2(\sigma_u 2s)^2(\sigma_g 2p)^2(\pi_u 2p)^4(\pi_g 2p)^2 \qquad (1)$$

---

† The following discussion is simply to familiarize the reader with the possible excited states of the oxygen molecule and is not meant to be a complete survey of all observations of electronically excited oxygen molecules.

gives rise to the states $^3\Sigma_g^-$, $^1\Delta_g$, and $^1\Sigma_g^+$, with $^3\Sigma_g^-$ being the ground state.

First definite evidence for the $^1\Delta_g$ state was obtained by Ellis and Kneser (3) in the infrared absorption of liquid oxygen, where it gives rise to a progression of prominent bands, starting at 12610A and extending to shorter wavelengths. Herzberg and Herzberg (4) observed the (0-0) and (0 -1) bands of the $^1\Delta_g \leftrightarrow {}^3\Sigma_g^-$ system at 12683A and 10674A in absorption. The (0-0) and (0-1) bands at 12683A and 15800A were subsequently observed in airglow emission by Vallance Jones and Harrison (5). Vallance Jones and Gattinger (6) estimated the Einstein A coefficient for spontaneous radiation of the $^1\Delta_g \rightarrow {}^3\Sigma_g^-$ system as 1.5×10^{-4} sec^{-1}.

The $^1\Sigma_g^+$ state has been observed in absorption both in gaseous (7) and liquid (8) oxygen, and in emission in airglow (9), aurora (10), discharged oxygen (11) and in certain types of flames (12). It gives rise to the atmospheric $^1\Sigma_g^+ \leftrightarrow {}^3\Sigma_g^-$ band system, with (0-0) band at 7619A. Childs and Mecke (8) determined the Einstein A coefficient to be 0.14 sec^{-1}.

The first excited electron configuration of oxygen of

$$KK(\sigma_g 2s)^2(\sigma_u 2s)^2(\sigma_g 2p)^2(\pi_u 2p)^3(\pi_g 2p)^3 \qquad (2)$$

gives rise to the states $^1\Sigma_u^-$, $^3\Sigma_u^+$, $^3\Sigma_u^-$, $^3\Delta_u$, $^1\Sigma_u^+$, $^1\Delta_u$.

The $^1\Sigma_u^-$ state has been observed only in absorption by Herzberg (13) who assigned five bands in the 2500-2700A region to the $^1\Sigma_u^- \leftarrow {}^3\Sigma_g^-$ system. The estimated lifetime of this state is >0.1 sec.

The $^3\Sigma_u^+$ state, which is the upper state of the Herzberg I $^3\Sigma_u^+ \leftrightarrow {}^3\Sigma_g^-$ system, has been observed in absorption (14) and in emission

in airglow (15) and in discharged oxygen (11,16). The system consists of a progression of closely spaced bands extending from 2400A to 4900A with the radiative lifetime of the $^3\Sigma^+$ state estimated at $\leq 10^{-3}$ sec.

The $^3\Sigma_u^-$ state gives rise to the Schumann-Runge $^3\Sigma_u^- \leftrightarrow {}^3\Sigma_g^-$ bands of the ultraviolet region, observed both in absorption (17) and in certain conditions in emission (18).

Herzberg (13) tentatively identified the $^3\Delta_u$ state on the basis of fragments of two bands assigned to the $^3\Delta_u \leftarrow {}^3\Sigma_g^-$ system, observed in absorption in the region between 2570A and 2630A. Chamberlain (19) proposed that the $^3\Delta_u \rightarrow {}^1\Delta_g$ system might account for three unidentified bands in the 3700 A region in blue airglow. Ingham (20), however, using a much higher resolution spectrograph, claims that the Herzberg I bands are the only identifiable emission attributable to molecular oxygen in blue airglow.

The $^1\Sigma_u^+$ and $^1\Delta_u$ states have not been observed. A brief summary of the electronically excited states of oxygen together with a description of the band systems they give rise to is given in table I.

Electronically Excited States of Oxygen Observed in Electrically Discharged Oxygen.

Which of these electronically excited states could be present in electrically discharged oxygen?

Since approximately ten percent of the oxygen passed through a microwave discharge undergoes dissociation into ground state $O(^3P)$ atoms, it is not unreasonable to expect that any excited states which can be formed from ground state atoms could be present in discharged oxygen.

TABLE I

Principal Band Systems of O_2

molecular state	band system	description band system	principal band heads		type of transition	reference
$a\ ^1\Delta_g$	$a^1\Delta_g \leftrightarrow X^3\Sigma_g$	triple Q-branch maxima	(0-0)	12683 A	magnetic	4,5,6
	Infrared atmospheric	slightly degraded to longer	(0-1)	15800 A	dipole	
		wavelengths	(1-0)	10674 A		
$b\ ^1\Sigma_g^+$	$b^1\Sigma_g^+ \leftrightarrow {}^3\Sigma_g^-$	weak heads degraded	(0-0)	7619 A	magnetic	6,7,8,9
	atmospheric	to longer wavelengths	(0-1)	8645 A	dipole	10,11
	$b^1\Sigma_g^+ \rightarrow a^1\Delta_g$	sharp Q-branch maxima	(0-0)	19080 A	electric quadrupole	31
$A\ ^3\Sigma_u^+$	$A^3\Sigma_u^+ \leftrightarrow X^3\Sigma_g^-$	single heads strongly	2400-4900 A			11
	Herzberg I	degraded to the red	region			
	$A^3\Sigma_u^+ \rightarrow b^1\Sigma_g^+$	single heads strongly	3500-4500 A			(11)
	Broida-Gaydon	degraded to the red	region			

$c\ ^1\Sigma_u^-$	$c\ ^1\Sigma_u^- \longleftarrow X^3\Sigma_g^-$ Herzberg II	single heads strongly degraded to the red	2500-2700 A region	electric dipole	13
$B\ ^3\Sigma_u^-$	$B^3\Sigma_u^- \longleftrightarrow X^3\Sigma_g^-$ Schumann-Runge	single heads strongly degraded to the red	1700-2500 A region		17,18
$C\ ^3\Delta_u$	$C^3\Delta_u \longleftarrow X^3\Sigma_g^-$ Herzberg III	three heads strongly degraded to the red	2570-2630 A region		13
	$C^3\Delta_u \longrightarrow a^1\Delta_g$	three heads strongly degraded to the red	3700 - 4300 A region		19

Figure I shows the potential energy diagram for O_2 as compiled by Gilmore (21). According to the Wigner-Whitmer correlation rules (22), two ground state oxygen atoms $O(^3P)$ on recombination can produce eighteen different electronic states of O_2, six of which lead to bound molecules, $^3\Sigma_g^-$, $^1\Delta_g$, $^1\Sigma_g^+$, $^3\Delta_u$, $^3\Sigma_u^+$, and $^1\Sigma_u^-$, and twelve of which give rise to repulsive states. The $^3\Sigma_u^-$ state is the only bound state formed by the combination of a ground state $O(^3P)$ atom and an excited $O(^1D)$ atom. The $^1\Delta_u$ state is formed by combination of two excited atoms, $O(^1D) + O(^1D)$, while the $^1\Sigma_u^+$ state also originates from two excited atoms, $O(^1D) + O(^1S)$. Consequently, the following excited states, $^1\Delta_g$, $^1\Sigma_g^+$, $^3\Sigma_u^+$, $^3\Delta_u$, and $^1\Sigma_u^-$ could conceivably be present in electrically discharged oxygen. (table II).

Several investigators have looked for evidence of electronically excited molecules in electrically discharged oxygen. Kaplan, (23) who observed the (0-0) and (0-1) bands of the atmospheric system in an oxygen enriched nitrogen afterglow, was the first to present spectroscopic evidence for the existence of the $^1\Sigma_g^+$ state in discharges. Broida, Bass and Kurzweg, (24), subsequently, observed the (0-0) and (0-1) bands in electrically discharged pure oxygen. However, they did not comment on whether the $^1\Sigma_g^+$ state originated in the discharge or was formed by three-body atom recombination in the afterglow. Young and Sharpless, (25), producing oxygen atoms by the reaction

$$N + NO \rightarrow N_2 + O, \tag{3}$$

also observed the (0-0) atmospheric band. They later showed that the atmospheric bands were being excited in the three-body atom recombination

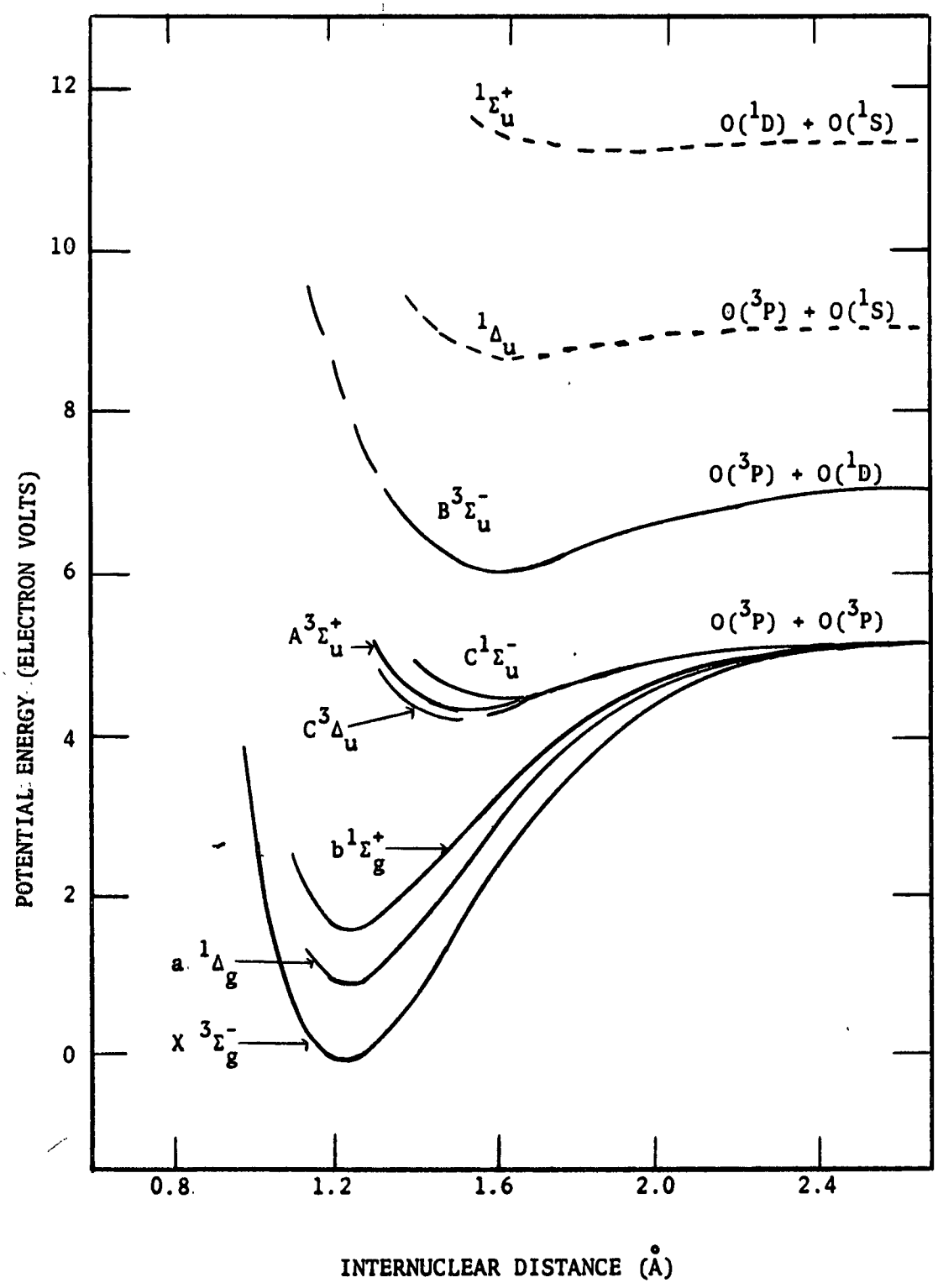

Figure 1: Potential Energy Diagram for O_2 as complied by R. F. Gilmore (21).

TABLE II

States of the Oxygen Molecule formed by recombination of $O(^3P)$, $O(^1D)$, $O(^1S)$ atoms

States of separate atoms	molecular states	electron configuration	excitation energy	radiative lifetime	reference
$^3P + {}^3P$	$X\ ^3\Sigma_g^-$ bound		0		
	$a\ ^1\Delta_g$ bound	$KK(\sigma_g 2s)^2(\sigma_u 2s)^2(\sigma_g 2p)^2(\pi_g 2p)^2$	7918 cm^{-1}	111 minutes	6
	$b\ ^1\Sigma_g^+$ bound		13195 cm^{-1}	7 sec	8
	$c\ ^1\Sigma_u^-$ bound		36679 cm^{-1}	> 0.1 sec.	13
	$A\ ^3\Sigma_u^+$ bound		36009 cm^{-1}	$\sim 10^{-3}$ sec	14
	$C\ ^3\Delta_u$ bound		34329 cm^{-1}	> 0.1 sec.	13
	$^1\Pi g$, $^1\Pi u$, $^3\Pi g$, $^3\Pi u$		repulsive states		
	$^5\Pi g$, $^5\Pi u$, $^5\Delta g$		repulsive states		
	$2\,^5\Sigma_g^+$, $^1\Sigma_g^+$, $^5\Sigma_u^-$, $^3\Sigma_u^+$		repulsive states		

TABLE II (continued)

$^3P + {}^1D$	$B\ {}^3\Sigma u^-$	$KK(\sigma_g 2s)^2(\sigma_u 2s)^2(\sigma_g 2p)^2(\pi_u 2p)^3(\pi_g 2p)^3$	49802 cm^{-1}
	+ 17 repulsive states		
$^1D + {}^1D$	$^1\Delta_u$	$KK(\sigma_g 2s)^2(\sigma_u 2s)^2(\sigma_g 2p)^2(\pi_u 2p)^3(\pi_g 2p)^3$	
	+ repulsive states		
$^1D + {}^1S$	$^1\Sigma_u^+$	$KK(\sigma_g 2s)^2(\sigma_u 2s)^2(\sigma_g 2p)^2(\sigma_u 2p)^3(\pi_g 2p)^3$	
	+ repulsive states		

reaction

$$O + O + M \rightarrow O_2(^1\Sigma_g^+) + M, \; M = \text{any third body} \tag{4}$$

with a rate constant of about 10^{-37} cm.$^{-6}$sec.$^{-1}$ and that the introduction of O_2 increased the intensity of the bands by a factor of five. The bands were quenched by the introduction of CO_2, N_2O and N_2 with the rate constant for the quenching reaction

$$O_2(^1\Sigma_g^+) + N_2 \rightarrow O_2(^3\Sigma_g^-) + N_2^* \tag{5}$$

being less that 10^{-18} cm.^{3} sec.$^{-1}$ (26). Thrush, Clyne, and Wayne, (27) in direct contrast to Young and Sharpless, found that the introduction of O_2 had no significant effect on the intensity of the atmospheric bands. They also observed that neither NO nor NO_2 had any significant effect on the band intensity, whereas the introduction of O_3 greatly reduced the intensity of the atmospheric bands and intensified the strength of the airglow emission associated with the reaction

$$O(^3P) + NO + M \rightarrow NO_2 + M + h\nu \tag{6}$$

indicating that $O(^3P)$ atoms are being formed. Consequently, they concluded that the reaction

$$O_2(^1\Sigma_g^+) + O_3(^1A) \rightarrow 2\,O_2(^3\Sigma_g^-) + O(^3P) \tag{7}$$

occurred to an appreciable extent.

The $^3\Sigma_u^+$ state which gives rise to the Herzberg I $^3\Sigma_u^+ \rightarrow {}^3\Sigma_g^-$ bands has been observed in discharged oxygen by Broida and Gaydon (11), who postulated that it must be formed by three-body atom recombination in the afterglow, according to the equation

$$O + O + M \xrightarrow{k_8} O_2(^3\Sigma_u^+) + M, \quad M = \text{any third body.} \tag{8}$$

Barth and Patapoff (28) confirmed that this was indeed the mechanism of formation of the $^3\Sigma_u^+$ state in a pure oxygen discharge. Young and

Sharpless (25), producing oxygen atoms by reaction 3, found k_8 equal to 2×10^{-37} cm.^{6} sec.$^{-1}$. They showed that reaction 8 was independent of the total pressure in the system, but quenched by the addition of O_2, N_2O, and CO_2. Broida and Gaydon identified a second series of bands having their origin in the $^3\Sigma_u^+$ state, corresponding to the transition $^3\Sigma_u^+ \rightarrow {}^1\Sigma_g^+$.

Herron and Schiff (29) and Forner and Hudson (30) have presented mass spectroscopic evidence for the existance of $^1\Delta_g$ state in discharged oxygen. Both have reported the presence of a species having an appearance potential of about 1 electron volt above normal oxygen in discharged oxygen. Herron and Schiff, comparing the initial slopes of the discharged oxygen curve and the normal oxygen curve, have estimated that ten percent of the total oxygen is in the $^1\Delta_g$ state. Ogryzlo, Elias and Schiff (31), measuring the heat liberated to a cobalt detector by an excited molecule stream, showed that the excited molecule, which they tentatively identified as $O_2(^1\Delta_g)$, was unaffected by the addition of NO, CO_2 and C_2H_4. All authors concluded in view of the high concentration of $O_2(^1\Delta_g)$ present that it must be formed as a primary discharge product, rather than by three-body atom recombination in the afterglow.

Summary:

The results of passing molecular oxygen through a microwave discharge can be summarized as follows. Approximately 10% of the oxygen is dissociated into ground state $O(^3P)$ atoms while another 10% is excited to the $^1\Delta_g$ state (2). The $^1\Sigma_g^+$ and $^3\Sigma_u^-$ states are produced in secondary reactions by three-body atom recombination, (25,28).

Primary process:

$$O_2(^3\Sigma_g^-) \xrightarrow{\text{discharge}} 2O(^3P) \qquad O_2(^3\Sigma_g^-) \longrightarrow O_2(^1\Delta_g) \tag{9}$$

Secondary process:

$$2O(^3P) + M \longrightarrow O_2(^3\Sigma_g^-) + M \qquad 2O(^3P) + M \longrightarrow O_2(^1\Sigma_g^+) + M \qquad 2O(^3P) + M \longrightarrow O_2(^3\Sigma_u^-) + M \tag{10}$$

When mercury is distilled through the discharge in order to destroy the oxygen atoms, the $^1\Delta_g$ state is still formed in approximately 10% concentration. The purpose of the present work is to determine if any other excited states exist in this system as the result of the secondary reactions of $O_2(^1\Delta_g)$ as well as to study the reactions of $O_2(^1\Delta_g)$ with added foreign gases.

EXPERIMENTAL

Materials:

Tank oxygen was obtained from Canadian Liquid Air and from the Matheson Company. Nitrogen was the most objectionable impurity since it would lead to the production of nitric oxide in the discharge. Canadian Liquid Air oxygen was found to contain the larger amount of nitrogen as indicated by the intensity of the nitrogen dioxide afterglow of the discharge products. Matheson Company oxygen (extra dry grade) was found to contain much less nitrogen and was, therefore, used throughout the experimental work, except where ultra nitrogen-free oxygen was required.

An attempt was made to remove more nitrogen by trapping the oxygen and distilling off eighty percent before using it. Since the oxygen thus prepared was found to give the same results, the procedure was abandoned.

In experiments in which ultra nitrogen-free oxygen was required oxygen was prepared by the thermal decomposition of potassium permanganate. The gas was passed through a dry ice-acetone trap to remove any water present. No nitrogen could be detected by looking for evidence of the nitrogen dioxide afterglow which was conspicuously absent.

Nitric oxide was obtained from the Matheson Company. Nitrogen dioxide, water, and nitrogen were the predominant impurities present. These were removed by three distillations at half an atmosphere pressure with the initial and final fifths discarded in each distillation.

Nitrogen dioxide was obtained from the Matheson Company. Nitric oxide and water were found to be the predominant impurities. Water was removed by fractional distillation and nitric oxide by the introduction of oxygen which converted it to nitrogen dioxide. Any unreacted oxygen was then pumped off by drawing the mixture through a dry ice trap.

The ammonia, dimethyl ether, hydrogen sulfide, carbon dioxide, hydrogen bromide, nitrogen, argon, and helium used in the quenching studies of $O_2(^1\Sigma_g^+)$ were obtained from the Matheson Company. Water was found to be the only objectionable impurity. All gases were dried by passing them over phosphorus pentoxide, except for ammonia which was passed over potassium hydroxide, and through either a dry ice-acetone or liquid nitrogen trap. The methane used was obtained from Phillips Petroleum Company. It was dried by passage through a dry ice-acetone trap.

The methyl alcohol, n-heptane, chloroform and carbon tetrachloride used were spectroscopic grade, guaranteed to contain less than 0.001% water. As a precaution they were dried by contact with anhydrous calcium sulfate.

The deuterium oxide was obtained from the Stewart Oxygen Company and was guaranteed to be 99.98% deuterium oxide.

Flow System

The flow system used for the majority of experiments is shown in Figure 2. The reaction tube had an internal diameter of 2.5 cm. and a length of 120 cm. It was not jacketed. The oxygen was discharged in a Pyrex tube about 10 cm. above the reaction tube. The added gases

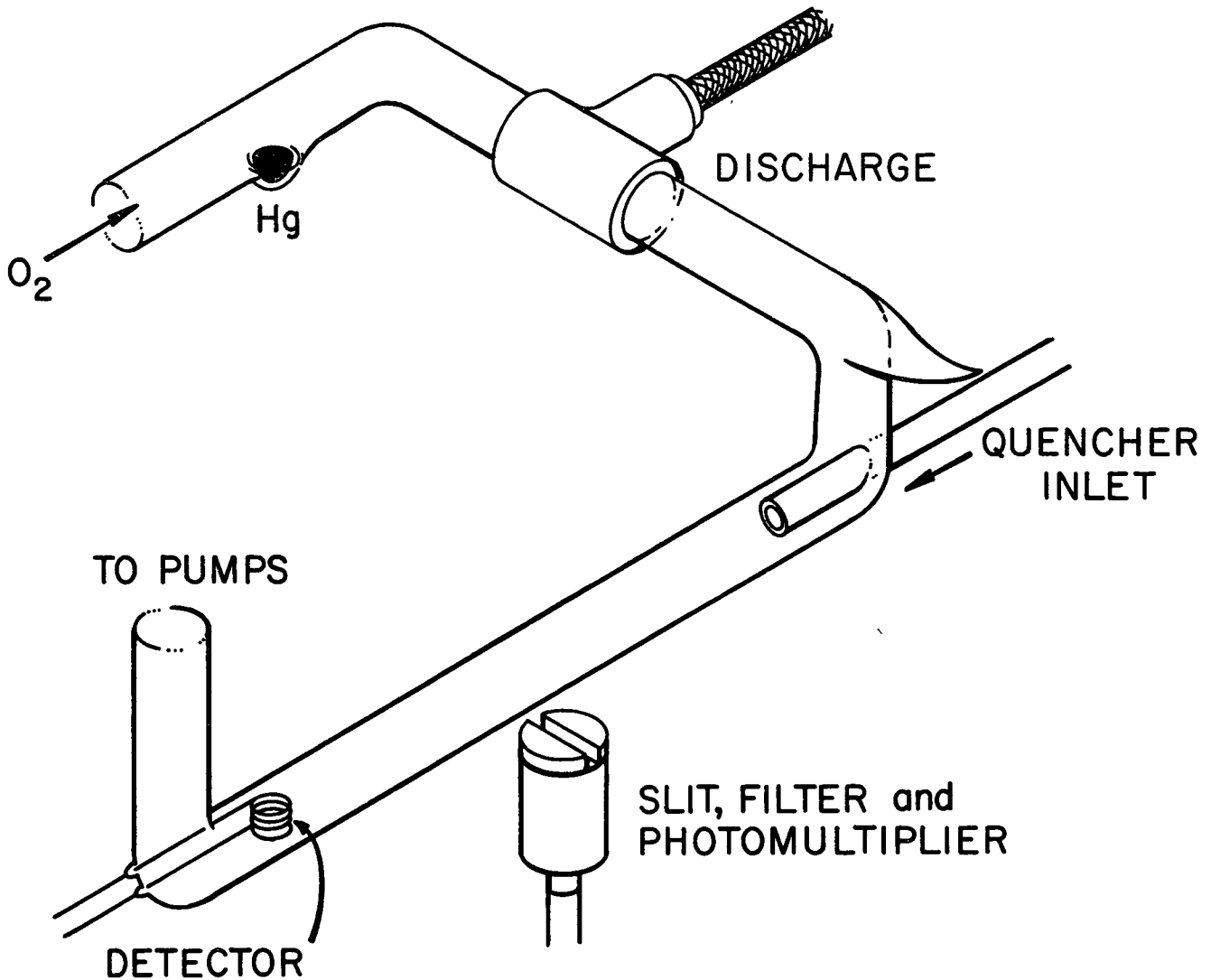

CORE OF APARATUS FOR "SINGLE OXYGEN" STUDIES

were introduced into the reaction tube through an inlet jet which extended 3 cm. into the reaction tube.

The reaction tube used for the temperature dependent studies $\{O_2(^1\Delta_g)\}_2$ was 1.5 cm. in diameter and 5 cm. in length. It was jacketed to permit the circulation of liquids or vapours over the whole length of the reaction tube. The jacket was covered with several layers of asbestos insulation. Two thermocouples were placed next to the wall of the inner reaction tube to record the temperature of the gas stream.

The flow rates of oxygen and added gas were controlled and measured by identical systems. The flow rates were varied by Edwards fine-control needle valves. The pressure difference established across a capillary was measured by a U-tube manometer filled with mercury in the case of oxygen and with dibutylphthalate in the case of the added gases. The flow rate of oxygen was determined by collecting the gas passing through the flow system when steady state conditions had been established. The flow rates of the noncondensable added gases were measured by observing the pressure drop, ΔP, due to outflow from a standard volume during a time, Δt, under normal experimental conditions. The average flow rate is:

$$f = \frac{(\Delta P)V_s}{(\Delta t)RT} \tag{11}$$

where V_s = standard volume from which the gas flowed during a measurement of flow rate. The flow rates of condensable added gases were determined by trapping the gas in a liquid nitrogen trap, transferring it to a weighing vessel and weighing it.

A constant pressure head was maintained for the flows of oxygen, carbon dioxide, nitrogen, helium, and argon by bubbling the excess gas through mercury. In the case of other gases used, a five-liter storage bulb had to be used to keep a constant pressure head during an experiment.

The pressure in the system was measured with a tilting McLeod gauge. The instrument, obtained from the Virtis Company, New York, measured pressures from 0.1 to 5.0 mm Hg with a reproducibility of 1%.

Excited Molecule Production:

A Raytheon Microwave Generator No. KV-1048B was used to obtain an electrodeless discharge. The unit generates a continuous 2450 megacycle wave with a maximum power output of 125 watts. When the output is directed at a stream of oxygen through a director, a discharge may be initiated under the proper conditions of pressure, flow and tube size by the application of a spark (from a Tesla coil).

The optimum discharge tube for maximum excited molecule production was a straight jacketed Pyrex tube, 10 cm. in length and 1.0 cm. in internal diameter, with the discharge area cooled by blowing cold air through the jacket. With linear flow rates in the vicinity of 260 cm. sec.$^{-1}$, the discharge could remain in operation at pressures between 0.2 and 10.0 mm Hg with the waveguide used in these experiments. A type C Raytheon director was stripped of all but its metal parts, and bent so the reflector encircled the gas carrying tube. Since the presence of water in the oxygen was found to almost totally destroy any $O_2(^1\Sigma_g^+)$ present, extra dry oxygen was used throughout the work.

The walls of the reaction tube were cleaned by rinsing with a 10% nitric acid solution, followed by several rinsings with water and a final rinsing with diethyl ether. The system was then allowed to pump down for three to four hours before use.

Under constant conditions of pressure and flow rate the excited molecule concentration was observed to increase linearly as the microwave power input increased between 10 and 75 watts.

Destruction of Oxygen Atoms:

Since oxygen atoms are produced in concentrations up to 10% in discharged oxygen, means had to be found for their elimination from the system without affecting the excited molecule concentration. Since Ogryzlo, Elias and Schiff (32) had shown that oxygen atoms recombine on a silver surface turning the surface black due to oxide formation, a coil of silver wire (30 gague, 60 cm. long) was suspended in the reaction tube, just in front of the oxygen stream. When sufficient silver wire was present in the system to remove the oxygen atoms, no excited molecules could be detected. A copper surface yielded similar results. In accordance with Ogryzlo's observations (2), it was found that a small amount of mercury distilled through the discharge completely removed the oxygen atoms, as evidenced by the extinction of the yellow-green nitrogen dioxide afterglow.† The concentration of the primary excited molecule $O_2(^1\Delta_g)$, does not appear to be affected by the presence or absence of oxygen atoms.

---

† The nitrogen dioxide afterglow, which is normally present because of trace amounts of nitrogen impurities in tank oxygen, is a very sensitive test for the presence of oxygen atoms.

Oxygen atoms can also be destroyed by the addition of nitrogen dioxide through the reaction

$$NO_2 + O \rightarrow NO + O_2 \qquad (12)$$

This method of destroying oxygen was used in only one or two particular instances.

Spectroscopic Studies:

The spectroscopic studies, undertaken to identify the excited molecules present in discharged oxygen, were conducted in a reaction system similar to the flow system used for kinetic studies. The reaction tube in this system had an optical window at one end (the excited molecule stream entering through a T joint) allowing a spectrograph to be directed along the tube to achieve a long light path. The outside of the reaction tube was coated with MgO paint to increase the light intensity within the tube.

The low resolution spectra were obtained using a Hilger-Watts glass prism spectrometer (f/4.5) equipped with a photoelectric detection system consisting of an RCA 7265 photomultiplier, having an S-20 response, or a liquid nitrogen cooled RCA 7102 photomultiplier having an S-1 response, a 82.5 cps chopper, an AC amplifier (Electronics Missels and Communications Inc., Lockin Amplifier Model RJB) and a recorder. The system could detect emissions in the range 3000 - 13000A.

The high resolution spectra were photographed on a Jarrell-Ash f/6.3 grating spectrograph, having 20A/mm despersion, using Kodak 103F or IN spectrographic plates.

Measurement of $O_2(^1\Sigma_g^+)$ and $O_2(^1\Delta_g)$ Concentrations:

The absolute concentration of $O_2(^1\Sigma_g^+)$ was obtained by measuring the absolute emission intensity of the 7619 A band due to the (0-0) transition of the $b^1\Sigma_g^+ \rightarrow X^3\Sigma_g^-$ system and comparing it with the chemiluminescence from the reaction

$$O + NO \rightarrow NO_2 + h\nu \tag{13}$$

according to the method described by Schiff, Fontijn and Meyer (32) who measured the absolute quantum yield for reaction 13. For this reaction the absolute emission intensity is given by

$$I(NO_2^*) = ck_{13}\,[NO][O] \tag{14}$$

while for the 7619 A band

$$I(7619) = ck_{15}[O_2(^1\Sigma_g^+)] \tag{15}$$

Hence, the concentration of $O_2(^1\Sigma_g^+)$ can be calculated from

$$[O_2(^1\Sigma_g^+)] = \frac{k_{13}I(7619)\,[NO][O]}{k_{15}I(NO_2^*)} \tag{16}$$

where c = optical constant for the measurements

$k_{15} = 1/\tau$ = Einstein A coefficient for spontaneous radiation

$= 0.14$ sec.$^{-1}$ (7)

k_{13} = rate constant for the NO + O reaction in the region 7525-7675 A

m $= 2.28 \times 10^{-18}$ cm.^{3} molecules^{-1} sec.$^{-1}$ (32)

[NO] = concentration of NO introduced in molecules/cm.^{3}

[O] = concentration of oxygen atoms from the discharge in atoms/cm.^{3}

The oxygen atom concentration is determined by titration with nitrogen dioxide according to the reaction

$$O + NO_2 \rightarrow NO + O_2 \tag{12}$$

The intensities of the 7619 A band and the nitrogen dioxide afterglow in the region 7525-7675 A were measured with an RCA 7625 photomultiplier according to the procedure described by Schiff et al (33).

Principal sources of error in determining the $O_2(^1\Sigma_g^+)$ concentration by a measurement of the absolute emission intensity of the 7619 A band are the errors in k_{15} and k_{13}. Schiff et al quote the accuracy of k_{13} to no better than $\pm$ 30%, while the accuracy of k_{15} is probably no better than an order of magnitude.

The absolute concentration of $O_2(^1\Delta_g)$ could not be successfully determined by measuring the absolute emission intensity of the 12680 A band of the (0-0) transition of the $a^1\Delta_g \rightarrow X^3\Sigma_g^-$ system because it occurred in a very difficult spectral region. Consequently, the $O_2(^1\Delta_g)$ concentration was determined with an isothermal calorimetric detector. The detector consists of a helically wound spiral of platinum wire electroplated with cobalt and movable under vacuum along the reaction tube. The platinum wire formed one arm of the Wheatstone bridge circuit shown in figure 3.

With the discharge off, that is, no excited molecules flowing, current is passed through the detector and the bridge is balanced by adjusting the current and/or the resistance of the decade resistance box. The current through the detector is then measured on an accurate potentiometer by measuring the current across the one ohm precission resistor. With the microwave discharge on and excited molecules present, the excited molecules are deactivated on the Co/Pt coil releasing 23 kcal. moles^{-1} (excitation energy of $O_2(^1\Delta_g)$) in the

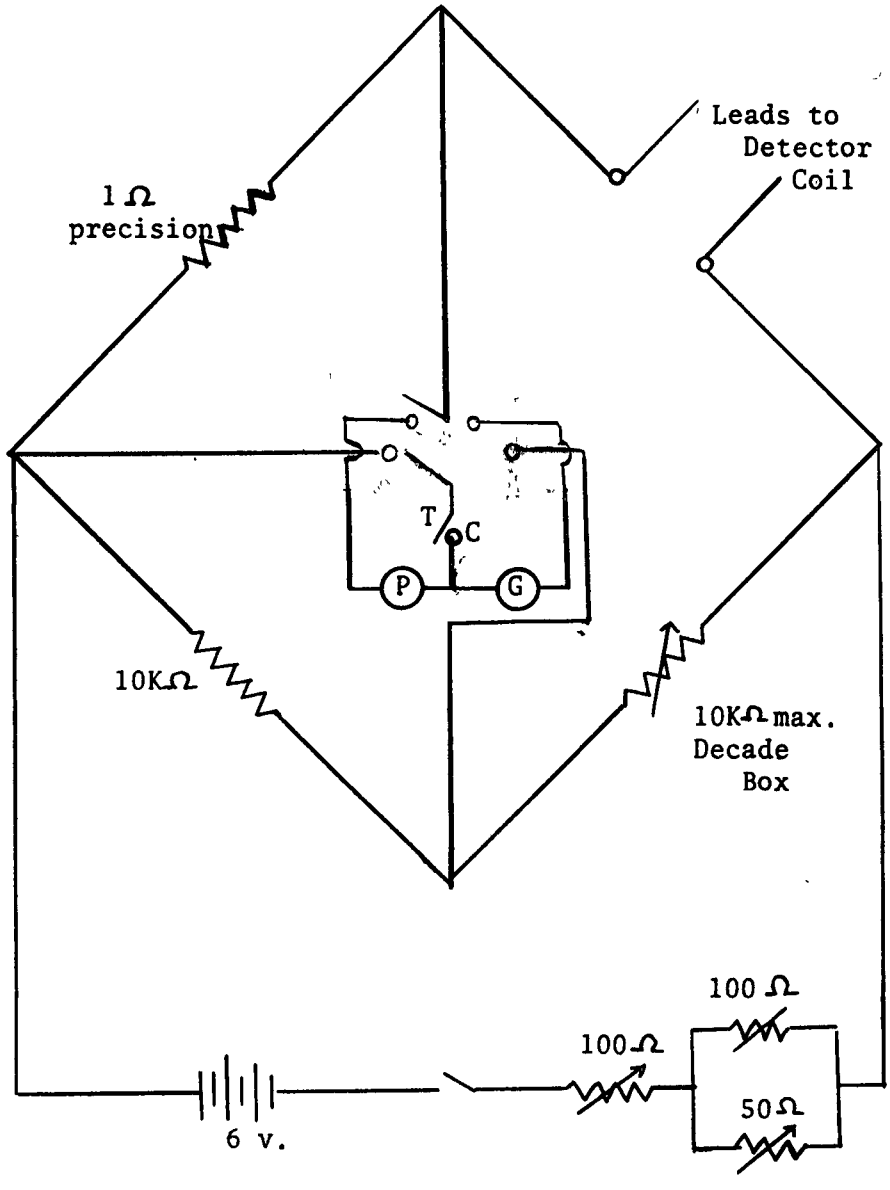

P. potentiometer terminal

C common "

G galvanometer "

T tapping key

Figure 3. Diagram of Detector Circuit.

form of heat. For the bridge to be balanced under these conditions the current through the detector must be decreased, returning the coil to its original temperature and thus to its original resistance. From the magnitudes of the decrease of the squares of the currents $\Delta(i^2)$, the excited molecule flow incident on the detector can be calculated from

$$O_2(^1\Delta_g) \text{ flow} = \frac{\Delta(i^2)R}{4.18E} \quad \frac{\text{moles}}{\text{sec.}} \tag{17}$$

where $\Delta(i^2)$ = current squared decrease = $(i_1^2) - (i_2^2)$

R = resistance of the detector

E = excitation energy of $O_2(^1\Delta_-)$ = 23 kcal./mole

Individual detector readings could be reproduced with a deviation of less than 2%.

The efficiency of the detector could be checked by looking to see if any emission at 12680 A due to the (0-0) $a^1\Delta_g \rightarrow X^3\Sigma_g^-$ transition was detectable down stream from the detector or by inserting a second detector into the gas stream down stream from the first. In each case the detector was observed to destroy better than 95% of the $O_2(^1\Delta_g)$ present.

Once it had been established that the intensity of the 6340 A band was proportional to the square of the $O_2(^1\Delta_g)$ concentration, changes in the $O_2(^1\Delta_g)$ concentration as a function of time or added gas could be easily and rapidly determined by measuring changes in the intensity of the 6340 A band with an RCA 7265 photomultiplier.

RESULTS

The Emission Bands:

When oxygen is passed through a microwave discharge a strong yellow-green afterglow is visible. This glow is due to the reaction of ground state oxygen atoms $O(^3P)$ with nitric oxide, formed from nitrogen impurities to produce the nitrogen dioxide airglow continuum.

$$O + NO \rightarrow NO_2^* \rightarrow NO_2 + h\nu \qquad (13)$$

Removal of oxygen atoms by distilling mercury through the discharge extinguishes nitrogen dioxide airglow continuum, leaving a faint red glow.

Figure 4 shows a low resolution spectrum of the emission detectable in an atom-free system with a Hilger-Watts f/4.5 glass prism spectrograph and a liquid nitrogen cooled RCA Victor 7102 photomultiplier. The peak at 12680 A is identified as the (0-0) transition of the "infrared atmospheric system" $a^1\Delta_g \rightarrow X^3\Sigma_g^-$, providing direct spectroscopic evidence for the presence of $O_2(^1\Delta_g)$ in discharged oxygen.

The peaks at 7619 A and 8645 A appear at the same wavelength as the (0-0) and (0-1) bands of the "atmospheric system" $b^1\Sigma_g^+ \rightarrow X^3\Sigma_g^-$. Figure 5 shows a high resolution spectrum of the 7619 A band taken with a Jarrell-Ash f/6.3 grating spectrograph. The peak is easily resolved into its P and R branches showing the rotational fine structure characteristic of the $b^1\Sigma_g^+ \rightarrow X^3\Sigma_g^-$ transition (7).

The peaks at 6340 A and 7030 A have not previously been observed in discharged oxygen and could not be assigned to any known

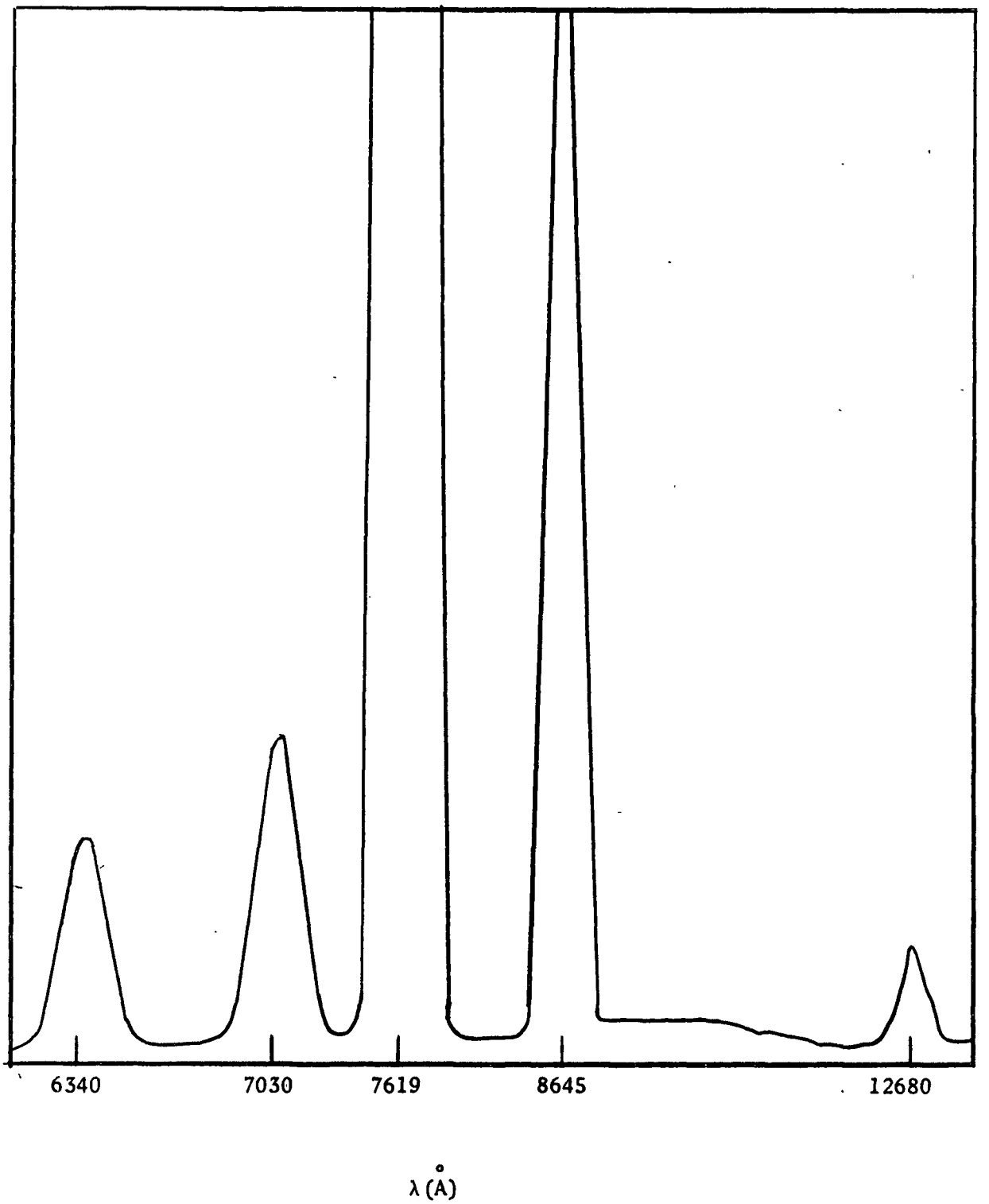

Figure 4:

The emission spectrum of electrically discharged oxygen afterglow as obtained with a Hilger-Watts f/4.5 glass prism spectrograph and a liquid nitrogen cooled RCA 7102 photomultiplier. All oxygen atoms have been removed by distilling mercury through the discharge. A 500-micron slit was used.

Figure 5.

High resolution spectrum of the 7619 A band as photographed with a Jarrell-Ash f/6.3 grating spectrograph, having 20A/mm dispersion. A 30-micron slit was used, requiring an exposure time of 15 minutes with Kodak IN spectroscopic plates.

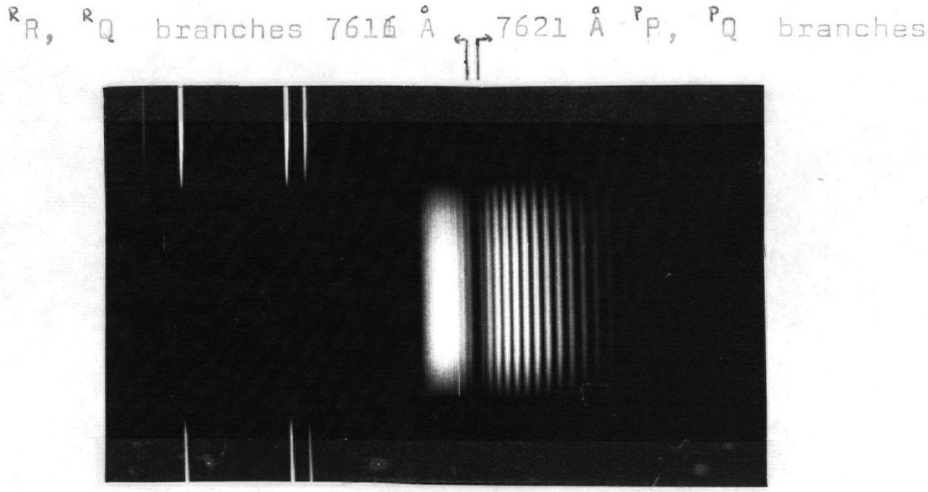

transition in O_2. Figure 6 shows the 6340 A band photographed under high resolution under identical conditions to the 7619 A band shown in figure 5. Unlike the 7619 A band where the rotational lines are easily resolved, the 6340 A band shows no sign of any rotation fine structure, but has a half-peak width of about 145 A.

At this point in the experimental work, it seemed expedient to investigate the possibility that the 6340 A and 7030 A bands were caused by impurity emissions. Two impurities commonly found in tank oxygen could give rise to emissions in this region. Water absorption peaks have been observed at 6340 A and 7000 A (34) and nitrogen dioxide emission bands occur throughout this region. (35) Therefore, ultra nitrogen-free oxygen was prepared by the thermal decomposition of potassium permanganate and thoroughly dried with phosphorus pentoxide. Furthermore, nitrogen, nitrogen dioxide, and water were added in small quantities both before and after the discharge to see if their presence or absence affected the intensity of the 6340 A and 7030 A bands. The intensity of the bands was affected neither by the purity of the oxygen used nor by contamination of the oxygen with nitrogen, nitrogen dioxide or water.

Ozone could not be the emitter since the addition of nitric oxide which would rapidly remove ozone by the reaction

$$\begin{array}{l} O_3 + NO \rightarrow NO_2^* + O_2 \\ \qquad\qquad\quad \hookrightarrow NO_2 + h\nu \end{array} \tag{18}$$

had no effect on the intensity of the 6340 A and 7030 A bands and failed to show the characteristic red flame (36).

The effect of other added foreign gases on the intensity of

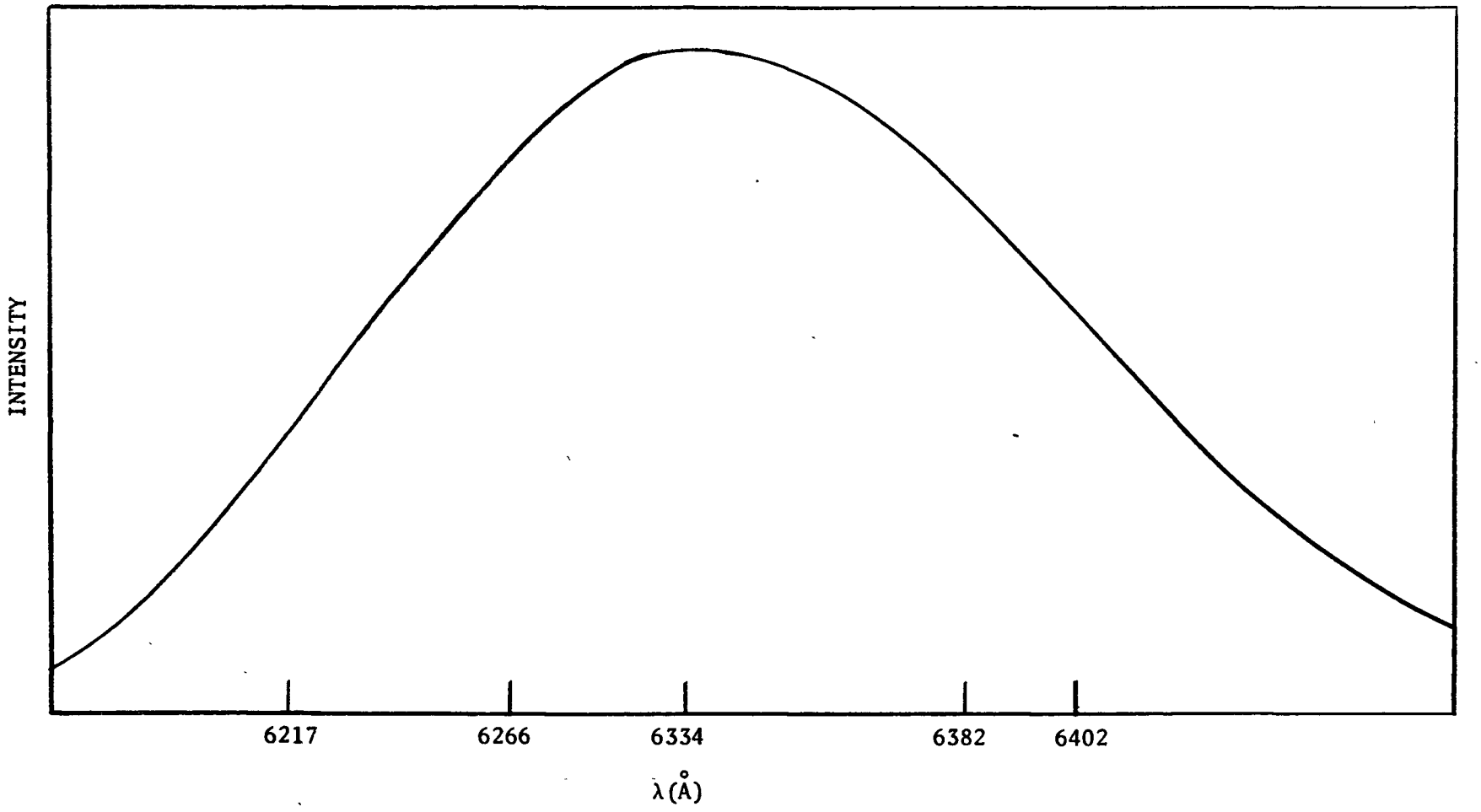

Figure 6:

Microdensitometer trace of the 6340 A band photographed with a Jarrell-Ash f/6.3 grating spectrograph (20A/mm. dispersion, 30-micron slit) on Kodak 103F plate, exposed for 72 hours.

the 6340 A and 7030 A bands was quickly checked by introducing small quantities of nitrous oxide, carbon monoxide, carbon dioxide, ammonia, helium, argon, and hydrogen after the discharge (see page 43 for a detailed discussion of excited state quenching). None of these added gases had any effect on the intensities of the 6340 A and 7030 A bands or on the intensity of the 12680 A band of the (0-0) transition of the $a^1\Delta_g \rightarrow X^3\Sigma_g^-$ system but some of the added gases almost totally extinguished the 7619 A and 8645 A bands of the (0-0) and (0-1) $b^1\Sigma_g^+ \rightarrow X^3\Sigma_g^-$ system.

<u>The Relationship between the 6340 A and 7030 A band intensities and the $O_2(^1\Delta_g)$ concentration.</u>

Under steady state conditions, the intensities of the 6340 A and 7030 A bands were measured with an RCA 7265 photomultiplier and the corresponding $O_2(^1\Delta_g)$ concentrations with an isothermal calorimetric detector. Under each set of experimental conditions, two sets of measurements were made, one at 75% microwave power input and the other at a lower microwave power input. The ratio of the band intensities and the $O_2(^1\Delta_g)$ concentration at the two microwave power inputs is given in table III. The band intensities and the $O_2(^1\Delta_g)$ concentration measured at the same microwave power input and at ten different pressures over a total oxygen pressure range from 1.0 to 5.2 mm Hg are given in table IV.

Table III

Ratios of the Intensities of the 6340 Å band, the intensities of the 7030 Å band and the $O_2(^1\Delta_g)$ concentrations.[a]

$I_1(6340)/I_2(6340)$	$I_1(7030)/I_2(7030)$	$[O_2(^1\Delta_g)]_1/[O_2(^1\Delta_g)]_2$
2.40	2.33	1.56
5.34	5.40	2.30
3.6	3.52	1.88
3.17	3.18	1.78
1.81	1.79	1.35
2.80	2.71	1.68
3.21	3.21	1.65
2.27	2.26	1.56
2.43	2.39	1.61

a The two sets of intensity and concentration measurements were made under identical experimental conditions but at two different microwave power inputs.

Table IV

Relationship between the intensity of the 6340 Å band, the intensity of the 7030 Å band and the $O_2(^1\Delta_g)$ concentration.[a]

P(torr)	I(6340) arbitrary units	I(7030)	$[O_2(^1\Delta_g)] \times 10^6$ moles $l.^{-1}$
1.0	43	25	7.5
1.5	59	34	8.8
2.0	88	53	10.7
2.4	107	63	12.0
3.1	128	74	13.0
3.5	150	85	13.5
3.8	163	94	14.3
4.3	190	111	15.3
4.8	220	126	16.8
5.2	230	130	17.4

a The measurements were made at constant microwave power input.

The Relationship between the $O_2(^1\Sigma_g^+)$ concentration and the $O_2(^1\Delta_g)$ concentration:

Under steady state conditions, the intensity of the 7619 A band, due to the (0-0) transition of the $b^1\Sigma_g^+ \rightarrow X^3\Sigma_g^-$ system, was measured with an RCA 7265 photomultiplier and the corresponding $O_2(^1\Delta_g)$ concentration with an isothermal calorimetric detector. Under each set of experimental conditions, two sets of measurements were made, one at 75% microwave power input and the other at lower microwave power input. The ratio of the band intensities and the $O_2(^1\Delta_g)$ concentration at the two microwave power inputs is given in table V. The 7619 A band intensity and the $O_2(^1\Delta_g)$ concentration measured at the same microwave power input at ten different pressures over a total oxygen pressure range from 1.0 to 5.2 mm Hg are given in table VI.

Using a smaller diameter fast flow system (flow rate $\sim$ 260 cm./sec.) a nonsteady state system was achieved which allowed the build up of $O_2(^1\Sigma_g^+)$ to its steady state value to be measured and observed. Figure 7 shows a typical plot of the intensity of the 7619 A band as a function of distance along the reaction tube indicating the build up of $O_2(^1\Sigma_g^+)$ to its steady state value. Over the same distance the $O_2(^1\Delta_g)$ concentration remained almost constant. For each of the curves shown in figure 7 the absolute $O_2(^1\Sigma_g^+)$ concentration was determined by measuring the absolute emission intensity of the 7619 A band. The steady state $O_2(^1\Sigma_g^+)$ concentrations and the corresponding $O_2(^1\Delta_g)$ concentrations are given in table VII.

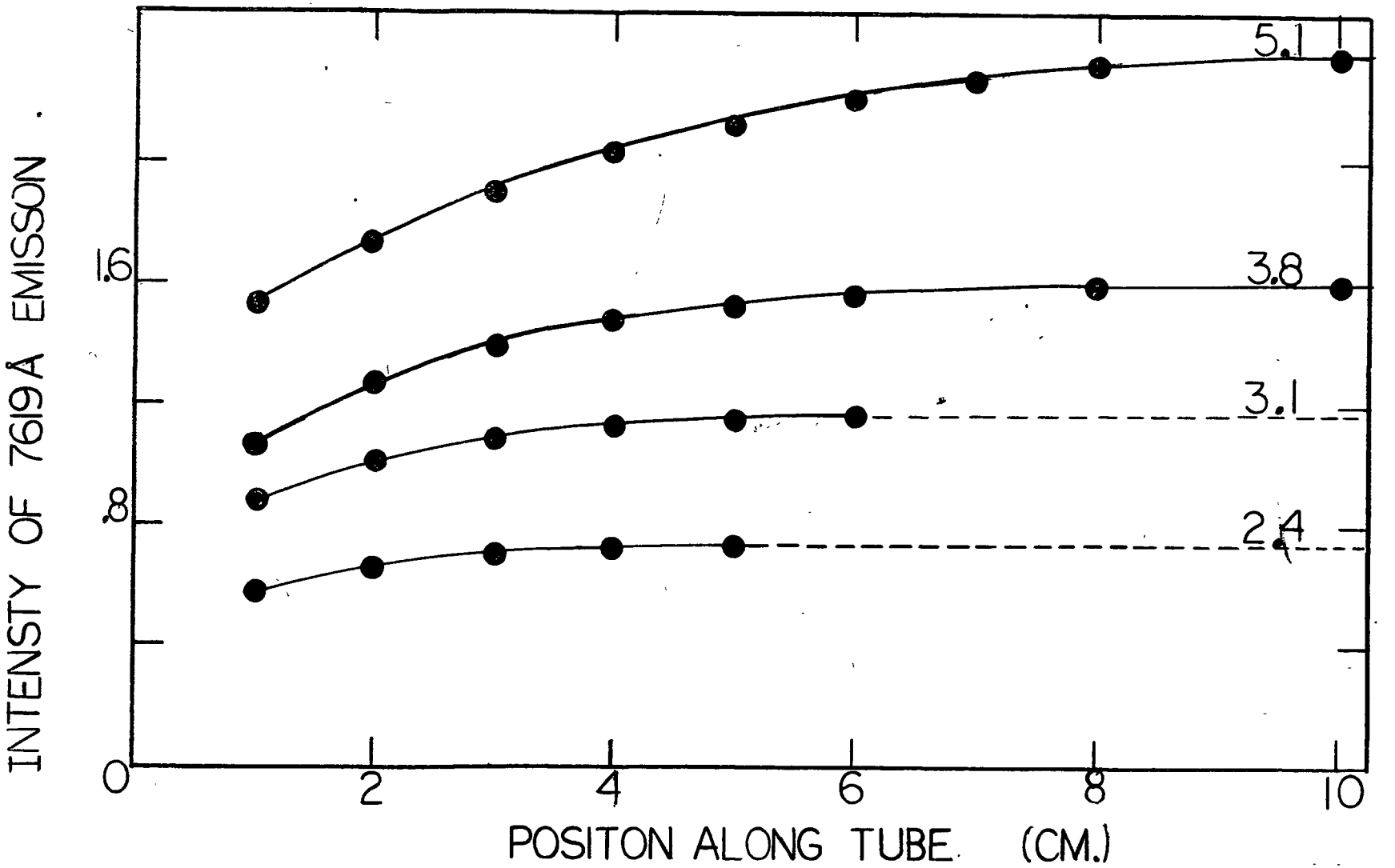

Figure 7: Plot of the intensity of the 7619 A band as a function of distance along the reaction tube. The values above each curve indicate the total oxygen pressure in the system in mm. Hg.

Table V

Ratios of the intensities of the 7619 Å band[a] and the $O_2(^1\Delta_g)$ concentrations.[b]

$I_1(7619)/I_2(7619)$	$[O_2(^1\Delta_g)]_1/[O_2(^1\Delta_g)]_2$
2.43	1.56
5.3	2.30
3.58	1.88
3.12	1.78
1.85	1.35
2.82	1.68

a The intensity of the 7619 Å band is a measure of the steady state $O_2(^1\Sigma_g^+)$ concentration.

b The two sets of intensity and concentration measurements were made under identical experimental conditions but at two different microwave power inputs.

Table VI

Relationship between the intensity of the 7619 Å band[a] and the $O_2(^1\Delta_g)$ concentration.[b]

P(torr)	I(7619) arbitrary units	$[O_2(^1\Delta_g)] \times 10^6$
1.0	450	7.5
1.5	600	8.8
2.0	850	10.7
2.4	1050	12.0
3.1	1350	13.0
3.5	1500	13.5
3.8	1600	14.3
4.3	1900	15.3
4.8	2150	16.8
5.2	2330	17.4

a See footnote a Table V .

b The measurements were made at constant microwave power input.

Table VII

Steady State $O_2(^1\Sigma_g^+)$ concentration and $O_2(^1\Delta_g)$ concentration.

P(torr)	$[O_2]x10^4$ moles/l	$[O_2(^1\Sigma_g^+)]x\ 10^9$ moles/l	$[O_2(^1\Delta_g)]x10^6$ moles/l	$\frac{K_f}{K_r}$ 1/moles
2.4	1.30	1.75	9.0	20.5
3.1	1.68	2.54	11.0	21.5
3.8	2.06	4.20	14.2	20.8
5.1	2.77	6.24	17.5	20.3

Decay of $O_2(^1\Delta_g)$

Figure 8 shows a plot of $O_2(^1\Delta_g)$ concentration as a function of distance along the reaction tube. Similar pairs of decay plots, one at 75% microwave power input and the other at a lower microwave power input, were determined at several pressures over the total pressure range, 0.5 to 5.2 mm Hg. As can be seen from figure 8, the decay of $O_2(^1\Delta_g)$ is very small, being less than 20%. Consequently, the decay was difficult to measure. In order to eliminate any random errors due to slight differences in wall conditions, the rate of decay, $d[O_2(^1\Delta_g)]/dt$, was determined at several positions for each pair of plots and the ratios of the corresponding decay rates $\{d[O_2(^1\Delta_g)]/dt\}_1/\{d[O_2(^1\Delta_g)]/dt\}_2$ was obtained. These ratios, togehter with the corresponding concentration ratios, $[O_2(^1\Delta_g)]_1/[O_2(^1\Delta_g)]_2$ are given in Table VIII.

Temperature dependence of the 6340 A band.

In order to determine the effect of altering the temperature on the intensity of the 6340 A band, the temperature of the gas stream was altered between 221° K and 475° K while all other experimental variables remained constant. A temperature of 221° K was obtained by circulating a solution of ethylene glycol, cooled in liquid nitrogen-alcohol slush bath, through the insulated jacket surrounding the five cm. long, 1.5 cm. in diameter reaction tube. Temperatures of 372° K and 475° K were obtained by distilling water and acetophenone, respectively, through the jacket.

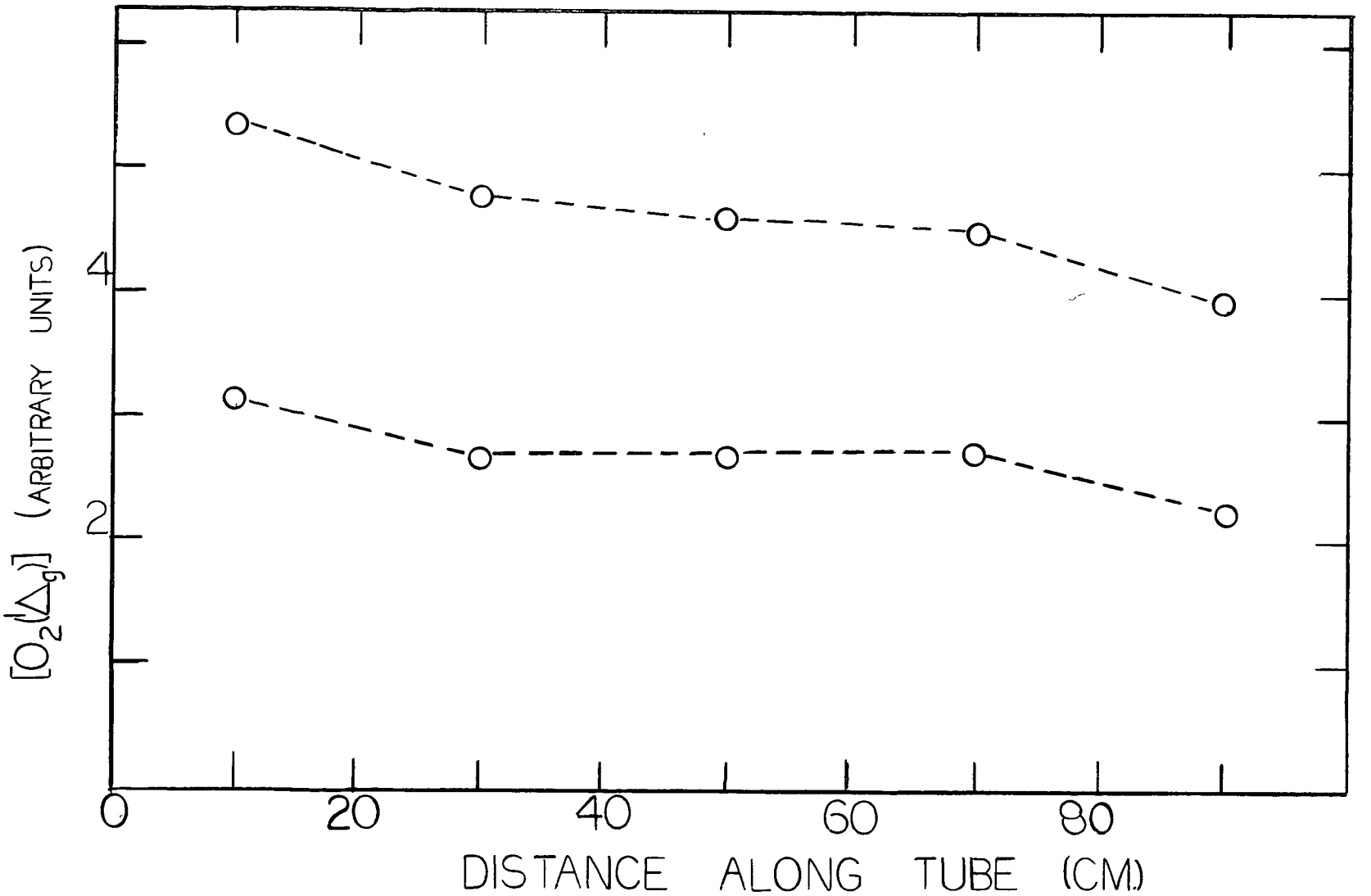

Figure 8: Plot of $O_2(^1\Delta_g)$ concentration against distance along the reaction tube.

Table VIII

Ratios of the decay rate, $d[O_2{}^1\Delta_g)]/dt$, and the average $O_2(^1\Delta_g)$ concentration.[a]

$(d[O_2(^1\Delta_g)]/dt)_1/(d[O_2(^1\Delta_g)]/dt)_2$	$[O_2(^1\Delta_g)]_1/[O_2(^1\Delta_g)]_2$
1.399	1.200
1.26	1.27
1.24	1.34
1.295	1.405
1.43	1.43
1.43	1.455
1.455	1.415
1.505	1.435
1.49	1.455
1.52	1.49
1.43	1.495
1.57	1.425
1.62	1.505
1.52	1.67
1.565	1.74
1.655	1.685
1.76	1.805
1.86	1.67
2.055	1.87
2.255	2.254

a See page 37 for a discussion of experimental procedure.

No change in pressure in the reaction tube could be measured when the temperature of the gas stream was changed. However, as the temperature of the gas stream was raised the half-peak width of the 6340 A band increased and the band height decreased. The integrated intensity of the 6340 A band, in arbitrary units, at four different temperatures is given in table IX.

Reactions of $O_2(^1\Delta_g)$

Several foreign gases were added to the excited molecule stream to test their effectiveness at deactivating $O_2(^1\Delta_g)$. The $O_2(^1\Delta_g)$ concentration was unaffected by the addition of argon, helium, nitrogen, carbon monoxide, carbon dioxide, water, deuterium oxide, ammonia, hydrogen sulfide, nitrous oxide, hydrogen bromide, carbon tetrachloride, chloroform, dimethyl ether, and n-heptane even when the partial pressure of these gases was 1/4 of the total pressure in the system.

Since Bayes and Winer (37) had observed that $O_2(^1\Delta_g)$ could oxidize 2,3-dimethylbutene-2 to its corresponding hydroperoxide, (2,3-dimethyl-3-hydroperoxybutene-1), ethylene and a series of its methyl substituted derivatives were added to the gas stream to see if they would react with $O_2(^1\Delta_g)$. Figure 9 shows the effect of equal concentrations of ethylene and five of its derivatives on $O_2(^1\Delta_g)$. Ethylene only slightly decreases the $O_2(^1\Delta_g)$ concentration whereas 2,3-dimethylbutene-2 almost completely quenches the $O_2(^1\Delta_g)$. The relative efficiencies of the series at quenching $O_2(^1\Delta_g)$ were

Table IX

Intensity of the 6340 Å band at four different temperatures.

T(°K)	I(6340 Å)
	integrated intensity in arbitrary units
221	153.5
296	100.0
373	70.3
473	49.7

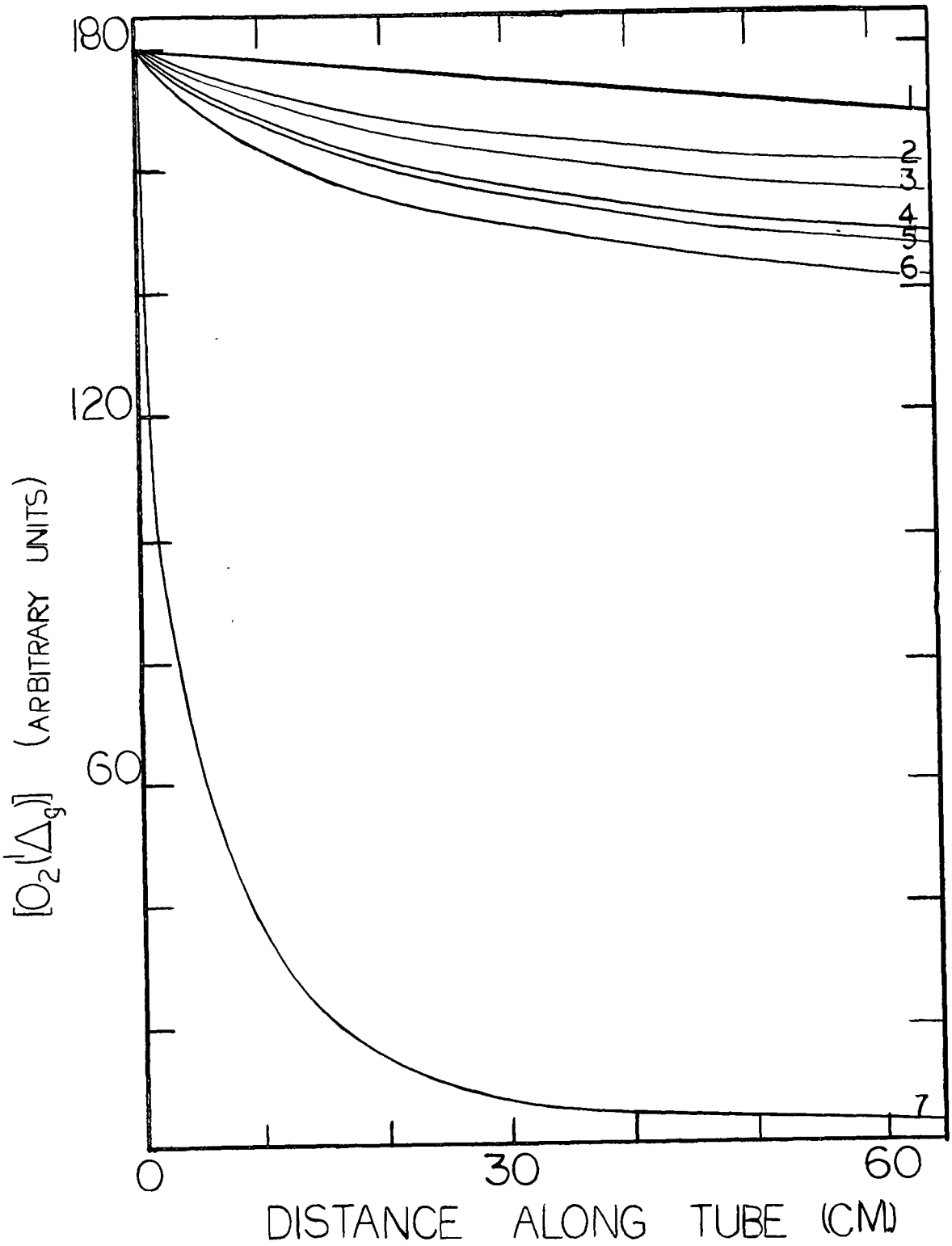

Figure 9: The effect of the addition of ethylene and its methyl substituted derivatives on the $O_2(^1\Delta_g)$ concentration

curve 1 no added gas
2 ethylene
3 propylene
4 cis-butene
5 transbutene
6 2-methylbutene-2
7 2,3-dimethylbutene-2

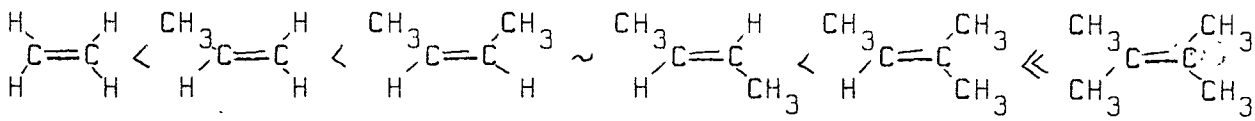

(19)

with 2,3-dimethylbutene-2 being approximately 100 times more efficient than 2-methylbutene-2.(†)

(†) Mr. Y. Kubo is continuing this work.

Reactions of $O_2(^1\Sigma_g^+)$

Several foreign gases were found to be very effective at deactivating $O_2(^1\Sigma_g^+)$ as indicated by the marked decrease in the intensity of the 7619 A band when these gases were introduced into the system. Figure 10 shows the effect of the addition of various quantities of water on the $O_2(^1\Sigma_g^+)$ concentration. In each case the $O_2(^1\Sigma_g^+)$ steady state concentration is decreased and a new steady state is established. Introduction of similar quantities of dry O_2 had no effect on the $O_2(^1\Sigma_g^+)$ concentration showing that the decrease in $O_2(^1\Sigma_g^+)$ on the addition of the foreign gases is not due to a slight increase in pressure in the system but is due to a real quenching effect.

At a constant pressure, the steady state concentration of $O_2(^1\Sigma_g^+)$ was determined both in the absence of and in the presence of various quantities of added foreign gas. In tables X to XXIV the $O_2(^1\Sigma_g^+)$ steady state concentration, as determined by the intensity of the 7619 A band, and the corresponding added foreign gas concentration are tabulated for the added gases; water, deuterium oxide, n-heptane, methanol, ammonia, dimethyl ether, hydrogen sulfide, carbon dioxide, chloroform, hydrogen bromide, methane, nitrogen, argon, carbon monoxide and helium.

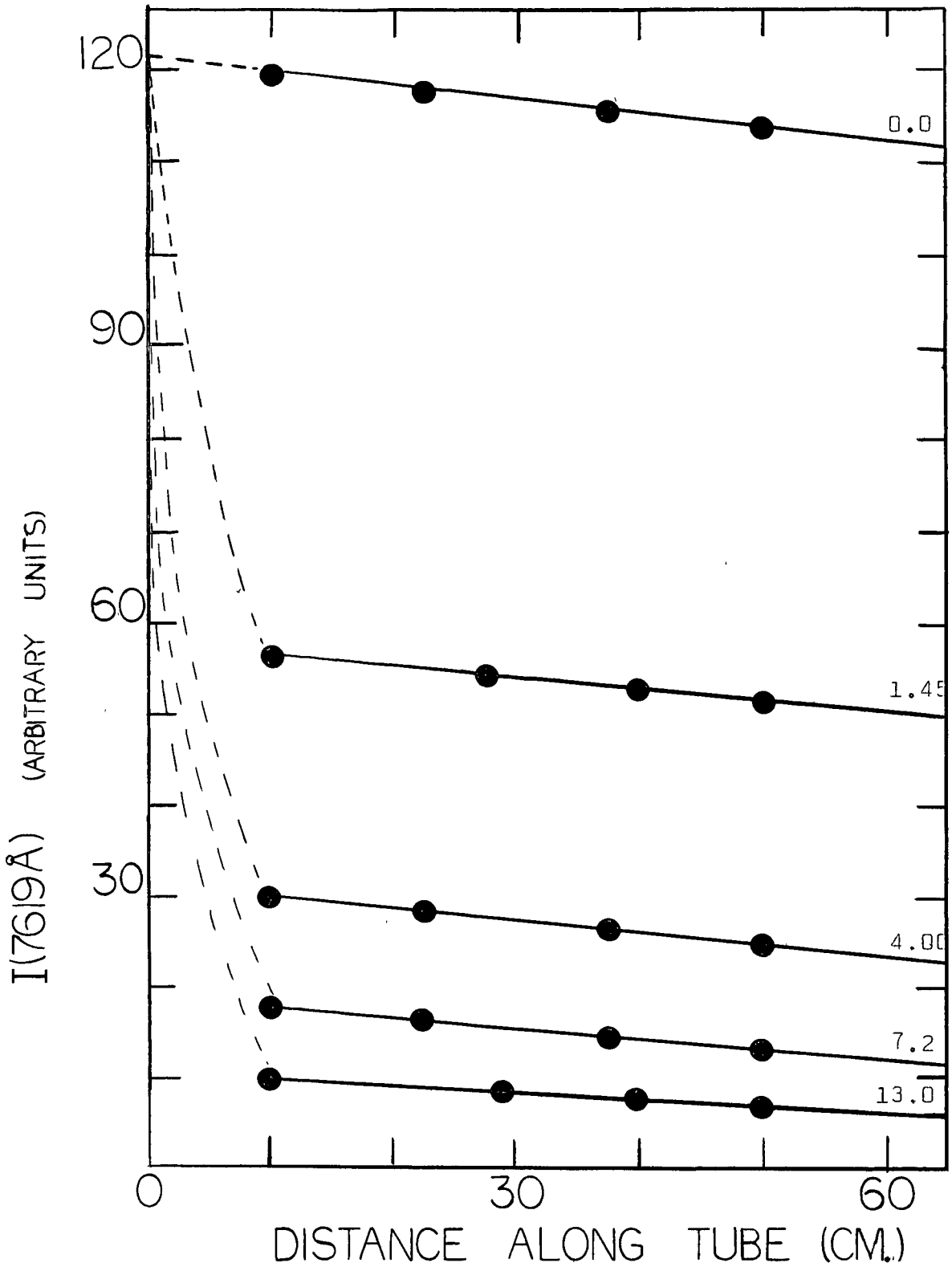

Figure 10: The effect of the addition of various amounts of water on the $O_2(^1\Sigma_g^+)$ concentration. The numbers on each line correspond to $[H_2O] \times 10^7$ moles/l.

Table X

Water as added gas

$[H_2O] \times 10^6$ moles $l.^{-1}$	$I(7619)^a$ arbitrary units
0.00	100.00
0.433	21.75
0.480	20.00
0.480	30.30
0.144	47.70
0.864	12.00
0.954	11.00
1.305	7.41
1.305	8.58
1.400	7.10
1.730	6.72

a The intensity of the 7619 A band is a measure of the $O_2(^1\Sigma_g^+)$ steady state concentration.

Table XI

Deuterium oxide as added gas.

$[D_2O] \times 10^6$ moles $l.^{-1}$	$I(7619)^a$ arbitrary units
0.000	100.00
0.192	51.3
0.168	41.9
0.289	40.0
0.289	31.3
0.385	34.1
0.385	26.2
1.000	13.6

a See footnote a Table X .

Table XII

n-heptane as added gas

$[C_7H_{16}] \times 10^6$ moles $l.^{-1}$	$I(7619)^a$ arbitrary units
0.0	100.0
0.12	65.4
0.312	44.1
0.336	39.9
0.505	25.2
0.557	21.9
0.562	30.9
0.795	23.4
1.005	18.4
1.13	17.8
1.13	17.25
1.27	11.5
1.27	11.6
1.29	12.7
1.53	13.2
1.53	13.1
2.59	9.87

a See footnote a Table X.

Table XIII

Methanol as added gas

$[CH_3OH] \times 10^6$ moles/l	I(7619)[a] arbitrary units
0.0	100.0
0.193	58.5
0.31	51.3
0.528	37.8
0.734	24.4
1.03	23.3
1.24	14.45
1.53	18.6
2.09	12.1
2.09	10.5
2.14	10.5
2.98	5.24

a See footnote a Table X.

Table XIV

Ammonia as added gas

$[NH_3] \times 10^6$ moles/l	I(7619)[a] arbitrary units
0.0	100.0
0.593	34.1
0.62	42.4
0.674	34.4
0.674	41.3
0.815	36.4
0.97	28.1
1.43	21.6
1.43	22.20
2.7	14.95
4.0	10.3
5.82	8.33

a See Footnote a Table X.

Table XV

Dimethyl ether as added gas

$[(CH_3)_2O] \times 10^6$ moles/l	I(7619)[a] arbitrary units
0.00	100.00
1.50	46.60
3.30	27.10
3.70	25.60
2.35	38.50
4.60	21.05
6.35	17.25

a See Footnote a Table X.

Table XVI

Hydrogen sulfide as added gas

$[H_2S] \times 10^6$ moles/l	I(7619)[a] arbitrary units
0.0	100.0
0.91	66.6
1.65	66.6
2.24	47.2
4.77	25.8
7.97	18.6

a See footnote a Table X.

Table XXVII

Carbon dioxide as added gas

$[CO_2] \times 10^6$ moles/l	I(7619)[a] arbitrary units
0.0	100.0
0.53	84.2
0.57	83.0
1.075	66.4
1.125	67.6
1.72	56.7
1.9	52.4
1.9	55.9
2.7	49.5
2.9	48.6
3.07	46.3
3.54	45.7
4.18	42.6

a See Footnote a Table X.

Table XXVIII

$CHCl_3$ as added gas

$[CHCl_3] \times 10^6$ moles/l	I(7619)[a] arbitrary units
0.0	100.00
1.81	66.7
1.81	63.7
1.72	67.2
1.72	65.0
1.29	73.0
1.29	71.4
0.73	82.0
0.43	91.0
0.43	85.4
1.17	94.0
2.8	59.5
1.76	88.6
1.86	81.3
3.2	45.9
3.2	49.1
0.79	57.5
1.22	56.2
3.4	51.8
3.4	54.1
0.62	83.4
1.24	75.3
1.48	69.9
1.055	81.8
0.55	87.8

a See footnote a Table X .

Table XIX

HBr as added gas

[HBr] x 10^6 moles/l	I(7619)[a] arbitrary units
0.00	100.00
1.00	80.00
0.80	74.00
2.10	74.00
3.20	57.30
8.30	40.00
6.00	47.60

a See Footnote a Table X.

Table XX

CH_4 as added gas

$[CH_4] \times 10^6$ moles/l	I(7619)[a] arbitrary units
0.0	100.00
1.67	86.3
4.57	68.6
7.85	58.3
10.0	43.8
10.9	51.3

a See Footnote a Table X.

Table XXI

Nitrogen as added gas

$[N_2] \times 10^6$ moles/l	I(7619)[a] arbitrary units
0.0	100.0
3.54	94.8
5.38	92.6
0.384	97.2
0.86	94.4
3.77	94.0
5.38	91.0
0.860	92.4
1.77	91.8
3.41	89.7
1.29	92.7
0.957	94.3
2.63	88.5

a See Footnote a Table X.

Table XXII

Argon as added gas

[Ar] x 10^6 moles/l	I(7619)[a] arbitrary units
0.0	100.00
0.337	98.5
4.25	90.4
1.48	92.3
1.48	93.0
8.27	84.3
8.45	81.0
1.00	94.3
8.54	86.0
4.92	85.5
4.78	88.5
1.94	93.5
7.4	83.3

a See Footnote a Table X.

Table XXIII

Carbon monoxide as added gas

[CO] x 10^6 moles/l	I(7619)[a] arbitrary units
0.0	100.00
1.195	96.2
1.82	93.5
1.86	97.2
3.55	92.3
3.7	92.6
5.7	90.1
5.86	90.1

a See Footnote a Table X.

Table XXIV

Helium as added gas

[He] x 10^6 moles/l	I(7619)[a] arbitrary units
0.0	100.00
1.2	94.3
2.4	92.6
3.5	91.0
5.2	83.4
7.1	78.7
8.0	77.0

a See Footnote a Table X.

Energy Pooling Processes

When either molecular iodine or nitrogen dioxide was added to an atom-free stream of excited molecules, the normal red emission was masked by a new visible emission. Figure 11 shows a low resolution spectrum of the emission obtained when nitrogen dioxide was introduced into the excited molecule stream. The emission, which appeared pale yellow to the eye, extended from 4800 A into the infrared.

The same emission can be obtained in a system containing both oxygen atoms and excited molecules in the following manner. When nitrogen dioxide is first added to a stream of oxygen atoms and excited molecules a very bright yellow-green glow due to the conventional nitrogen dioxide airglow continuum is obtained. This glow is extinguished at the end point of the titration of oxygen atoms with nitrogen dioxide

$$O + NO_2 \rightarrow O_2 + NO \tag{12}$$

However, if more nitrogen dioxide is added to the gas stream a pale yellow glow due to the new emission gradually becomes visible. Therefore, the observed emission is not due to traces of oxygen atoms because the large concentrations of nitrogen dioxide would rapidly destroy any oxygen atoms present.

Curve B in figure 2 shows the effect of water on the new yellow emission. When sufficient water was introduced to quench the $O_2(^1\Sigma_g^+)$ completely, the new yellow glow disappeared.

In order to determine the dependence of the new emission on the $O_2(^1\Sigma_g^+)$ and $O_2(^1\Delta_g)$ concentrations, the maximum intensity of the new yellow emission, the intensity of the 6340 A band and the intensity of the 7619 A band were determined, under steady state conditions, at several

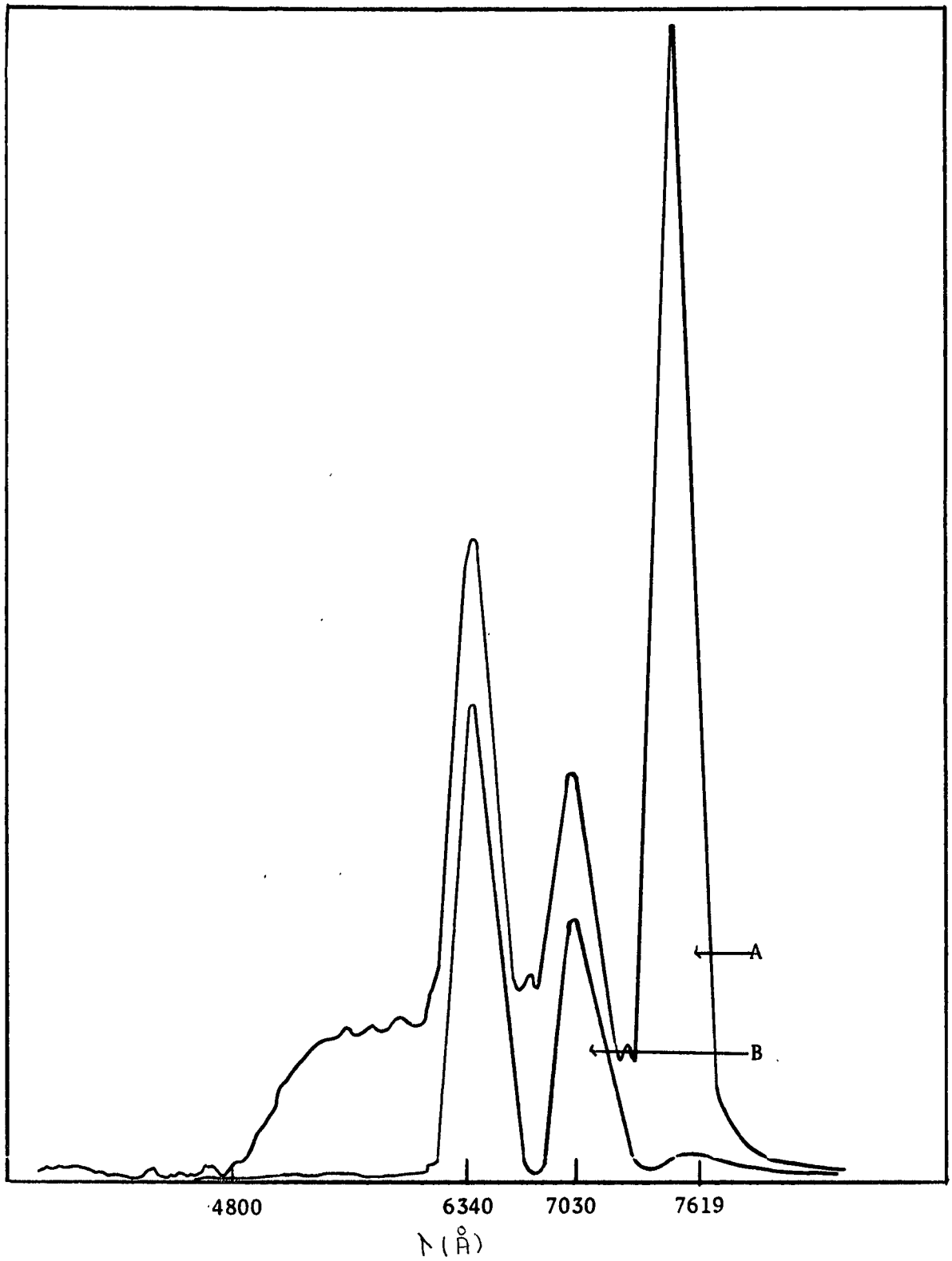

Figure 11:

Curve A: Low resolution spectrum of the NO_2^* emission taken with a Basch and Lomb grating monochrometer and an RCA 7265 photomultiplier.

Curba B: The effect of the introduction of water on the NO_2^* emission.

different total oxygen pressures. Under each set of experimental conditions two sets of measurements were made, one at 75% microwave power input and the other at a lower microwave power input. The ratio of the intensities at two microwave power inputs is given in Table XXV.

When molecular iodine vapour was introduced into a stream of excited molecules a very intense buttercup yellow glow, visible in room light, was produced. This glow is not due to or dependent upon trace amounts of oxygen atoms because when sufficient nitrogen dioxide was introduced to remove any traces of oxygen atoms, the emission remains undiminished in intensity. However, when sufficient water is added to the system to completely quench the $O_2(^1\Sigma_g^+)$, the yellow emission is almost totally extinguished. The excited molecule $O_2(^1\Sigma_g^+)$ is also being produced in the reaction, because when the yellow emission is at its maximum (†) the $O_2(^1\Sigma_g^+)$ concentration is ten times its steady state value.

Figure 12 shows a microdensitometer tracing of a high resolution spectrum of this yellow emission taken with a Jarrell-Ash f/6.3 grating spectrograph. The spectrum consists of a series of bands beginning at 5000 A and extending into the infrared. The spectral resolution was not sufficiently high to resolve each of the peaks completely into its composite bands. However, the resolution was sufficient to permit an identification of the emitting state as the $^3\pi_{ou}^+$ state, by comparison of the observed wavelengths with those

---

(†) Under a given set of experimental conditions (given $O_2(^1\Sigma_g^+)$ steady state concentration) the maximum yellow emission is obtained by introducing various amounts of iodine until the emission is brightest.

Table XXV

Ratios[a] of the intensities of the 6340 Å band[c], the intensities of the 7619 Å band[b], and the intensities of the NO_2^* emission.

$I_1(NO_2^*)/I_2(NO_2^*)$	$I_1(6340)/I_2(6340)$	$I_1(7619)/I_2(7619)$
2.66	2.11	1.623
2.14	1.79	2.08
2.33	1.80	1.80
5.30	2.80	2.81
3.60	2.39	2.22

a The two sets of intensity measurements were made under identical experimental conditions but at two different microwave power inputs.

b The intensity of the 7619 Å band is a measure of the steady state $O_2(^1\Sigma_g^+)$ concentration.

c The intensity of the 6340 Å band is directly proportional to the square of the $O_2(^1\Delta_g)$ concentration.

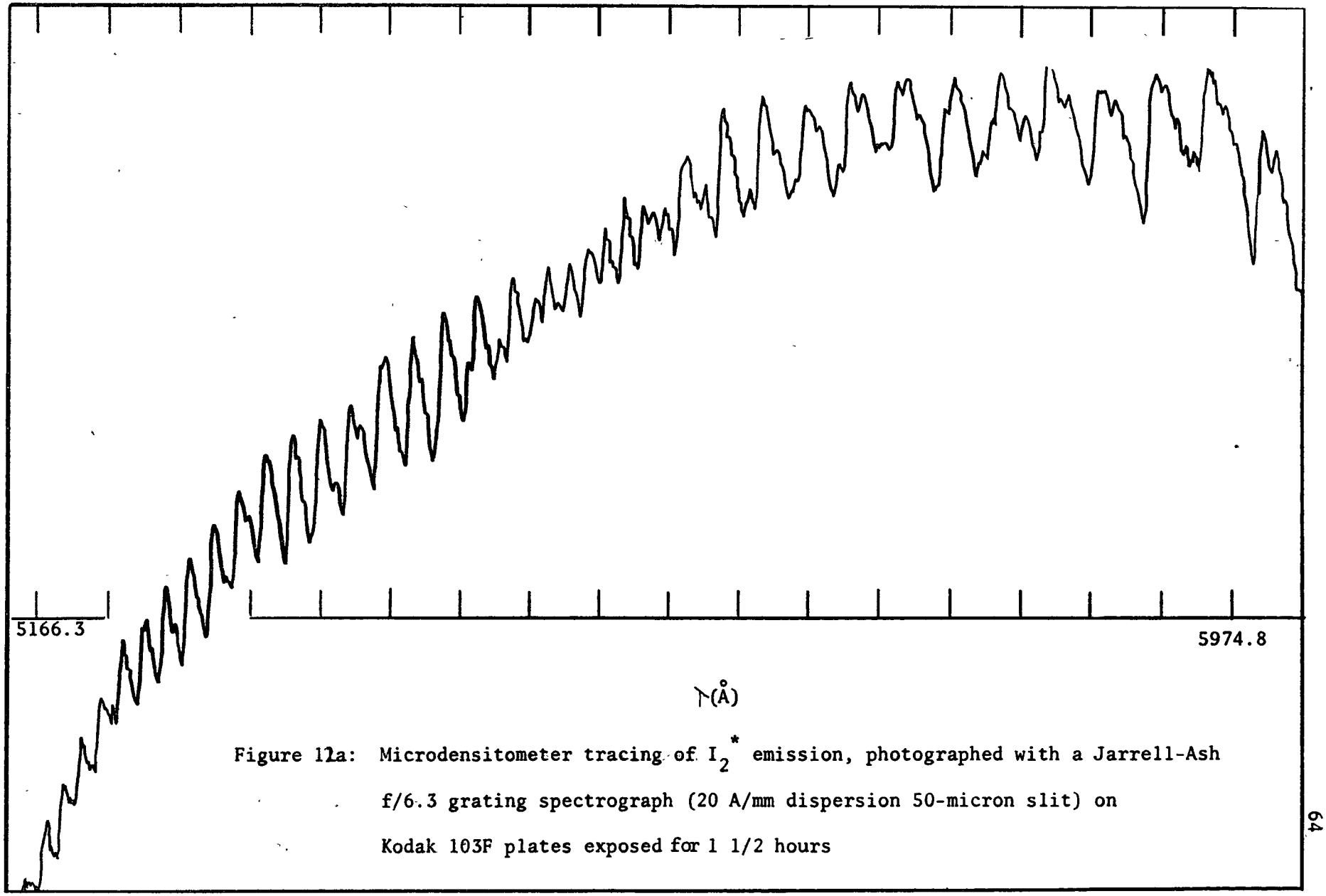

Figure 12a: Microdensitometer tracing of I_2^* emission, photographed with a Jarrell-Ash f/6.3 grating spectrograph (20 A/mm dispersion 50-micron slit) on Kodak 103F plates exposed for 1 1/2 hours

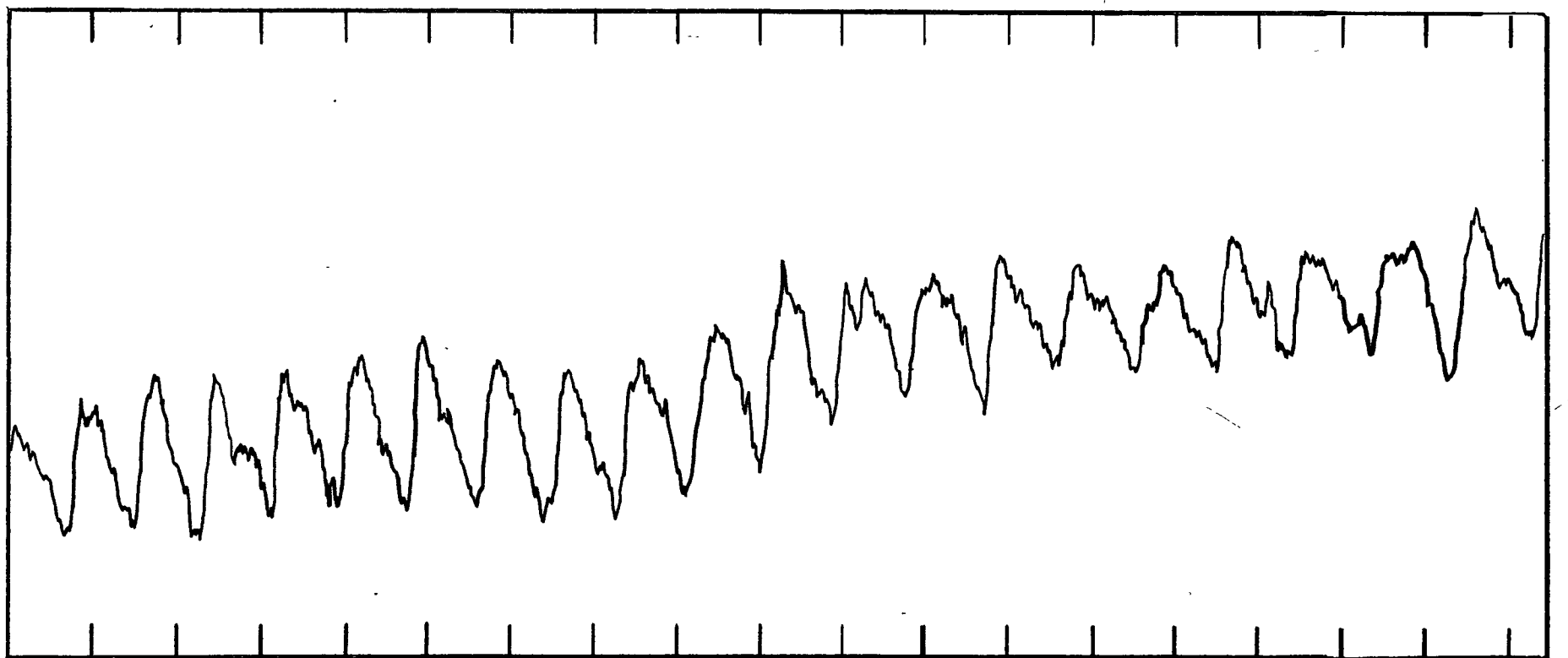

Figure 12b

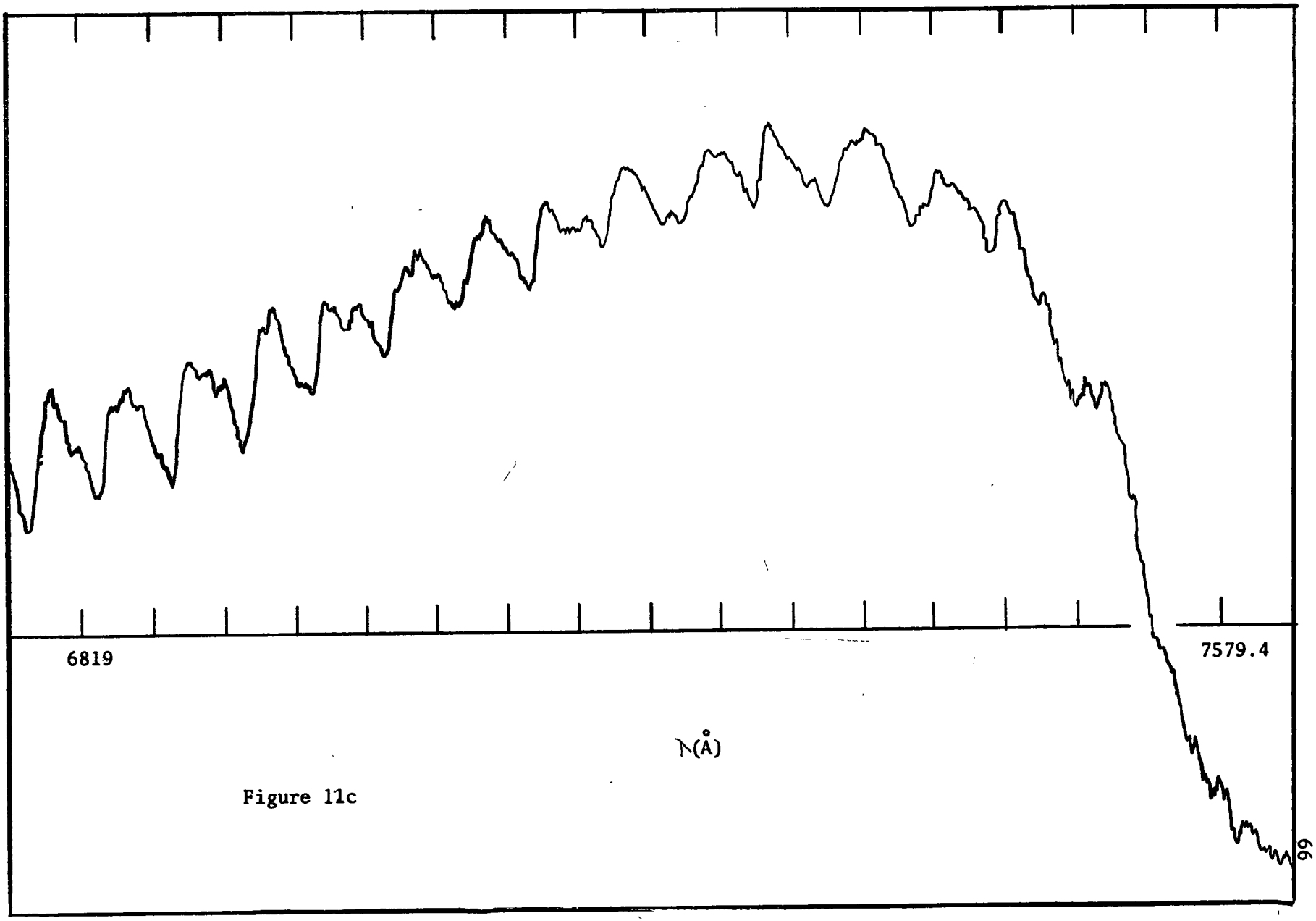

Figure 11c

calculated using the vibrational constants for the $X^1\Sigma_g^+$ state as given by Herzberg (39) and for the $^3\pi_{ou}^+$ state as determined by Steinfeld et al (40). The $^3\pi_{ou}^+$ state can be formed by recombination of an excited iodine atom ($I\ ^2P_{1/2}$) and a ground state atom ($I\ ^2P_{3/2}$). A very strong line was observed at 13,200 A (38) which could be assigned to the $^2P_{1/2} \rightarrow {}^2P_{3/2}$ transition of atomic iodine, indicating the presence of excited iodine atoms in the system.

DISCUSSION

Spectroanalysis:

Observation of the 7619 A and 8645 A bands due to the (0-0) and (0-1) transitions of the $b^1\Sigma_g^+ \rightarrow X^3\Sigma_g^-$ system was expected, since $^1\Sigma_g^+$ had previously been observed in electrically discharged oxygen. Observation of the 12680 A band of the (0-0) transition of the $a^1\Delta_g \rightarrow X^3\Sigma_g^-$ system, confirming the presence of $^1\Delta_g$ in discharged oxygen was not unexpected since its presence had previously been inferred by several indirect observations. However, observation of two new emission bands at 6340 A and 7030 A was completely unexpected.

Preliminary experiments showed that the 6340 A band, unlike the emission bands normally associated with O_2^*, was a broad band, having a half-peak width of 145 A and totally lacking rotational fine structure and that neither the 6340 A and 7030 A bands nor the 12,680 A were collisionally deactived by added foreign gases. Further experiments showed that the 6340 A and 7030 A bands were not due to water or nitrogen dioxide impurities in the oxygen or to ozone.

At this point in the investigation the similarity between the 6340 A and 7030 A bands in discharged oxygen and the red chemiluminescence from the hydrogen-peroxide-chlorine reaction observed by Seliger (41) became apparent. The emission spectrum from the chlorine-hydrogen peroxide reaction exhibited bands at 6340 A, 7030 A, and 12680 A. Since $O_2(^1\Delta_g)$ and $O_2(^1\Sigma_g^+)$ are clearly formed in the reaction, it was concluded that the emitter responsible for the 6340 A and 7030 A bands must be oxygen.

A thorough search was made of other possible excited states of O_2 to see if any could give rise to two very broad structureless bands at 6340 A and 7030 A. As shown on the potential energy diagram for oxygen illustrated in figure 1 the $A^3\Sigma_u^+$, $C^3\Delta_u$, and $c^1\Sigma_u^-$ states can also be formed by recombination of ground state $O(^3P)$ atoms. The $A^3\Sigma_u^+$ state gives rise to the Herzberg I $A^3\Sigma_u^+ \rightarrow X^3\Sigma_g^-$ bands and the Broida-Gaydon $A^3\Sigma_u^+ \rightarrow b^1\Sigma_g^+$ bands. Both systems are characterized by a closely spaced progression of bands having single heads strongly degraded to the red with the most intense Herzberg I bands in the 3000-3600 A region (11) and the most intense Broida-Gaydon bands in the 4000-4500 A region.(†) The $A^3\Sigma_u^+$ state, however, could not be the source of the 6340 A and 7030 A bands because it is very rapidly quenched by the addition carbon dioxide and nitrous oxide whereas the intensity of the 6340 A and 7030 A bands is unaffected by the addition of these gases (26).

The $c^1\Sigma_u^-$ state gives rise to the Herzberg II $c^1\Sigma_u^- \rightarrow X^3\Sigma_g^-$ system which is characterized by a closely spaced progression of bands having single heads strongly degraded to the red. The $C^3\Delta_u$ state gives rise to the Chamberlain $C^3\Delta_u \rightarrow a^1\Delta_g$ system which is characterized by bands having three heads strongly degraded to the red. (table I)

(†) Herzberg I bands were observed in the 3200 A region in the products of electrically discharged oxygen in the presence of oxygen atoms. The bands were quenched as soon as the atoms were destroyed.

Although the 6340 A and 7030 A bands are due to an oxygen emitter, they are not due to a conventional excited oxygen molecule O_2^*.

Throughout all these experiments one fact emerged; the behaviour of the 6340 A and 7030 A bands closely paralled the behaviour of the 12680 A band of the (0-0) $a^1\Delta_g \rightarrow X^3\Sigma_g^-$ system. Neither $O_2(^1\Delta_g)$ nor the new bands were deactivated by any of the foreign gases added. Coupled with this observation was the fact that twice the electronic energy of $O_2(^1\Delta_g)$ is equal to 15765 cm.$^{-1}$ or 6343 A. Consequently, it is proposed that the 6340 A and 7030 A bands are the result of a simultaneous electronic transition in two $O_2(^1\Delta_g)$ molecules in which the energy of both molecules appears as a single photon. The 6340 A band results when both molecules undergo a (0-0) transition in the $a^1\Delta_g \rightarrow X^3\Sigma_g^-$ system of O_2 while the 7030 A band results when one molecule makes the (0-0) transition and the other the (0-1) transition.

To test this theory, it was necessary to determine the relationship between the intensities of the 6340 A and 7030 A bands and the concentration of $O_2(^1\Delta_g)$ in the gas stream.

A modified form of the van't Hoff differential method is used throughout this work in order to determine the relationship between the emission intensity I of a band and the O_2^* concentration. The method is based upon the fact that the instantaneous rate of light emission, (dhv/dt), in a reaction of the nth order involving only one emitting substance is proportional to the nth power of its concentration. The emission intensity I is dhv/dt

$$I = \frac{dhv}{dt} = k[O_2^*]^n \tag{20}$$

By making two sets of measurements of the emission intensity and the O_2^* concentration under each set of experimental conditions (temperature, pressure, flow rate, etc.) but at two different microwave power inputs, the ratio Ia/Ib could be obtained

$$\frac{Ia}{Ib} = \frac{k[O_2^*]_a^n}{k[O_2^*]_b^n} = \left\{\frac{[O_2^*]a}{[O_2^*]b}\right\}^n \tag{21}$$

which gives

$$\log (I_a/I_b) = n \log ([O_2^*]_a/[O_2^*]_b) \tag{22}$$

A plot of $\log (I_a/I_b)$ versus $\log ([O_2^*]_a/[O_2^*]_b)$ will give a straight line with intercept zero and slope n.

The data of table III is analysed in this manner. Figure 13 shows a plot of $\log\left\{\frac{I_a(6340)}{I_b(6340)}\right\}$ versus $\log\left\{\frac{[O_2(^1\Delta_g)]_a}{[O_2(^1\Delta_g)]_b}\right\}$ and $\log\left\{\frac{I_a(7030)}{I_b(7030)}\right\}$ versus $\log\left\{\frac{[O_2(^1\Delta_g)]_a}{[O_2(^1b_g)]_b}\right\}$. In each case a straight line is obtained and a least squares analysis of the data gives slopes of 1.99 and 2.01 respectively. This provides good evidence that the intensities of the 6340 A and 7030 A bands are proportional to the square of the $O_2(^1\Delta_g)$ concentration.

If the relationship

$$I(6340) \propto I(7030) \propto [O_2(^1\Delta_g)]^2 \tag{23}$$

(†) The advantages of this method of analysis are a) any effects due to the total pressure in the system cancel out when the ratio is taken b) in many places relative concentrations and intensities could be used instead of absolute concentrations and intensities.

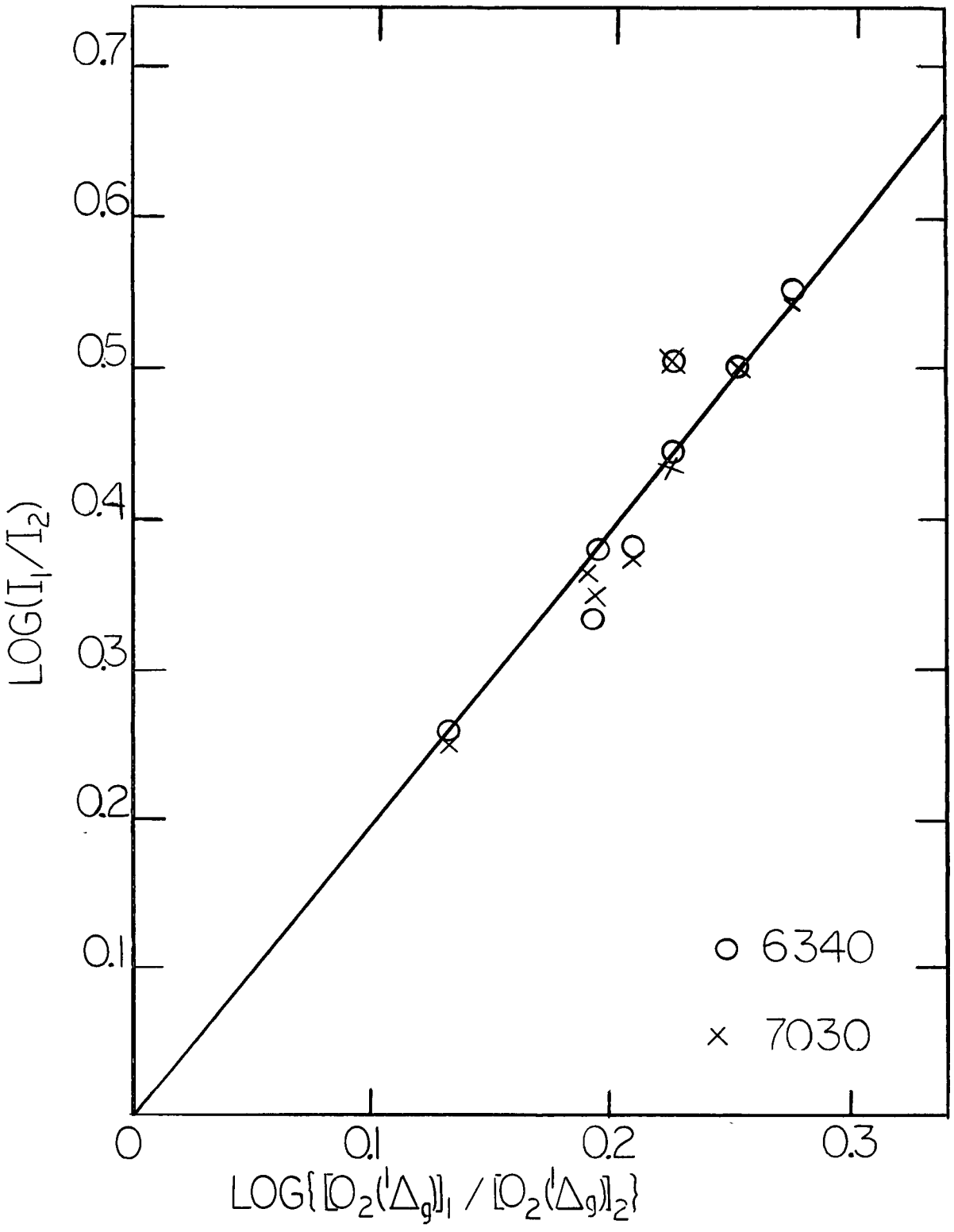

Figure 13: Plot of Log (I_1/I_2) against Log $\{(O_2(^1\Delta_g)\}_1/\{O_2(^1\Delta_g)]_2\}$

is independent of the total pressure in the system, a plot of $[O_2(^1\Delta_g)]^2/I(6340)$ or $[O_2(^1\Delta_g)]^2/I(7030)$ versus pressure will yield a straight line with slope zero. Figure 14 shows the data of table IV plotted in this way. For each plot a straight line having a slope of essentially zero is obtained, indicating that I(6340) and I(7030) are proportional to the square of the $O_2(^1\Delta_g)$ concentration regardless of the total oxygen pressure in the system.

These experiments provide strong support for the theory that the 6340 A and 7030 A bands are due to a simultaneous electronic transition in two $O_2(^1\Delta_g)$ molecules.

Additional supporting evidence comes the fact that simultaneous electronic transitions in two O_2 molecules have been shown to account for the observed absorpiton spectrum of compressed, gaseous, liquid and solid oxygen.

Ellis and Kneser (3), in addition to observing bands due to the (0-0), (1-0) and (2-0) transitions of the $X^3\Sigma_g^- \rightarrow a^1\Delta_g$ system and to the (0-0) and (1-0) transitions of the $X^3\Sigma_g^- \rightarrow b^1\Sigma_g^+$ system in liquid oxygen, observed bands at 6320 A, 5780 A and 5335 A which they attribute to simultaneous electronic transitions of the form

$$^3\Sigma_g^- + {}^3\Sigma_g^- \rightarrow {}^1\Delta_g + {}^1\Delta_g \qquad \text{I} \qquad (24)$$

bands at 4775 A and 4475 A, attributed to

$$^3\Sigma_g^- + {}^3\Sigma_g^- \rightarrow {}^1\Delta_g + {}^1\Sigma_g^+ \qquad \text{II} \qquad (25)$$

and bands at 3815 A, 3617 A and 3453 A attributed to

$$^3\Sigma_g^- + {}^3\Sigma_g^- \rightarrow {}^1\Sigma_g^+ + {}^1\Sigma_g^+ \qquad \text{III} \qquad (26)$$

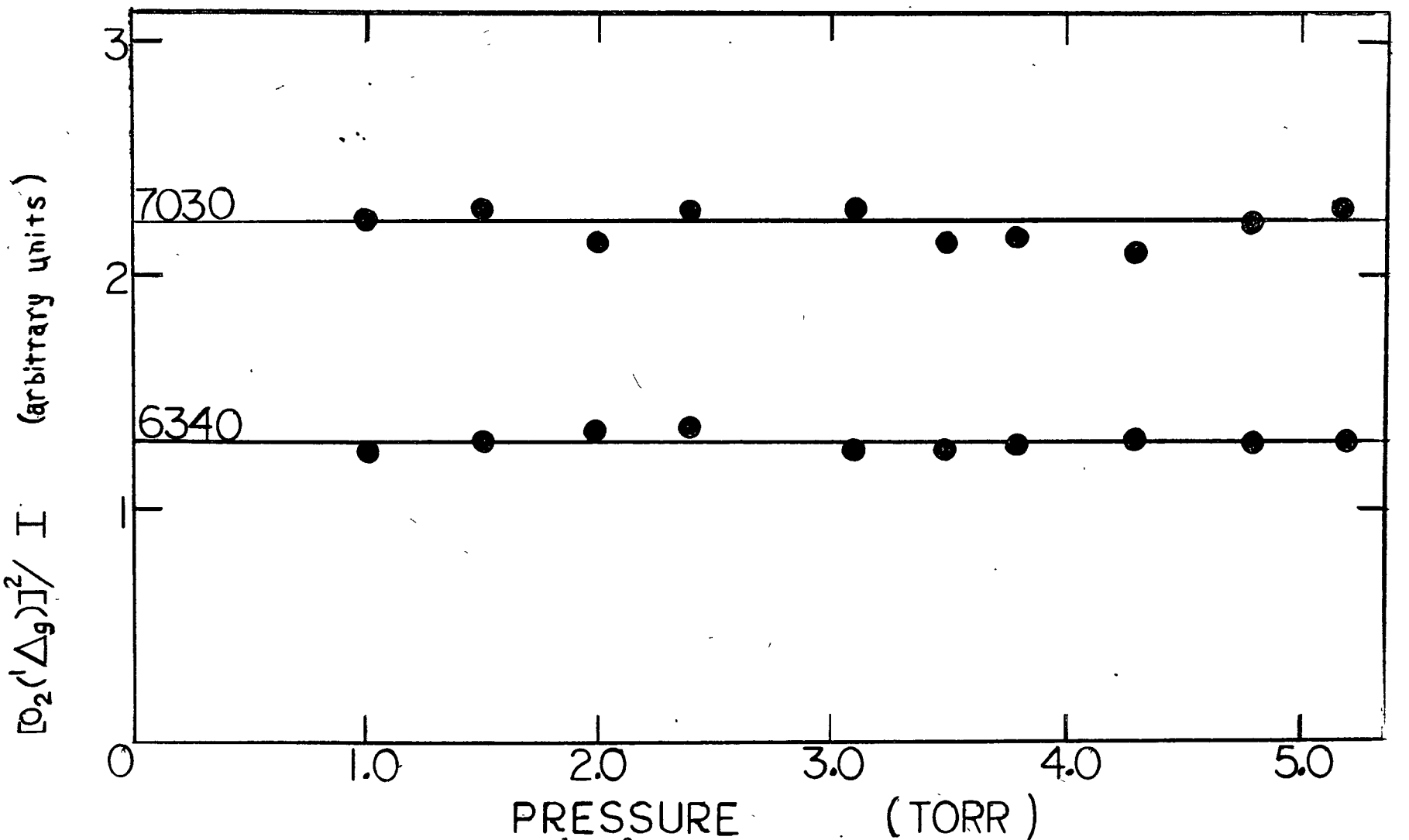

Figure 14: Plot of the ratio $[O_2(^1\Delta_g)]^2/I$ against pressure.

Their assumption that these bands were due to simultaneous electronic transitions in two O_2 molecules was supported by their observation that the frequencies of the band maxima could be represented approximately by the formula

$$v = mv_A + nv_B + v'w' \tag{27}$$

where v_A = frequency of the (0-0) $X^3\Sigma_g^- \rightarrow a^1\Delta_g$

v_B = frequency of the (0-0) $X^3\Sigma_g^- \rightarrow b^1\Sigma_g^+$

m and n = 0, 1, 2 $(m+n \leq 2)$

v' = 0,1,2,3, ...

w' = 1450 cm.$^{-1}$ (approximate value for w'_e = 1509 cm.$^{-1}$ and 1433 cm.$^{-1}$ in $^1\Delta_g$ and $^1\Sigma_g^+$ states, respectively) used by Ellis and Kneser.

Salow and Steiner (42), who studied the pressure dependence of the bands of series I, II and III, showed that they were independent of the pressure of added gases and depended on the square of the oxygen pressure, supporting Ellis and Kneser's assignments. Dianov-Klokov (43) who studied the temperature and pressure dependence of the absorption bands in liquid and highly compressed gaseous oxygen, claimed that the theory of simultaneous transitions successfully accounted for the position of all the absorption bands in the 12600 A to 3000 A region and was consistent with the observed intensity distribution and with the temperature coefficient of the intensities.

However, Kasha and Khan (44), at first questioned, the identification of the emitting species responsible for the red bands as $\{O_2(^1\Delta_g)\}_2$. Although Seliger (41) first observed the 6340 A band as the sole emission from the hydrogen peroxide-chlorine reaction, he

made no attempt at identifying it. Kasha and Khan (44), upon reinvestigating the hydrogen peroxide-chlorine reaction, observed both the 6340 A and 7030 A bands and tentatively assigned them to the (0-0) and (0-1) bands of the $b^1\Sigma_g^+ \rightarrow X^3\Sigma_g^-$ system, solvent shifted 2593 cm^{-1}. However, Browne and Ogryzlo (45), also studying the hydrogen peroxide-chlorine emission, showed that in addition to the 6340 A and 7030 A bands a third band at 5800 A could also be assigned to $\{O_2(^1\Delta_g)\}_2$, with bands at 12680 A and 10670 A assignable to the (0-0) and (0-1) transitions of the $a^1\Delta_g \rightarrow X^3\Sigma_g^-$ system and bands at 7619 A, 7708 A and 8645 A assignable to the (0-0), (1-1) and (0-1) transitions of the $b^1\Sigma_g^+ \rightarrow X^3\Sigma_g^-$ system. Kasha and Khan (46), now agreeing that $\{O_2(^1\Delta_g)\}_2$ is the emitter responsible for the 6340 A and 7030 A bands, have very recently observed a new emission band at 4780 A which they assigned to an $\{O_2(^1\Sigma_g^+)O_2(^1\Delta_g)\}$ double molecule. This observation raises the question as to why emission bands corresponding to $\{O_2(^1\Sigma_g^+)\}_2$ and $\{O_2(^1\Delta_g)O_2(^1\Sigma_g^+)\}$ were not observed in electrically discharged oxygen, since they are well known in the absorption spectra of high-pressure gaseous, liquid and solid oxygen. The answer appears to lie in the low concentration of $O_2(^1\Sigma_g^+)$ in electrically discharged oxygen; whereas on the average 6-8% of the total oxygen concentration is excited to the $^1\Delta_g$ state, less than 0.003% is found in the $^1\Sigma_g^+$ state.

The relationship between the intensity of the 6340 A band and the $O_2(^1\Delta_g)$ concentration has been the subject of several investigations. Table XXVI shows the results of these investigations and the methods used to measure the intensity of the 6340 A band and the $O_2(^1\Delta_g)$ concentration. Bader and Ogryzlo (47) and Finlay

Table XXVI

Methods Used to measure the Absolute Concentrations of $O_2(^1\Delta_g)$ and $O_2(^1\Sigma_g^+)$

experimenters	measurement of I(6340)	measurement of $[O_2(^1\Delta_g)]$	relationship
Bader & Ogryzlo (42)	RCA 7265 photomultiplier	isothermal calorimetric detector	$I(6340) \alpha [O_2(^1\Delta_g)]^2$
Finlay & Whitlow (43)	RCA 7265 photomultiplier	RCA PD 523 germanium photodiode	$I(6340) \alpha [O_2(^1\Delta_g)]^2$
Schiff et al (44)	RCA 7102 photomultiplier	RCA 7102 photomultiplier (liquid air cooled)	$I(6340) \alpha [O_2(^1\Delta_g)]$
present work	RCA 7265 photomultiplier	isothermal calorimetric detector	$I(6340) \alpha [O_2(^1\Delta_g)]^2$

and Whitlow (48), in agreement with the present work, find that the intensity of the 6340 A band is directly proportional to the square of the $O_2(^1\Delta_g)$ concentration, whereas Schiff et al (49) find a linear relationship between the intensity of the 6340 A band and the $O_2(^1\Delta_g)$ concentration.

Accurate measurement of the $O_2(^1\Delta_g)$ concentration by measuring the absolute emission intensity of the 12680 A band due to the (0-0) transition of the $a^1\Delta_g \rightarrow X^3\Sigma_g^-$ system is extremely difficult. The sensitivity of the RCA 7102 photomultiplier, used by Schiff et al, is less than 1% of its maximum sensitivity at 12680 A, with the result that the signal to noise ratio is very low. It is also questionable whether the photomultiplier response is linear in this region. The RCA PD 523 germanium photodiode, used by Finlay and Whitlow, has a very high signal to noise ratio with a maximum sensitivity in the range 8000-16000 A. Unfortunately the RCA PD 523 germanium photodiode is manufactured exclusively for the Defence Research Board of Canada and is not commercially available. Consequently, in the work of Bader and Ogryzlo and in the present work, the concentration of $O_2(^1\Delta_g)$ was measured with an isothermal calorimetric detector. The efficiency of the detector could be checked by seeing if there was any emission observable at 12680 A down stream from the detector or by inserting a second detector into the gas stream down stream from the first. In each case the detector was observed to destroy better than 95% of the $O_2(^1\Delta_g)$ present. Individual detector readings were reproducible with less than 2% deviation. Thus the discrepency between the results of Schiff et al and the present work could be explained by the method they used to measure the $O_2(^1\Delta_g)$ concentration.

Relationship between the $O_2(^1\Sigma_g^+)$ concentration and the $O_2(^1\Delta_g)$ concentration.

What is the relationship between the $O_2(^1\Sigma_g^+)$ concentration and the $O_2(^1\Delta_g)$ concentration? Figure 15 shows a plot of $\log\left\{\frac{[O_2(^1\Sigma_g^+)]_1}{[O_2(^1\Sigma_g^+)]_2}\right\}$ versus $\log\left\{\frac{[O_2(^1\Delta_g)]_1}{[O_2(^1\Delta_g)]_2}\right\}$ for the data of Table V.

A straight line is obtained and a least squares analysis of the data gives a slope of 2.04. This indicates that under steady conditions the $O_2(^1\Sigma_g^+)$ concentration is proportional to the square of the $O_2(^1\Delta_g)$ concentration. Figure 16 shows that a plot of $[O_2(^1\Delta_g)]^2/[O_2(^1\Sigma_g^+)]$ versus pressure for the data of Table VI gives a straight line with slope essentially equal to zero, indicating that, under steady state conditions, the relationship

$$[O_2(^1\Sigma_g^+)] \propto [O_2(^1\Delta_g)]^2 \tag{28}$$

is independent of the total pressure in the system.

The existence of this relationship between the $O_2(^1\Sigma_g^+)$ concentration and the $O_2(^1\Delta_g)$ concentration suggests that $O_2(^1\Sigma_g^+)$ is being formed in the energy pooling process

$$2\ O_2(^1\Delta_g) \rightarrow O_2(^1\Sigma_g^+) + O_2(^3\Sigma_g^-) \tag{29}$$

Since this relationship is independent of the total pressure in the system and is obeyed along the length of the reaction tube, either one of two mechanisms for the formation and removal of $O_2(^1\Sigma_g^+)$ can be operative.

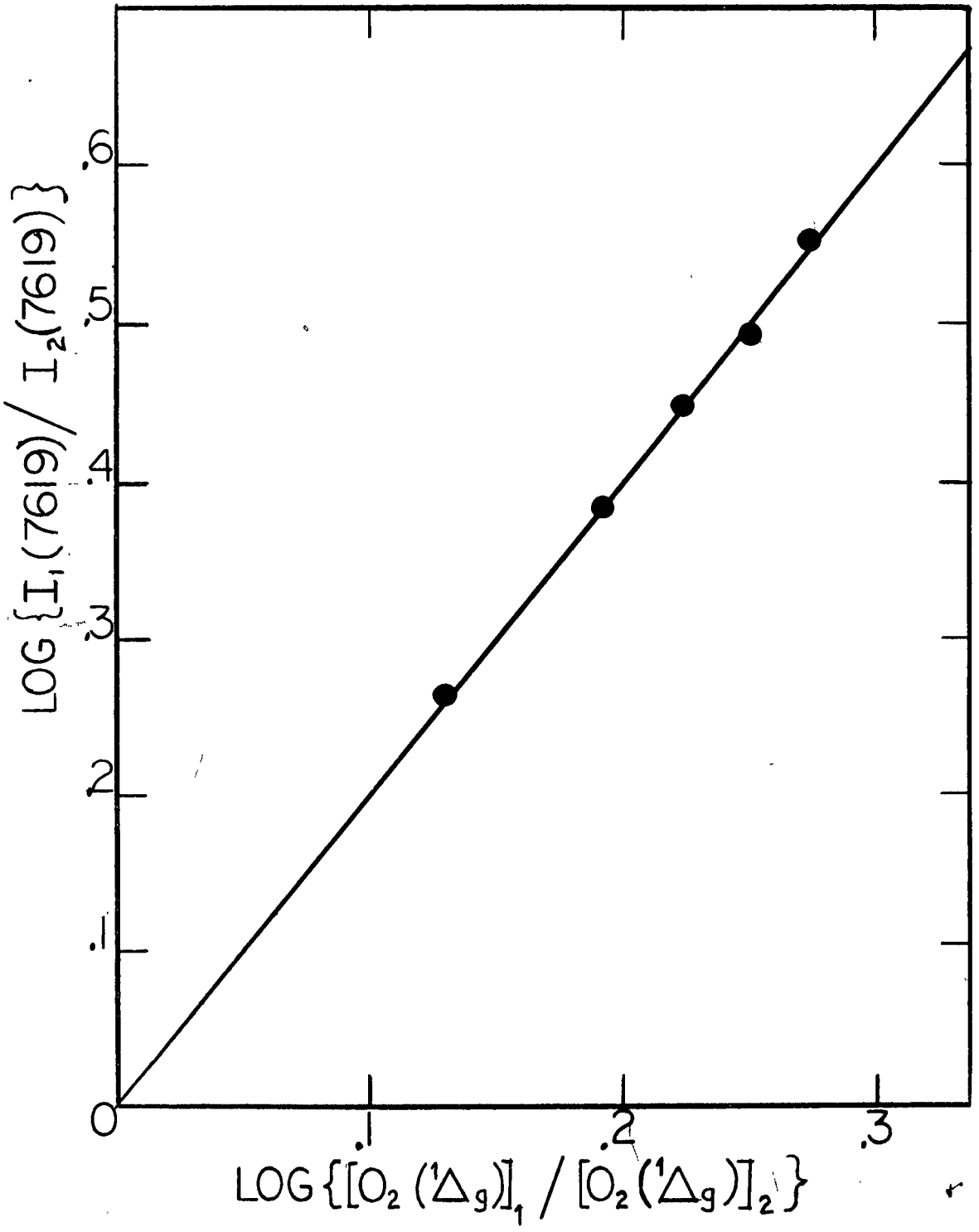

Figure 15: Plot of Log $(I(7619)_1/I(7619)_2)$ against Log $\{[O_g(^1\Delta_2)]_1/[O_2(^1\Delta_g)]_2\}$

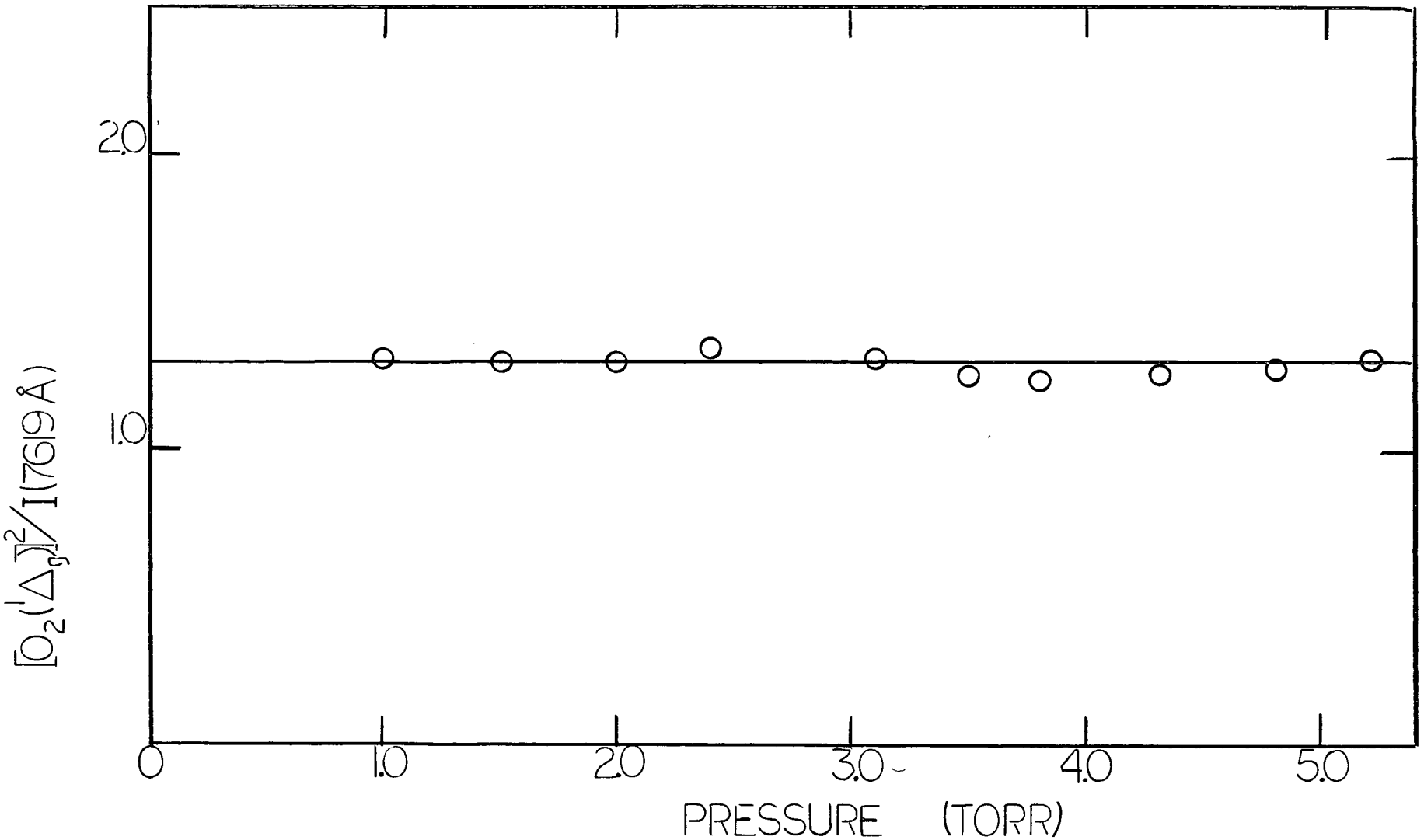

Figure 16: Plot of the ratio $[O_2(^1\Delta_g)]^2$ / I(7619) against pressure.

Mechanism A: $2\,O_2\,(^1\Delta_g) \xrightarrow{k_{29}} O_2(^1\Sigma_g^+) + O_2(^3\Sigma_g^-)$ (29)

$O_2\,(^1\Sigma_g^+) \xrightarrow{k_{30}} O_2(^3\Sigma_g^-)$ (30)

Mechanism B:

$O_2(^3\Sigma_g^-) + 2O_2(^1\Delta_g) \xrightarrow{k_{31}} O_2(^1\Sigma_g^+) + 2O_2(^3\Sigma_g^-)$ (31)

$O_2(^1\Sigma_g^+) + O_2(^3\Sigma_g^-) \xrightarrow{k_{32}} 2O_2(^3\Sigma_g^-)$ (32)

In both mechanisms the steady state concentration of $O_2(^1\Sigma_g^+)$ is proportional to the square of the $O_2(^1\Delta_g)$ concentration and independent of the total pressure in the system. Consequently, the ratio

$$\frac{[O_2(^1\Sigma_g^+)]}{[O_2(^1\Delta_g)]^2} = \frac{k_{29}}{k_{30}} \quad \text{or} \quad \frac{k_{31}}{k_{32}} \tag{33}$$

depending on whichever mechanism is operative, can be determined from the steady state concentrations of $O_2(^1\Sigma_g^+)$ and $O_2(^1\Delta_g)$.

In order to determine the formation and removal constants individually it is necessary to achieve a nonsteady state system. As is shown in figure 7 a nonsteady state system was achieved, which allowed the build-up of $O_2(^1\Sigma_g^+)$ to its steady state value to be measured. The two mechanisms for the formation and removal of $O_2(^1\Sigma_g^+)$ could now be analyzed as follows: If one uses the simplified symbols

$\Delta = O_2(^1\Delta_g)$

$\Sigma = O_2(^1\Sigma_g^+)$

$O_2 = O_2(^3\Sigma_g^-)$

then for mechanism A,

$$\frac{d[\Sigma]}{dt} = k_{29}[\Delta]^2 - k_{30}[\Sigma] \tag{34}$$

with steady state value

$$\frac{[\Sigma]_{ss}}{[\Delta]_{ss}^2} = \frac{k_{29}}{k_{30}} \tag{35}$$

Solving for k_{30} and substituting into equation 34 one gets

$$\frac{d[\Sigma]}{dt} = k_{29}[\Delta]^2 - k_{29}\frac{[\Sigma][\Delta]_{ss}^2}{[\Sigma]_{ss}} \tag{36}$$

Since the $O_2(^1\Delta_g)$ concentration remains almost constant along the reaction tube equation 36 reduces to an equation of the form

$$\frac{dx}{dt} = a-bx,$$

where (37)

$$x = [\Sigma] \qquad b = k_{29}\,[\Delta]_{ss}^2/[\Sigma]_{ss}$$

$$a = k_{29}[\Delta]^2$$

which upon integration gives

$$2.303\{[\Sigma]_{ss}/[\Delta]_{ss}^2\}\log\{[\Delta]^2-[\Delta]_{ss}^2[\Sigma]/[\Sigma]_{ss}\}=k_{29}t + \text{constant} \tag{38}$$

For mechanism B

$$\frac{d[\Sigma]}{dt} = k_{31}[\Delta]^2[O_2] - k_{32}[\Sigma][O_2] \tag{39}$$

with steady state value

$$\frac{[\Sigma]_{ss}}{[\Delta]^2_{ss}} = \frac{k_{31}}{k_{32}} \tag{40}$$

Solving for k_{32}, substituting into equation 39 and integrating one gets

$$\left\{2.303 \frac{[\Sigma]_{ss}}{[\Delta]^2_{ss}}\right\} \log \left\{[\Delta]^2 - \frac{[\Delta]^2_{ss}}{[\Sigma]_{ss}} [\Sigma]\right\} = k_{31}\, t[O_2] + \text{constant} \tag{41}$$

Comparing equations 39 and 41

$$k_{42} = k_{31}\, [O_2] = k_{29} \tag{42}$$

A plot of the left hand side of equation 38 or 41 against t will give a straight line with slope equal to k_{42}. Mechanism A will be operative if k_{42} equals a constant, independent of the total pressure in the system and mechanism B will be operative if $k_{42}/[O_2]$ equals a constant. Figure 17 shows such a plot for the data of Figure 7 and Table VII. In each case a straight line can be drawn through all the points. All the lines are parallel. The value of the slope k_{42} obtained for different total oxygen pressures are given in Table XXVII. These values are constant and independent of the total oxygen pressure in the system, indicating that k_{42} equals k_{29} and that mechanism A is operative. The values of k_{31}, on the other hand are not constant but decrease as the total pressure in the system increases. The average value of k_{29} equals 1.3×10^3 l.moles^{-1}sec.$^{-1}$ The value of k_{30}, calculated from the steady state value and k_{29}, is 64.7 sec.$^{-1}$ Therefore, mechanism A satisfactorily explains the formation and removal of $O_2(^1\Sigma^+_g)$ in the afterglow.

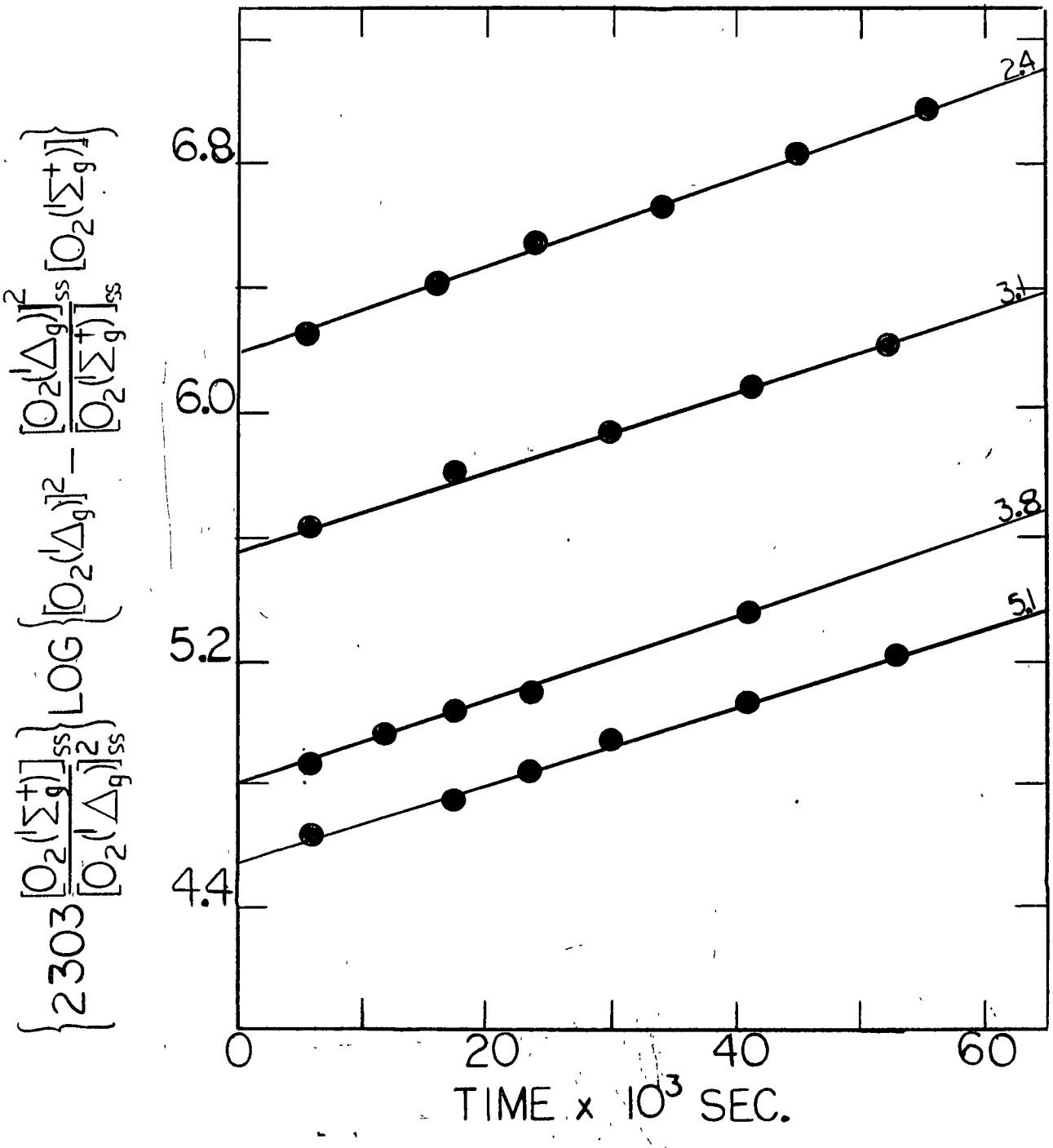

Figure 17:

Plot of $\left\{2.303 \frac{[O_2(^1\Sigma_g^+)]_{ss}}{[O_2(^1\Delta_g)]^2_{ss}}\right\} \log \left\{[O_2(^1\Delta_g)]^2 - \frac{[O_2(^1\Delta_g)]^2_{ss}}{[O_2(^1\Sigma_g^+)]_{ss}} [O_2(^1\Sigma_g^+)]\right\}$

against t. The values above each line indicate the total oxygen pressure in the system in mm. Hg.

Table XXVII

Rate Constants for the Formation of $O_2(^1\Sigma_g^+)$ by mechanism A and mechanism B

	mechanism A		mechanism B
P(torr)	$k_{29} \times 10^{-3}$ l. moles^{-1} sec.$^{-1}$	k_{30} sec.$^{-1}$	$k_{31} \times 10^{-6}$ l.^{2} moles^{-2} sec.$^{-1}$
2.4	1.40	68.3	10.8
3.1	1.30	60.5	7.75
3.8	1.37	66.0	6.66
5.1	1.30	64.0	4.70

In mechanism A, k_{30} represents the overall first order decay and has the form

$$k_{30} = k_{rad.} + k_{nonrad.} \tag{43}$$

The rate constant for the radiative decay of $O_2(^1\Sigma_g^+)$ according to the equation

$$O_2(^1\Sigma_g^+) \rightarrow O_2(^3\Sigma_g^-) + h\nu(7619) \tag{44}$$

has a value of 0.14 $sec.^{-1}$ (8) and for the radiative decay according to

$$O_2(^1\Sigma_g^+) \rightarrow O_2(^1\Delta_g) + h\nu(19080A) \tag{45}$$

a value of 2.5×10^{-3} sec.(31). Therefore, $k_{nonrad.}$, equals 64.6 $sec.^{-1}$

The rate constants k_{30} and $k_{nonrad.}$ are constant within experimental error over the pressure range (2.4 - 5.1 torr) in which the measurements were made. If one assumes that the nonradiative decay of $O_2(^1\Sigma_g^+)$ occurs on the walls of the reaction tube and that $k_{nonrad.}$ equals k_{wall}, the surface deactivation coefficient, ε, may be approximated as follows (52)

$$\varepsilon = \frac{\text{rate}}{\text{total number of collisions with the wall}} \tag{46}$$

$$= \frac{NVk_{wall}}{{}^1/_4\, N\bar{c}S}$$

$$= \frac{2r}{\bar{c}}\, k_{wall}$$

where N = number of molecules per volume element

V = volume = $\pi r^2 L$

S = surface area = $2\,\pi r\, L$

$\bar{c}$ = mean molecular velocity

r = radius of cylindrical reaction tube = 0.75 cm.

The surface deactivation coefficient which corresponds to the probability that $O_2(^1\Sigma_g^+)$ will undergo deactivation on collision with the walls, equals 0.0022, implying that deactivation occurs on approximately every 460 collisions with the wall.

Now, if the nonradiative decay of $O_2(^1\Sigma_g^+)$ occurs on the walls, it is possible that the rate of diffusion to the walls could be the rate controlling step and that k_{wall} would decrease as the pressure in the system increased. According to Benson (52), diffusion is the rate controlling step in wall deactivation if the time required for the molecule to diffuse to the walls, t_D, is greater than the average time for deactivation of a molecule by collision with the walls, t_{cw}. From the kinetic theory of Brownian motion, the time required for a molecule to diffuse a distance X is given approximately by

$$t_D \sim X^2/D \tag{47}$$

where D = diffusion coefficient

Now, the average time for deactivation of a molecule by collision with the walls is

$$t_{cw} = \frac{1}{k_{wall}} = \frac{2r}{\bar{c}\varepsilon} \tag{48}$$

For the average excited molecule in a vessel which is a distance X from the walls, diffusion will be the rate controlling step in wall deactivation if $t_D \geq t_{cw}$. Since the diffusion coefficient, D, is inversely proportional to the pressure

$$D = D_{ref.} P_{ref.}/P \tag{49}$$

the critical pressure P above which diffusion is important may be calculated from the relation

$$t_D \geq t_{cw} \tag{50}$$

$$\frac{X^2}{(D_{ref.} P_{ref.}/P} \geq \frac{2r}{\bar{c}\varepsilon} \tag{51}$$

which reduced to

$$P \geq \frac{2}{3} \frac{T_{ref.} P_{ref.}}{r\varepsilon} \tag{52}$$

if one assumes that $x \sim r_o$, the radius of the cylindrical reaction vessel and that $D_{ref.} \sim 1/3\ T_{ref.}\bar{c}$. The critical pressure is 2.36 torr. Consequently, over the pressure range at which the measurements were made (2.4 - 5.1 torr) diffusion control is important. However, since the pressure range is so small the effect of diffusion would be difficult to detect.

Young and Black (50), who were the first to measure the rate constant for reaction 29, obtained a larger value for k_{29} = $1.8 \times 10^{7 \pm 0.5}$ l.moles^{-1} sec.$^{-1}$, giving a difference of 10^4 in the two determinations. The major experimental difficulty is in separately evaluating the rate of formation $k_{form.}$ and the rate if loss k_{loss} for $O_2(^1\Sigma_g^+)$. In the present work this was possible but Young and Black were compelled to estimate k_{loss}. From the fact that the slopes of the Stern-Volmer plots of $I_o(7619)/I(7619)$ against partial pressure of added CO_2 or N_2 were independent of the total pressure in the system, they concluded that the decay of $O_2(^1\Sigma_g^+)$ was predominantly nondiffusion controlled. They then estimated k_{loss} from flow and geometry conditions to be 10, with a maximum error of 10. Consequently, their maximum value of k_{loss}

be 100, which is quite close to the value of k_{30} = 64.7 sec.$^{-1}$ obtained in the present work. Therefore, the difference in the two measurements is not due to an error in estimating k_{loss}.

This raises the question as to the accuracy of the measurements of the $O_2(^1\Sigma_g^+)$ and $O_2(^1\Delta_g)$ concentrations. In both cases the $O_2(^1\Sigma_g^+)$ concentration was measured by measuring the absolute emission intensity of the 7619 A band so that the error in both measurements would be approximately the same. Young and Black determined the $O_2(^1\Delta_g)$ concentration by measuring the absolute emission intensity of the 12680 A band whereas in the present work the $O_2(^1\Delta_g)$ concentration was measured with an isothermal calorimetric detector. Since the relative merits of these two methods have been discussed previously (page 76), it is sufficient to note that a larger error will occur in the absolute emission intensity measurement. An error of an order of magnitude in the measurement of the $O_2(^1\Delta_g)$ concentration will produce an error of 10^2 in k_{29}.

Additional evidence that Young and Black's value of k_{29} is large by several orders of magnitude comes from Bayes and Winer's (37) study of the oxidization of 2,3-dimethylbutene-2 by $O_2(^1\Delta_g)$. They showed that Young and Black's value of k_{29} would predict that the decay of $O_2(^1\Delta_g)$ in their system would be second order whereas the observed decay was pressure independent first order and it would predict an impossibly low $O_2(^1\Delta_g)$ concentration in view of the percentage of 2,3-dimethylbutene-2 oxidized. In fact Young and Black's value of k_{29} predicted that only 0.006 % (or 2 x 10^{13} molecules/cm.^{3} at a pressure of 7 torr) of the total oxygen concentration was excited to the $^1\Delta_g$ state, whereas, from the percentage hydrocarbon oxidized, Bayes and Winer estimated that the initial $^1\Delta_g$

concentration was closer to 10% (or 3×10^{15} molecules/cm.^{3}) of the total oxygen concentration. This value of 10% excitation to the $^1\Delta_g$ state is comparable to the 6-8% excitation found in the present study.

Decay of $O_2(^1\Delta_g)$

Since $O_2(^1\Delta_g)$ decays by the second order energy pooling processes

$$2\ O_2\ (^1\Delta_g) \rightarrow O_2\ (^1\Sigma_g^+) + O_2\ (^3\Sigma_g^-) \tag{29}$$

$$2\ O_2\ (^1\Delta_g) \rightarrow \{O_2(^3\Sigma_g^-)\}_2 \text{ or } \{2\ O_2(^3\Sigma_g^-)\} + h\nu(6340 \text{ and } 7030) \tag{53}$$

it is of interest to find out if these are the dominant modes of decay. The rate of deactivation of $O_2(^1\Delta_g)$ can be expressed as follows.

$$R = \frac{d[O_2(^1\Delta_g)]}{dt} = -k_{54}[O_2(^1\Delta_g)]^n \tag{54}$$

where k_{54} = the overall rate constant for the reaction

n = the order of the reaction with respect to $O_2(^1\Delta_g)$ concentration

According to the modified van't Hoff method (page 70) a plot of $\log(R_1/R_2)$ against $\log\{[O_2(^1\Delta_g)]_1/[O_2(^1\Delta_g)]_2\}$ will give a straight line with slope n. Figure 18 shows such a plot for the data of Table VIII. A least squares analysis of the data gives a slope of 1.02, indicating that the decay of $O_2(^1\Delta_g)$ is predominantly first order.

The observed first order rate constant k_{54} is now examined phenomenologically as

$$k = k_{1st} + k_{2nd}[O_2] \tag{55}$$

where k_{1st} = pseudo first order rate constant

k_{2nd} = pseudo second order rate constant

Figure 19 shows a plot of $k_{obs}(k_{54})$ against total oxygen pressure. A least squares analysis of the data gives an intercept, k_{1st}, equal to

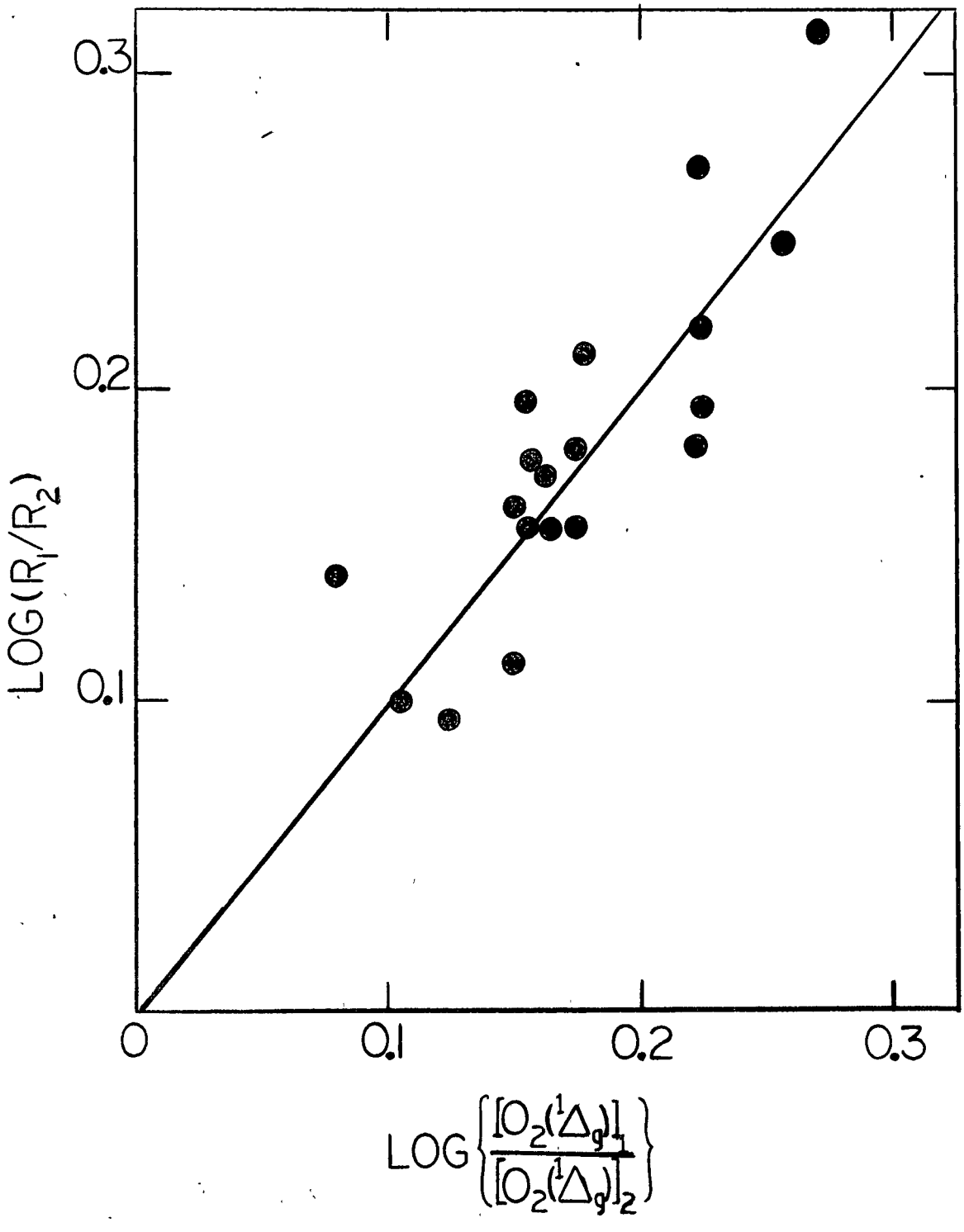

Figure 18: Plot of $\mathrm{Log}(R_1/R_2)$ against $\{[O_2(^1\Delta_g)]_1/[O_2(^1\Delta_g)]_2\}$

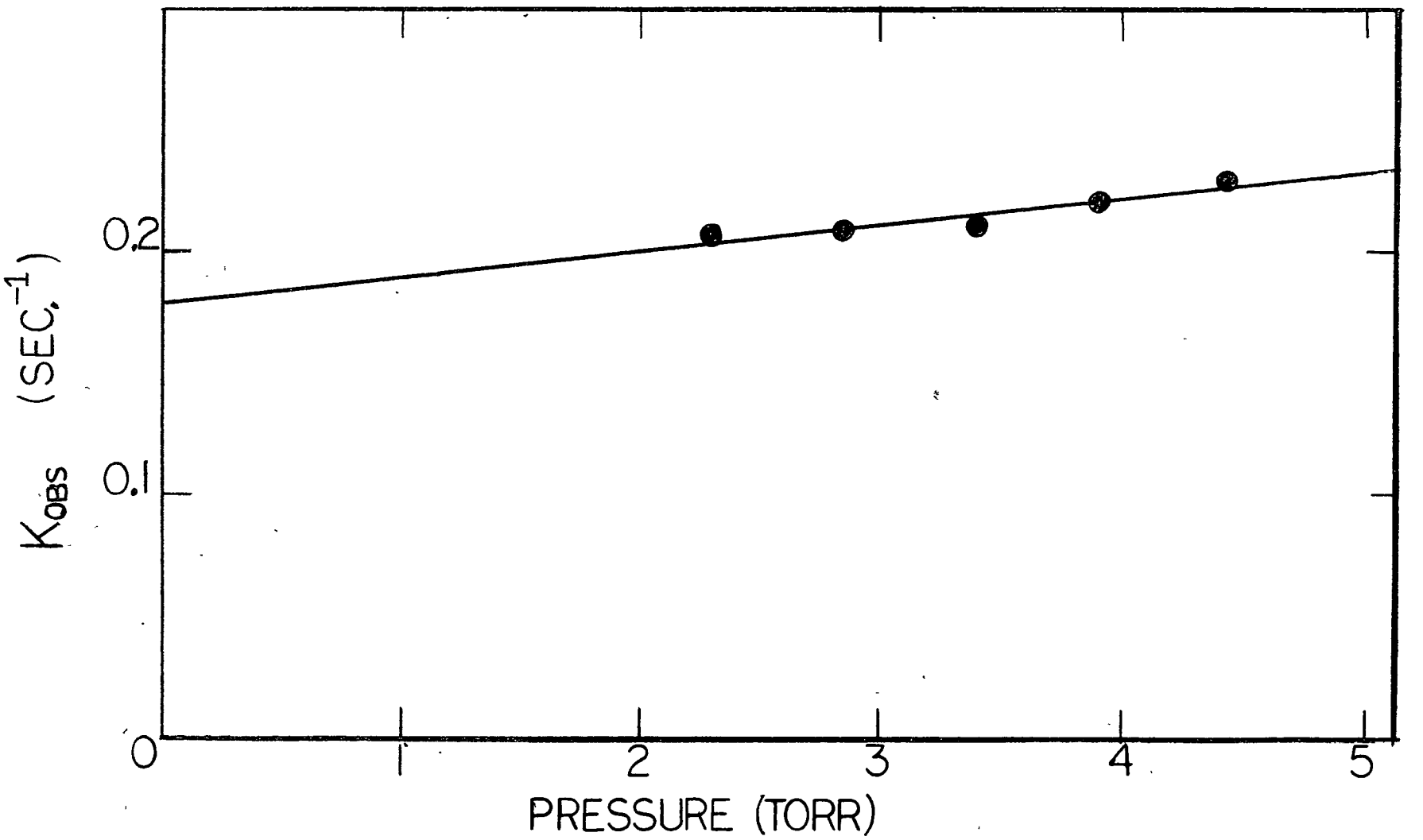

Figure 19: Plot of the observed first order decay constant, $k_{obs.}$, for $O_2(^1\Delta_g)$ against pressure.

0.178 sec.$^{-1}$ and a slope

$$k_{2nd} = (1.98 \pm 0.829) \times 10^2 \text{ l.moles}^{-1} \text{ sec.}^{-1}$$

where the limits on k_{2nd} are the probable error.

A resonable mechanism to explain the observed decay of $O_2(^1\Delta_g)$ would be

$$O_2(^1\Delta_g) \xrightarrow{k_{56}} O_2(^3\Sigma_g^-) + h\nu(12680 \text{ A}) \quad (56)$$

$$O_2(^1\Delta_g) \xrightarrow{k_{wall}} O_2(^3\Sigma_g^-) \quad (57)$$

$$O_2(^1\Delta_g) + O_2(^3\Sigma_g^-) \xrightarrow{k_{58}} 2O_2(^3\Sigma_g^-) \quad (58)$$

$$2O_2(^1\Delta_g) \rightarrow \{O_2(^3\Sigma_g^-)\}_2 (\text{or } 2O_2(^3\Sigma_g^-)) + h\nu(6340 \text{ and } 7030) \quad (53)$$

$$2O_2(^1\Delta_g) \xrightarrow{k_{29}} O_2(^1\Sigma_g^+) + O_2(^3\Sigma_g^-) \quad (29)$$

$$2O_2(^1\Delta_g) \rightarrow \text{products} \quad (59)$$

with $k_{obs} = k_{56} + k_{wall} + k_{58}[O_2] + (k_{53}+k_{29}+k_{59})[O_2(^1\Delta_g)]$ (60)

Decay by reaction 56 which would contribute to the pseudo first order decay constant is negligible since $k_{56} = 1.5 \times 10^{-4}$ sec.$^{-1}$ (6) in comparison with $k_{1st} = 0.178$ sec.$^{-1}$ Since the percentage $O_2(^1\Delta_g)$ concentration was observed to be approximately independent of the oxygen pressure, equation 60 reduced to

$$k_{obs} = k_{wall} + [k_{58} + c(k_{53}+k_{29}+k_{59})]\ [O_2] \quad (61)$$

where C=0.065 = average mole fraction of $O_2(^1\Delta_g)$. However, before one can equate k_{wall} to k_{1st}, one has to show that k_{wall} is independent of the total pressure in the system. Bayes and Winer (37), in their study of the oxidization of 2,3-dimethylbutene-2 by $O_2(^1\Delta_g)$ concluded that the first order decay of $O_2(^1\Delta_g)$ was pressure independent wall

decay.

If one assumes that k_{wall} is independent of the total pressure in the system and that, therefore, $k_{wall} = k_{1st} = 0.178$ sec.$^{-1}$, the surface deactivation coefficient, ε, calculated from equation 46, equals 10^{-5}. This value of ε implies that $O_2(^1\Delta_g)$ will undergo deactivation on every 10^5 wall collisions, in comparison with Bayes and Winer's observation that deactivation occured on every 3.5×10^4 wall collisions. The pressure above which diffusion to the walls will become important and above which k_{wall} will cease to be independent of the pressure, can be calculated from equation 52 with $r_o = 1.25$ cm., and $\varepsilon = 10^{-5}$. Since the critical pressure is 310 torr. and since the measurements under consideration were made in the pressure range 2.0 - 5.0 torr, the assumption that k_{wall} is independent of the pressure is justified and

$$k_{1st} = k_{wall} = 0.178 \text{ sec.}^{-1} \tag{62}$$

Therefore, the pseudo second order rate constant, k_{2nd} equals

$$k_{2nd} = [k_{58} + c(k_{53}+k_{29}+k_{59})] \tag{63}$$

Owing to the scatter of points, the slope of the least squares line of figure 19 is of little significance. Consequently, the least squares slope plus twice the probable error will be used as an upper limit for k_{2nd}

$$k_{2nd} \leq 3.635 \times 10^2 \text{ l. moles}^{-1}\text{sec.}^{-1} \tag{64}$$

Since $k_{53} = 0.28$ l.moles^{-1}sec.$^{-1}$ and $k_{29} = 1.3 \times 10^3$ l.moles^{-1}sec.$^{-1}$

if one assumes k_{59} equals zero the upper limit for k_{58} is 2.77×10^2 l. moles^{-1} sec.$^{-1}$ which corresponds to one deactivation in every 3.8×10^8 collisions with O_2 in comparison with Bayes and Winer's (37) observation of one deactivation in every 6.8×10^8 gas phase collisions.

On the other hand, if one assumes k_{58} equals zero, the maximum decay of $O_2(^1\Delta_g)$ by all processes second order in $O_2(^1\Delta_g)$ is 5.6×10^3 l. moles^{-1}sec.$^{-1}$ Since the sum of $k_{29} + k_{53}$ is $\sim 1.3 \times 10^3$ l. moles^{-1} sec.$^{-1}$, k_{59} has an upper limit of 4.3×10^3 l. moles^{-1}sec.$^{-1}$.

The Species $\{O_2(^1\Delta_g)\}_2$

The excited molecule, $O_2(^1\Delta_g)$ can undergo at least two energy pooling processes

$$2\ O_2(^1\Delta_g) \rightarrow 2\ O_2(^3\Sigma_g^-) \quad (\text{or}\{O_2(^3\Sigma_g^-)\}_2) + h\nu \tag{53}$$

$$2\ O_2(^1\Delta_g) \rightarrow O_2(^1\Sigma_g^+) + O_2(^3\Sigma_g^-) \tag{29}$$

The first process (reaction 46) implies a simultaneous electronic transition in two $O_2(^1\Delta_g)$ molecules, resulting in the energy of both molecules appearing as a single photon. The 6340 A band results when both molecules undergo a (0-0) transition in the $a^1\Delta_g \rightarrow X^3\Sigma_g^-$ system of O_2 while the 7030 A band appears when one molecule makes a (0-0) transition and the other a (0-1) transition.

The second process, the formation of $O_2(^1\Sigma_g^+)$, is analogous to the formation of an excited singlet and a ground state singlet by triplet-triplet annihilation in aromatic hydrocarbons (53) or to the familiar disproportionation reactions in oxidization-reduction processes. As in the case of triplet-triplet annihilations, the energy of both the initial excited molecules, here singlets, is pooled to produce an excited singlet of higher energy and a ground state molecule. Since in the case of triplet-triplet annihilation an excimer is first formed which can either emit directly or disproportionate (54), it is not unreasonable to expect that reactions 29 and 46 have a common intermediate, $\{O_2(^1\Delta_g)\}_2$, which can undergo one of the following processes

a) return to two unassociated $O_2(^1\Delta_g)$

b) undergo a simultaneous electronic transition with the emission of a single photon

c) disproportionate to form $O_2(^1\Sigma_g^+)$ and $O_2(^3\Sigma_g^-)$

What is the nature of this common $\{O_2(^1\Delta_g)\}_2$ intermediate? Is the intermediate a bound double molecule, a metastable double molecule or a colliding pair of molecules (55)? Some information on the nature of the intermediate can be obtained by considering how the intensity of the 6340 A band varies as the temperature of the gas is altered. Since the 6340 A band lies almost exactly at twice the excitation energy to two $O_2(^1\Delta_g)$ molecules (6343 A) and since the spacing between the 6340 A and the 7030 A bands is exactly the vibrational spacing in an isolated $O_2(^3\Sigma_g^-)$ molecule, it does not appear that the interaction between the two molecules can be very great. However, a weak interaction could still leave the band position unaltered but make the emitter a double molecule.

The temperature of the gas was altered between 221°K and 473°K while all other experimental variables remained constant. Since no change in the pressure in the reaction tube could be measured when the temperature was changed, the concentration of $O_2(^1\Delta_g)$ can be calculated with sufficient accuracy by the ideal gas law;

$C = P/RT$ where P = partial pressure of $O_2(^1\Delta_g)$ (65)

Mechanism A:

If the common intermediate, $\{O_2(^1\Delta_g)\}_2$ is either a metastable double molecule or a bound double molecule, one may write, using the

simplified symbols

$$O_2(^1\Delta_g) = \Delta$$

$$O_2(^1\Sigma_g^+) = \Sigma$$

$$O_2(^3\Sigma_g^-) = O_2$$

$$\Delta + \Delta + M \underset{k_{-66}}{\overset{k_{66}}{\rightleftharpoons}} \Delta_2 + M \qquad M = \text{any third body} \tag{66}$$

$$\Delta_2 \overset{k_{67}}{\rightarrow} \Sigma + O_2 \tag{67}$$

$$\Delta_2 \overset{k_{68}}{\rightarrow} 2\ O_2\ (\text{or } (O_2)_2) + h\nu \tag{68}$$

where k_{68} = the emission probability defined by

$$I = \frac{dh\nu}{dt} = k_{68}\ [\Delta_2] \tag{69}$$

I = 6340 A band intensity

Now, under steady state conditions

$$k_{66}\ [\Delta]^2[M] = k_{-66}\ [\Delta_2][M] + k_{67}\ [\Delta_2] + k_{68}[\Delta_2] \tag{70}$$

so that

$$[\Delta_2] = \frac{k_{66}\ [\Delta]^2[M]}{k_{-66}[M] + k_{67} + k_{68}} \tag{71}$$

Since it was observed that the rate of formation of $O_2(^1\Sigma_g^+)$ was independent of the total pressure in the system, that the ratio $\Delta^2/I(6340)$ was independent of the total pressure in the system and that the intensity of the 6340 A band was unaffected by the addition

of foreign gases if this mechanism is operative then it is necessary that

$$k_{-66}\,[M] \gg k_{67} + k_{68} \tag{72}$$

So that k_{obs} for the light emitting process equals

$$k_{obs} = k_{68} K_c \quad \text{independent of the concentration of M or the nature of M} \tag{73}$$

$$\text{where } Kc = k_{66}/k_{-66} = \frac{[\Delta_2]}{[\Delta]^2} \tag{74}$$

From equation 65, the Δ concentration is given by

$$[\Delta] = P/RT \quad \text{where P = partial pressure of } \Delta \tag{75}$$

so that equation (74) becomes

$$K_c = \frac{(I/k68)}{(P/RT)^2} = \frac{IR^2\,T^2}{k_{68}P^2} \tag{76}$$

$$\text{Now, } Kp = Kc(RT)^{\Delta v} \tag{77}$$

where Δv = number of moles of gaseous product minus the number of moles of gaseous reactant

$$\text{Therefore, } Kp = Kc(RT)^{-1} = \frac{IRT}{k_{68}\,P^2} \tag{78}$$

with the temperature dependence of Kp described by the usual thermodynamic relationship

$$\frac{d\ \ln Kp}{d\ (1/T)} = \frac{-\Delta H^\circ}{R} \tag{79}$$

or $Kp = \text{constant} \times e^{-\Delta H^\circ/(RT)}$ for constant ΔH° (80)

Substituting for Kp in equation 78 one gets

$$\frac{IRT}{k_{68}P^2} = \text{constant} \times e^{-\Delta H^\circ/RT} \tag{81}$$

which at constant P gives

$$IT = \text{constant} \times e^{-\Delta H^\circ/RT} \tag{82}$$

or

$$\log (IT) = \left(\frac{-\Delta H^\circ}{2.303\ R}\right)\frac{1}{T} + \text{constant} \tag{83}$$

Therefore, a plot of log (IT) versus 1/T will give a straight line with slope equal to $-\Delta H^\circ/(2.303R)$. Figure 20 shows the data of Table IX plotted in this way. A straight line is obtained, with a slope of 68.6 deg. ΔH° is then calculated to be -314 cal. mole^{-1}. Since

$$\Delta H = \Delta E + \Delta PV = \Delta E + \Delta v(RT) \tag{84}$$

ΔE, the change in internal energy on association (averaged over the temperature range 221°K to 473°K), which is approximately equal to minus the bond dissociation energy (averaged over the same temperature range), is +373 cal. mole^{-1}. Since a positive value is obtained for ΔE, the common intermediate, $\{O_2(^1\Delta_g)\}_2$, is not bound. The possibility however still exists that the common intermediate is a metastable double molecule. (55)

Mechanism B:

If, on the other hand the common intermediate, $\{O_2(^1\Delta_g)\}_2$, is simply a pair of colliding molecules, then the following processes must be considered

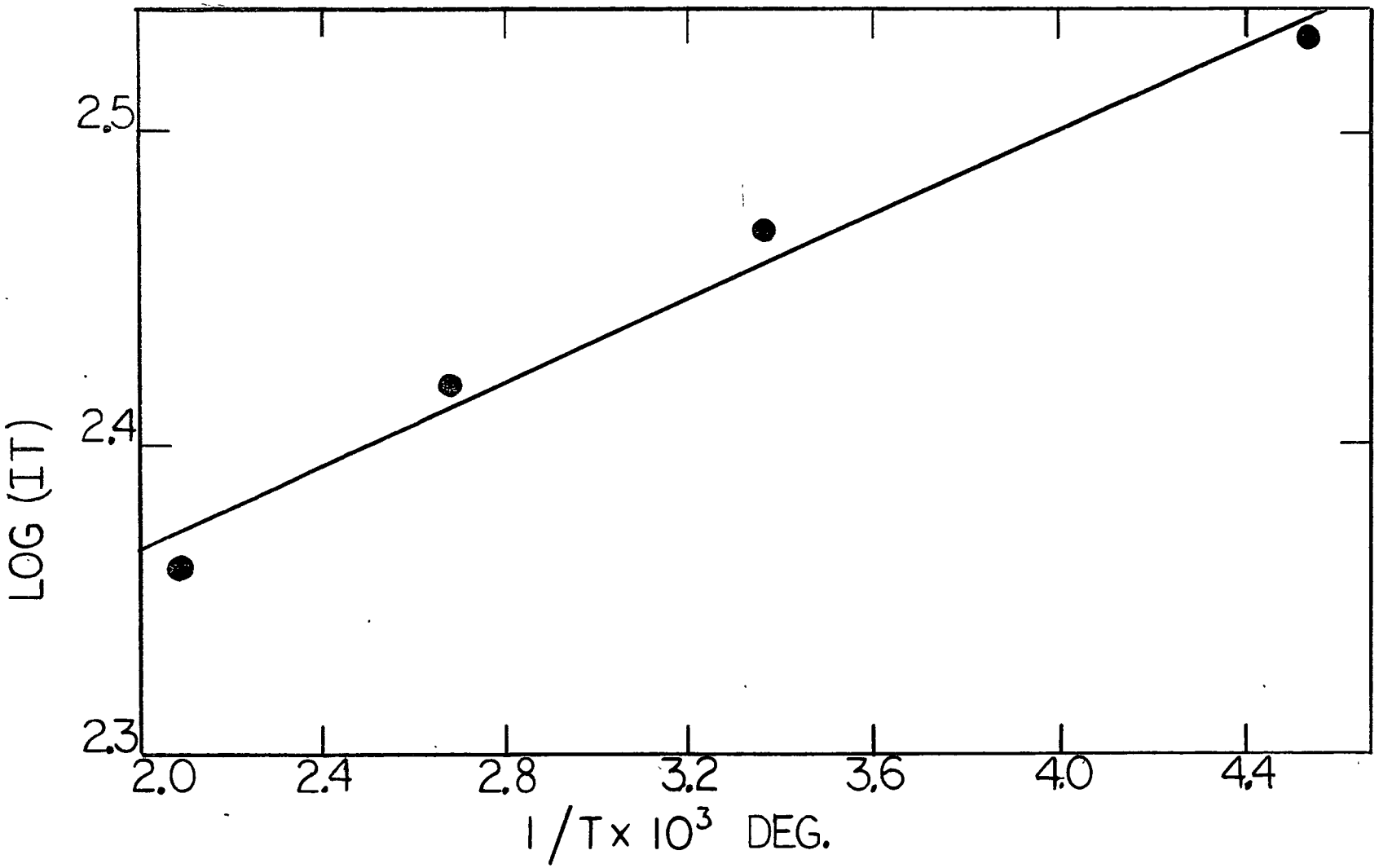

Figure 20: Plot of Log (IT) against 1/T.

$$\Delta + \Delta \underset{k_{-85}}{\overset{k_{85}}{\rightleftharpoons}} \Delta_2 \text{ (M is not involved)} \tag{85}$$

$$\Delta_2 \xrightarrow{k_{67}} \Sigma + O_2 \tag{67}$$

$$\Delta_2 \xrightarrow{k_{68}} 2\ O_2 \text{ (or } (O_2)_2) + h\nu \tag{68}$$

then k_{obs} for the light emitting process has the form

$$k_{obs} = \frac{k_{68}k_{85}}{k_{-85} + k_{67} + k_{68}} \tag{86}$$

Since the intensity of the 6340 A band is proportional to the square of the Δ concentration

$$I = k_{obs}\ \Delta^2 = k_{obs}\ \frac{P^2}{R^2T^2} \tag{87}$$

Assuming that the observed temperature dependence of light emission is the same as the temperature dependence of the collision number(†), k_{obs} will have a $T^{1/2}$ temperature dependence. Substituting for k_{obs} in equation 87 one gets

$$I = \text{constant } P^2/R^2T^{3/2} \tag{88}$$

$$\text{or } IT^{3/2} = \text{constant at constant P} \tag{89}$$

As shown in Table XXVIII, $IT^{3/2}$ is a constant within experimental error indicating that the emitting complex and hence the common

---

(†) A sufficient condition is that $(k_{-85} + k_{68} + k_{67})$ and k_{68} have the same temperature dependence.

intermediate could be a colliding pair of molecules if the assumed temperature dependence of k_{obs} is essentially correct.

The preceeding discussion can be summarized as follows:

mechanism A → $k_{-66}[M]$ is not $\gg (k_{67} + k_{68})$ → rejected on exp. evidence

mechanism A → $k_{-66}[M] \gg (k_{67} + k_{68})$ → bound double molecule rejected on exp. evidence

mechanism A → $k_{-66}[M] \gg (k_{67} + k_{68})$ → metastable double molecule consistent with exp. evidence

mechanism B → colliding pair of molecules consistent with exp. evidence.

Table XXVIII

Value of log (IT) and $IT^{3/2}$

T(°K)	IT	log(IT)	$IT^{3/2}$
221	340	2.53	5.07×10^3
296	296	2.47	5.10
373	262	2.42	5.06
473	236	2.37	5.12

Consequently , on the basis of available experimental evidence, the common intermediate $\{O_2(^1\Delta_g)\}_2$ which can either emit at 6340 A or 7030 A or disproportionate to form $O_2(^1\Sigma_g^+)$ can be either a metastable double molecule or a colliding pair of molecules but not a bound double molecule.

Considering the two processes, light emission and disproportionation, the ratio of the observed rate constants for the case of the metastable double molecule is

$$R = \frac{k_{obs}\text{(light emission)}}{k_{obs}\text{ (disproportionation)}} = \frac{k_{53}}{k_{29}} = \frac{k_{68}}{k_{67}}\ \frac{K_c}{K_c} = \frac{k_{68}}{k_{67}} \tag{91}$$

and for the case of the colliding pair of molecules the ratio is

$$R = \frac{k_{obs}\text{(light emission)}}{k_{obs}\text{(disproportionation)}} = \frac{(k_{68}\ k_{85})/(k_{-85}+k_{68}+k_{67})}{(k_{67}\ k_{85})/(k_{-85}+k_{68}+k_{67})} = \frac{k_{68}}{k_{67}} \tag{92}$$

For either intermediate the same ratio of observed rate constants for light emission and for disproportionation is obtained, indicating that the rate controlling steps for the two processes are the light emitting step or the disproportionation step. In the present work k_{29} (k_{obs} for disproportionation) was found to equal 1.3×10^3 l.moles^{-1}sec.$^{-1}$ while Browne (51) found k_{53}(k_{obs} for light emission) to equal 0.28 l.mole^{-1}sec.$^{-1}$, indicating that disproportation is 4.8×10^3 more probable than light emission. A possible explanation is that light emission requires the common intermediate to have a specific orientation which is not required for disproportionation.

Bader and Ogryzlo (47), on the other hand found $(O_2(^1\Delta_g))_2$ to be a bound double molecule with $-\Delta E^\circ$ equal to 600 cal. mole^{-1}. This discrepency can be explained by considering the apparatus used by Bader and Ogryzlo to study the effect of altering the temperature on the intensity of the 6340 A band. Since in these experiments it was essential to view only a very short region of the gas stream so that no appreciable decay of the excited molecules occurred in the viewing region, Bader and Ogryzlo shortened the effective length of their reaction tube by inserting a piece of cobalt wire a few centimeters from the viewing window. Cobalt wire very effectively removes $O_2(^1\Delta_g)$ at room temperature, but it was found in this work that, as the temperature of the gas stream is lowered, the efficiency of the cobalt wire decreased markedly so that $O_2(^1\Delta_g)$ is not being completely removed at the lower temperature. Therefore, Bader and Ogryzlo obtained an apparent very large increase in emission intensity of the 6340 A band as the temperature of the gas was lowered, which they interpreted as indicating that the emitting species was a bound double molecule.

Reactions of $O_2(^1\Sigma_g^+)$

The rate of deactivation of $O_2(^1\Sigma_g^+)$ by added foreign gases can be calculated as follows. If one uses the simplified symbols

$$O_2(^1\Sigma_g^+) = \Sigma$$

$$O_2(^1\Delta_g) = \Delta$$

$$O_2(^3\Sigma_g^-) = O_2$$

In a pure oxygen system the formation and removal of $O_2(^1\Sigma_g^+)$ are by

$$2\,\Delta \xrightarrow{k_{29}} \Sigma + O_2 \tag{29}$$

$$\Sigma \xrightarrow{k_{30}} O_2 \tag{30}$$

When a quencher is added to the system, $O_2(^1\Sigma_g^+)$ is also removed by

$$\Sigma + Q \rightarrow O_2 + Q \tag{93}$$

Under steady state conditions in the pure oxygen system

$$k_{29}[\Delta]_o^2 = k_{30}[\Sigma]_o \tag{94}$$

while in the presence of the added quenching gas

$$k_{29}[\Delta]^2 = k_{30}[\Sigma] + k_{93}[\Sigma][Q] \tag{95}$$

Dividing equation 95 by equation 94, one gets

$$\frac{[\Delta]^2}{[\Delta]_o^2} = \frac{[\Sigma]}{[\Sigma]_o}\left\{1 + \frac{k_{93}[Q]}{k_{30}}\right\} \tag{96}$$

Since none of the quenching gases used in this set of experiments affected the $O_2(^1\Delta_g)$ concentration, $[\Delta] = [\Delta]_o$ so that equation 96 reduces to the

standard Stern-Volmer relationship

$$\frac{I_o(7619)}{I(7619)} = \frac{[\Sigma]_o}{[\Sigma]} = 1 + \frac{k_{93}}{k_{30}}[Q] \qquad (97)$$

A plot of $I_o(7619)/I(7619)$ against quencher concentration, [Q], will give a straight line with intercept I and slope k_{93}/k_{30}. Figure 21 shows a series of these plots for different added foreign gases as calculated from the data of Tables XX-XXIV. All the plots obey the Stern-Volmer relationship. From the value of $k_{30} = 64.7\ sec^{-1}$. and the slopes k_{93}/k_{30}, k_{93} can be evaluated for the various added foreigh gas. Table XXIX shows the values of k_{93} (k_{quench}) obtained.

The excited molecule $O_2(^1\Sigma_g^+)$ can be quenched either to the ground state $O_2(^3\Sigma_g^-)$ to the first excited state, $O_2(^1\Delta_g)$. Experimentally, it could not be determined which reaction occurred. This is because the $O_2(^1\Sigma_g^+)$ concentration is only 10^{-4} of the $O_2(^1\Delta_g)$ concentration, so that even if all the $O_2(^1\Sigma_g^+)$ was quenched to the $^1\Delta_g$ state, the increase in $O_2(^1\Delta_g)$ concentration would be so small that it could not be detected. Throughout the quenching process the $O_2(^1\Delta_g)$ concentration remained unaltered.

Several attempts were made to correlate quenching efficiency with some known molecular parameter.

Almost immediately, an emperical correlation between quenching efficiency and boiling point was observed. Figure 23 shows a plot of log $k_{quencher}$ against boiling point. With the exception of chloroform, the correlation between boiling point and quenching efficiency is quite good, with the coefficient of linear correlation having a value of 0.92. However, a similar emperical correlation was observed by Russell and Simons (56)

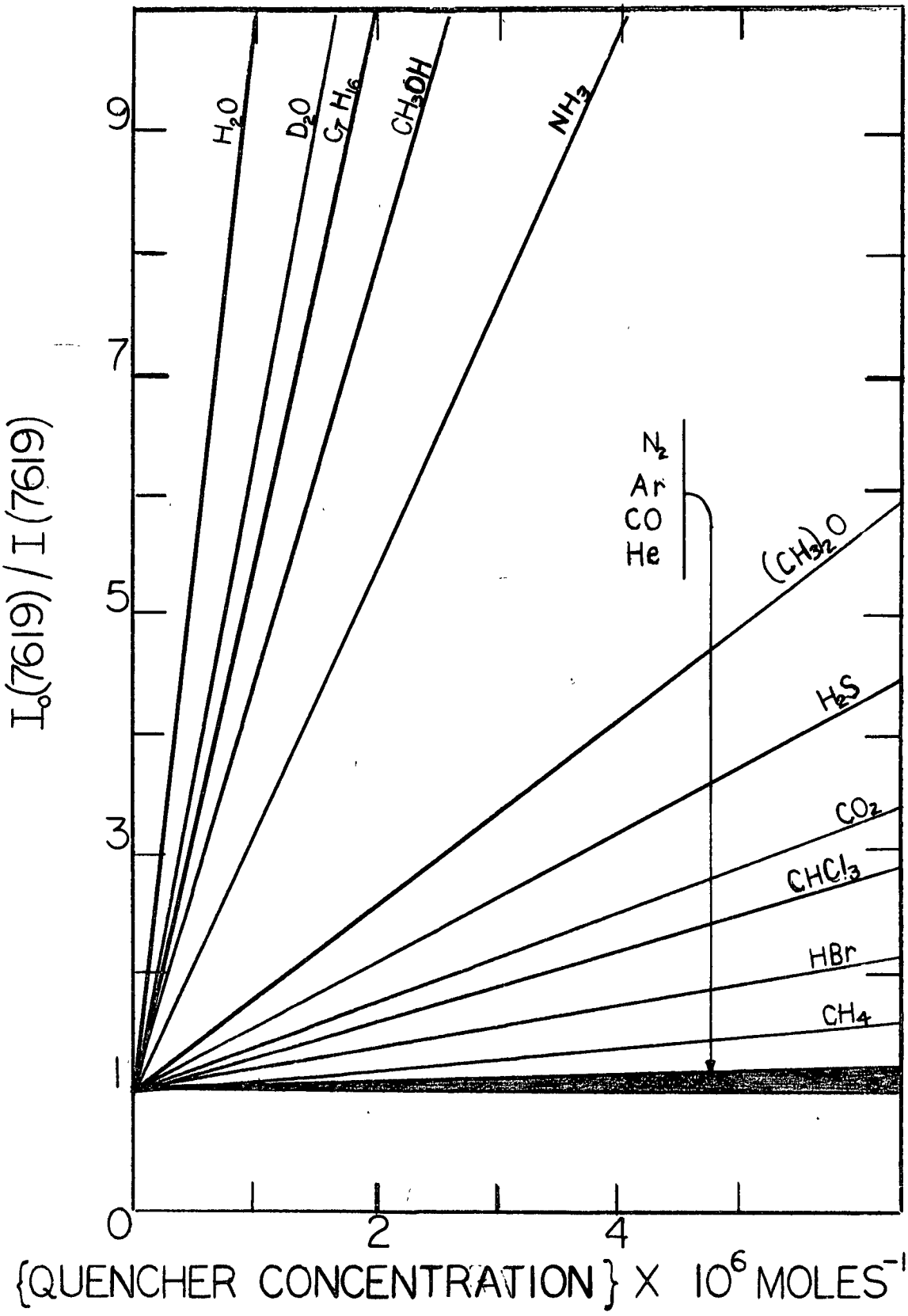

Figure 21: Plot of $I_0(7619)/I(7619)$ against quencher concentration where I_0/I equals the steady state ratio at the same distance along the reaction tube.

Table XXIX

Rate Constants for $O_2(^1\Sigma_g^+)$ quenching.

Added gas	Kqencher/Kwall	Kquencher (l/moles sec)
H_2O	8.07×10^6	5.3×10^8
D_2O	6.2×10^6	4.1×10^8
nC_7H_{16}	4.6×10^6	3.0×10^8
CH_3OH	3.65×10^6	2.4×10^8
NH_3	2.2×10^6	1.5×10^8
$(CH_3)_2O$	7.8×10^5	5.15×10^7
H_2S	5.5×10^5	3.6×10^7
CO_2	3.4×10^5	2.3×10^7
$CHCl_3$	3.07×10^5	2.0×10^7
HBr	1.9×10^5	1.25×10^7
CH_4	1.0×10^5	6.6×10^6
N_2	3.1×10^5	2.1×10^6
Ar	2.8×10^5	1.9×10^6
CO	2.2×10^5	1.5×10^6
He	0.9×10^4	0.6×10^6

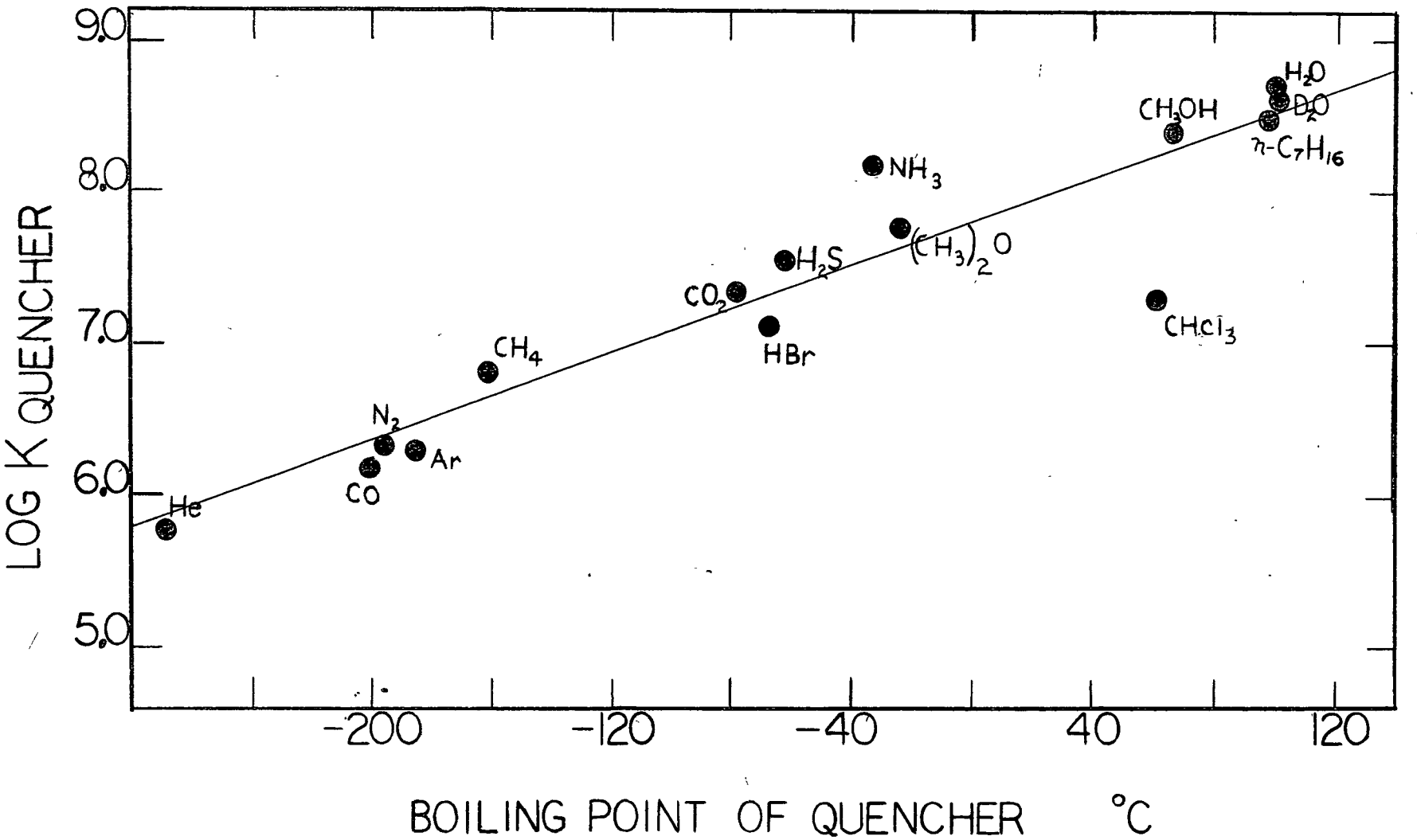

Figure 22:

Plot of Log $k_{quencher}$ against boiling point of the quencher.

between boiling point and third body efficiency an iodine atom recombination. Figure 23 shows a plot of log $k_{quencher}$ against log $k_{third\ body}$. A very high correlation (r = 0.95) exists between the efficiency of an added gas at quenching $O_2(^1\Sigma_g^+)$ and its efficiency at promoting iodine atom recombination. This is to be expected because both effects correlate with the boiling point of the added gas. However, molecular oxygen which is quite effective at promoting iodine atom recombination does not quench $O_2(^1\Sigma_g^+)$. Consequently, a more meaningful correlation was sought.

It is well known that energy transfer can occur by a resonance mechanism if there is an excited state of the acceptor, in this case the quencher, which requires exactly the same energy as is available in the donor, $O_2(^1\Sigma_g^+)$. (57). Exact resonance will occur if the quencher has an excited state requiring 13,120 cm.$^{-1}$ in the case of $^1\Sigma_g^+ \rightarrow {}^3\Sigma_g^-$ quenching or 5,238 cm.$^{-1}$ in the case of $^1\Sigma_g^+ \rightarrow {}^1\Delta_g$ quenching. None of the quenchers tried had a low lying electronic state at either 5,238 cm.$^{-1}$ or 13,120 cm.$^{-1}$ above the ground state, in all cases the first known excited state lie at considerably higher energy. Consequently, for a resonance mechanism to be operative, energy transfer must occur, of necessity, to a vibrationally excited level of the ground state. In the case of the majority of quenchers, this means that a number of vibrational modes would have to be excited simultaneously in order to achieve a resonance condition.

For the quenchers,(†), water, deuterium oxide, ammonia, hydrogen sulfide, carbon dioxide chloroform and methane, a linear combination of the

---

(†) The fundamental vibrational frequencies of these quenchers are well known. (58)

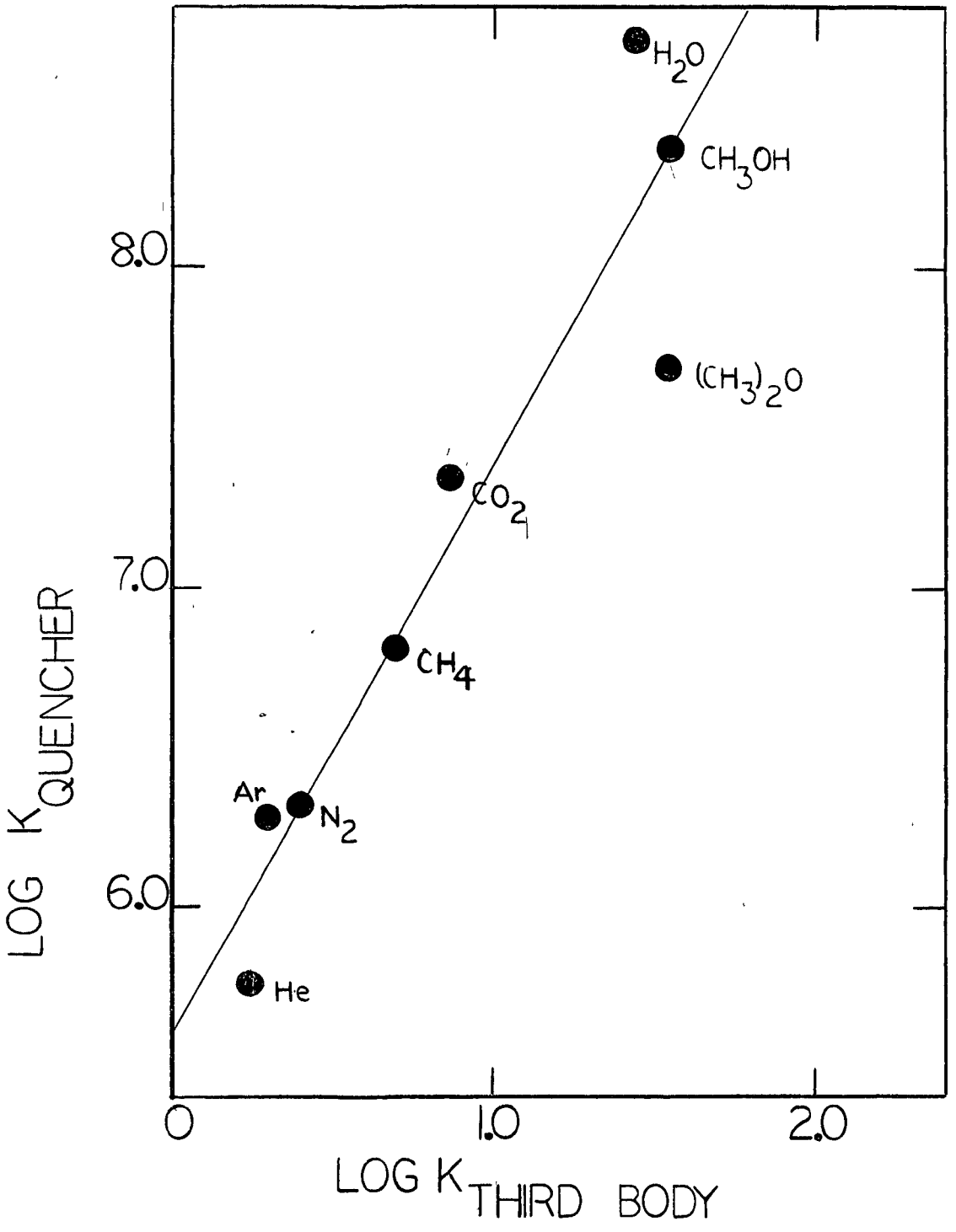

Figure 23: Plot of Log $k_{quencher}$ against log $k_{third\ body}$

fundamental vibrational modes of the form

$$v = a_1v_1 + a_2v_2 + a_3v_3 + \ldots + a_nv_n \tag{98}$$

where $v_1, v_2 \ldots v_n$ are the fundamental vibrational frequencies of the quencher

$a_1, a_2 \ldots a_n$ are integers

was calculated. A suitable linear combination of vibrational modes requiring approximately 5238 cm^{-1} could be found for a 1 the quenchers tried, (Table XXX). Similarily, a suitable linear combination of vibrational modes requiring 13,120 cm^{-1} could be found for all the quenchers, with the exception of water, the most efficient quencher tried. Consequently, it appears that quenching efficiency cannot be attributed to a resonance condition existing between $O_2(^1\Sigma_g^+)$ and the quencher.

Table XXX

Linear Combinations of Vibrational Modes of the Quenchers Approximating 5,238 cm.$^{-1}$ or 13120 cm.$^{-1}$

quencher[a]	linear combination	frequency cm^{-1}	ΔE cm^{-1}	linear combination	frequency cm^{-1}	ΔE cm^{-1}
H_2O	v_1+v_2	5247	9	v_2+v_3	12,863	257
D_2O	$2v_2+v_3$	5135	103	$3v_1+2v_2+v_3$	13,143	23
NH_3	v_1+2v_2	5237	1	$3v_2+3v_3$	13,092	28
H_2S	v_1+2v_2	5191	47	$4v_1+v_3$	13,128	8
CO_2	$4v_1$	5280	42	$2v_2+5v_3$	13,086	34
$CHCl_3$	$v_1+v_2+2v_5$	5230	8	$4v_1+v_2+v_3$	13,163	43
CH_4	$4v_4$	5224	14	$3v_1+2v_2+v_4$	13,100	20

a arrange in decreasing order of k_{93}

It can be noted, however, that polyatomic molecules are on the average more effective quenchers of $O_2(^1\Sigma_g^+)$ than diatomic molecules, that water, which known to be a very efficient quencher of vibrationally excited oxygen (59), is observed to be the most efficient quencher tried and that, with the exception of n-heptane, polar molecules were more efficient quenchers than nonpolar molecules.

Since polar molecules were observed to be more efficient quenchers than nonpolar molecules, it is reasonable to expect that a correlation will exist between quenching efficiency and the magnitude of the intermolecular potential between $O_2(^1\Sigma_g^+)$ and the quencher. The magnitude of the intermolecular potential between two molecules is determined in part by the depth of the potential well, e_{ij}, formed when two molecules come together along an attractive curve. For a polar and nonpolar molecule, e_{ij} can be calculated as follows (60):

$$e_{ij} = \sqrt{e_i e_j}\ \zeta^2 \tag{99}$$

$$\zeta = (1 + \frac{1}{4}\alpha_n^* \mu_p^{*2} \sqrt{e_p/e_n}) = (1 + \frac{1}{2} 2\alpha_n^* t_p^* \sqrt{e_p/e_n}) \tag{100}$$

where e_n = Leonnard-Jones potential (†) parameter for the nonpolar molecule

e_p = Stockmayer potential (†) parameter for the polar molecule

α_n^* = reduced polarizability of the nonpolar molecule = α_n/σ_n^3

μ_p^* = reduced dipole moment of the polar molecule = $\mu_p/\sqrt{e_p\sigma_p^3}$

(†) The values for the required parameters were obtained from reference (60).

μ_p = dipole moment of the polar molecule

$t_p^* = \mu_p^*/\sqrt{8}$

while for two nonpolar molecules e_{ij} can be approximated by (101)

$$e_{ij} = \sqrt{e_i e_j}$$

where e_i, e_j = Leonnard-Jones potential parameters for the two nonpolar molecules

The values of e_{ij} calculated for the various quenchers is shown in Table XXXI. Figure 23 shows a plot of log $k_{quencher}$ against e_{ij}/k, where k is Boltzman's constant. The correlation between e_{ij}/k and quenching efficiency is fairly good with the exception of n-heptane. The linear coefficient of correlation is 0.9 indicating a high degree of correlation. Consequently, it appears that the magnitude of the intermolecular potential between $O_2(^1\Sigma_g^+)$ and the quencher is a major factor determining quenching efficiency in the present system.

Table XXXI

Values of e_{ij}, the intermolecular potential between $O_2(^1\Sigma_g^+)$ and the quencher.

quencher[a]	e_{ij}/k
H_2O	311
C_7H_{16}	179
CH_3OH	224
NH_3	206
$(CH_3)_2O$	221
H_2S	200
CO_2	147
$CHCl_3$	178
CH_4	124
N_2	102
Ar	118
CO	112
He	10.7

a arranged in decreasing order of k_{93}

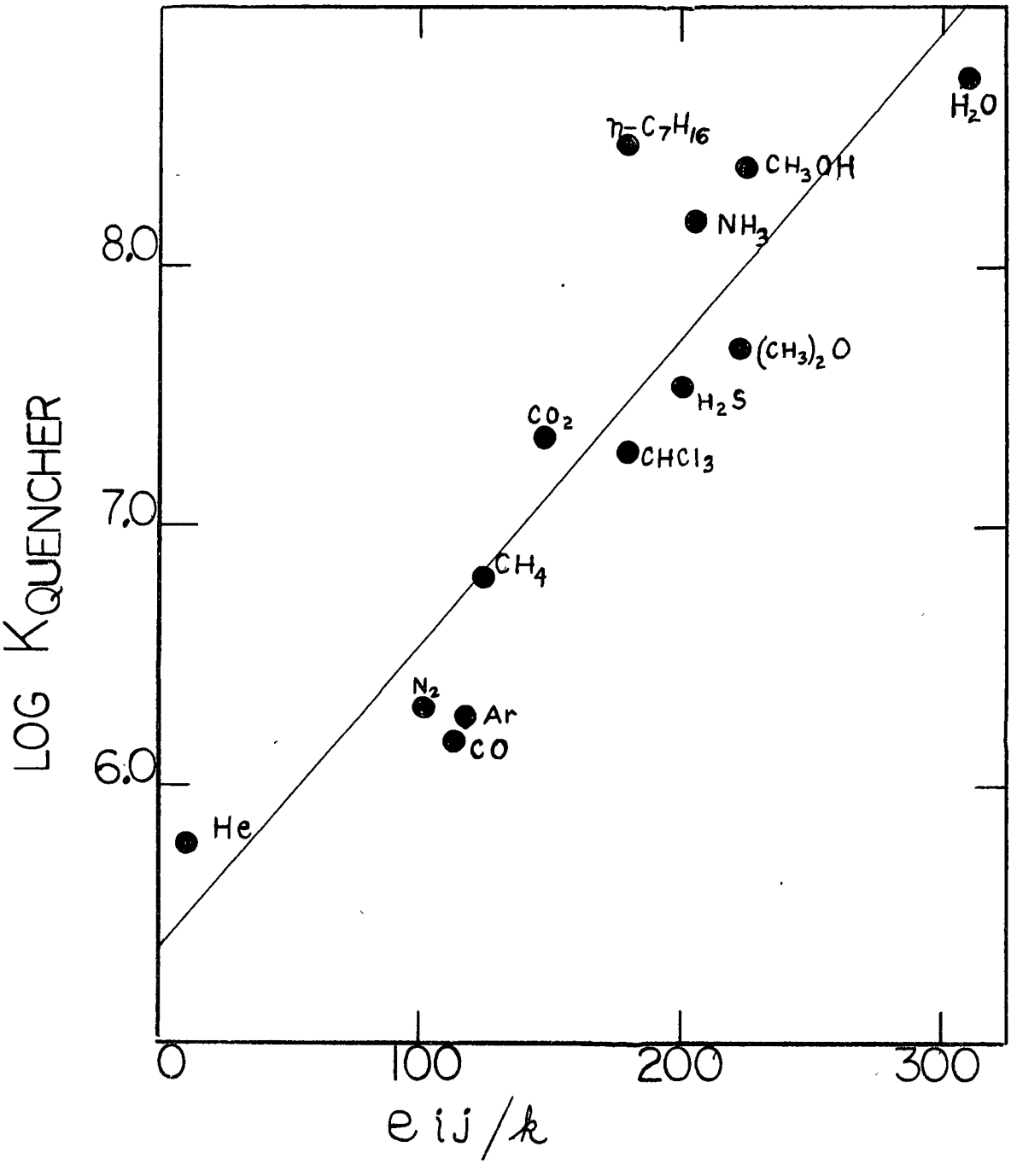

Figure 24:

Plot of Log $k_{quencher}$ against e_{ij}/k, the magnitude of the intermolecular potential between $O_2(^1\Sigma_g^+)$ and the quencher.

Energy Pooling Processes.

When nitrogen dioxide is introduced into an atom-free stream of excited molecules a pale yellow glow, extending from 4800 A into the infrared is observed. This emission which is due to an excited state of nitrogen dioxide, NO_2^*, is dependent on the presence of $O_2(^1\Sigma_g^+)$ for when the $O_2(^1\Sigma_g^+)$ is quenched by the addition of water, the emission is also quenched. Since the emission begins at 4800 A which corresponds to the sum of the excitation energies of $O_2(^1\Sigma_g^+)$ and $O_2(^1\Delta_g)$ (4761 A) it is not unreasonable to expect that both species are involved in the energy pooling process resulting in NO_2^*.

Assuming that both $O_2(^1\Sigma_g^+)$ and $O_2(^1\Delta_g)$ are involved in the energy pooling process, the intensity of the NO_2^* emission can be expressed as follows:

$$I(NO_2^*) = k[O_2(^1\Delta_g)]^n[O_2(^1\Sigma_g^+)]^m \tag{102}$$

where k = emission probability

n = order of the reaction with respect to $O_2(^1\Delta_g)$ concentration

m = order of the reaction with respect to $O_2(^1\Sigma_g^+)$ concentration

Since for a fixed quencher concentration, the $O_2(^1\Sigma_g^+)$ concentration is proportional to the square of the $O_2(^1\Delta_g)$ concentration, equation 102 reduced to

$$I(NO_2^*) = k[O_2(^1\Delta_g)]^P \tag{103}$$

where p = 2m + n

Therefore, a plot of log $\{(I_1(NO_2^*))/(I_2(NO_2^*))\}$ versus log $\{[O_2(^1\Delta_g)]_1/[O_2(^1\Delta_g)]_2\}$ will give a straight line with slope P. Figure 24 shows such a plot for the data of Table XXV. A straight line is

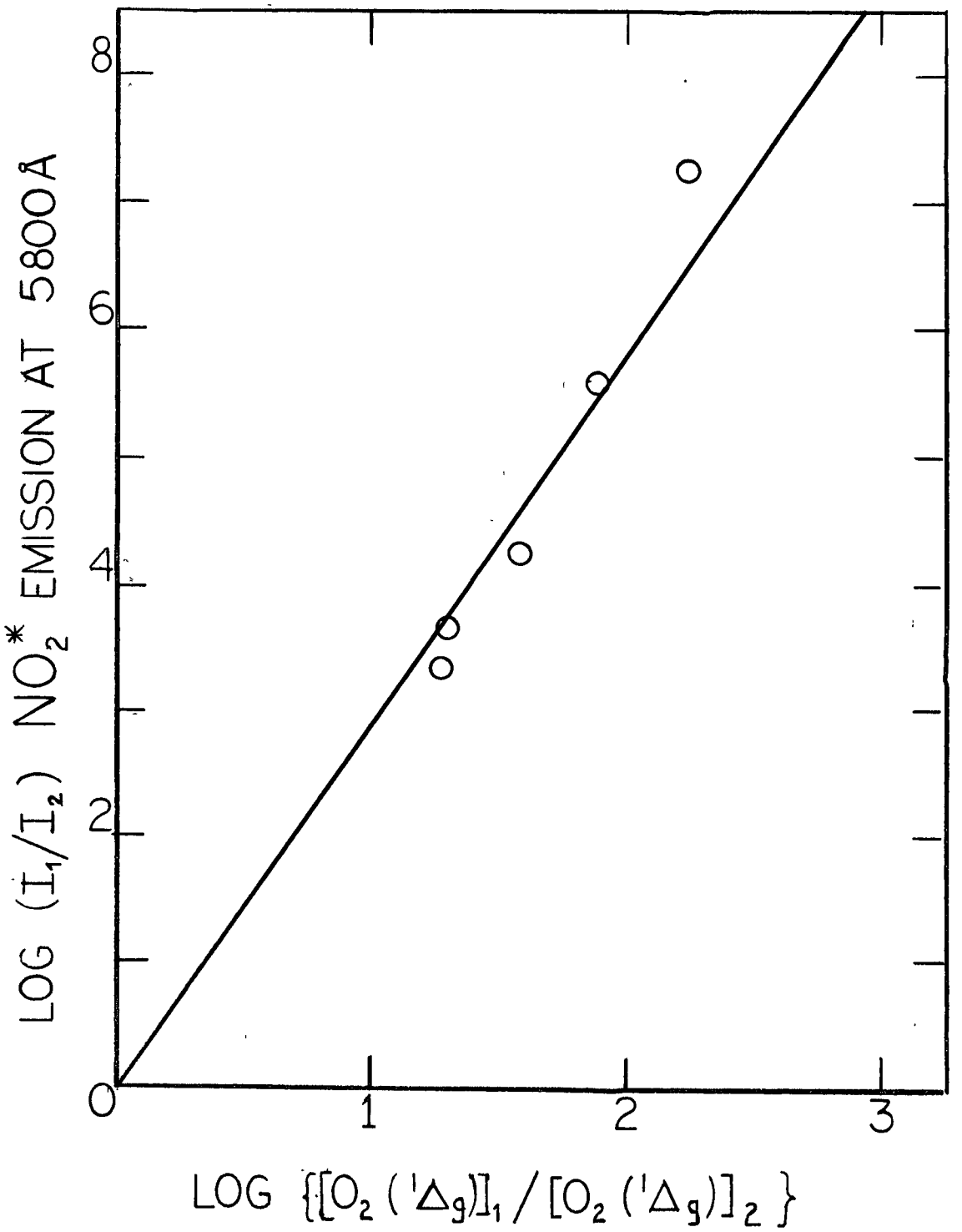

Figure 25

Plot of Log $\{I(NO_2^*)_1/I(NO_2^*)_2\}$ against Log $\{[O_2(^1\Delta_g)]_1/[O_2(^1\Delta_g)]_2\}$

obtained with a slope of 3. Since the NO_2^* emission is dependent on the $O_2(^1\Sigma_g^+)$ concentration the observation that p = 2m + n = 3, implies that m = n = 1, so that the overall equation for the production of the NO_2^* emission may be written

$$NO_2 + O_2(^1\Delta_g) + O_2(^1\Sigma_g^+) \rightarrow NO_2^* + 2\,O_2(^3\Sigma_g^-) \qquad (104)$$

$$NO_2^* \rightarrow NO_2 + h\nu(\geq 4800\ A)$$

In view of the available experimental evidence it is not possible to say how the emitting species NO_2^* is formed. However two possibilities are; a) a low lying state of NO_2 receives energy from either $O_2(^1\Sigma_g^+)$ or $O_2(^1\Delta_g)$ before the second transfer occurs b) direct transfer to NO_2 takes place from an $\{O_2(^1\Delta_g)\ O_2(^1\Sigma_g^+)\}$ double molecule (or collision complex). Although this complex has not been observed due to the very low $O_2(^1\Sigma_g^+)$ concentration in the system, it has been observed in the reaction of hydrogen peroxide with chlorine. (46).

The reaction of molecular iodine with excited molecular oxygen which leads to emission from the $^3\pi_{ou}^+$ state of I_2^* is both dependent upon and produces $O_2(^1\Sigma_g^+)$. The I_2 emission is in all probability, like the NO_2^* emission, dependent upon both $O_2(^1\Delta_g)$ and $O_2(^1\Sigma_g^+)$.(†) The excited molecule $O_2(^1\Sigma_g^+)$, which has an excitation energy of 37.5 kcal./mole, has sufficient energy to dissociate $I_2(^1\Sigma_g^+)$ into two ground state atoms $I(^2P_{3/2})$. The excited atom $I(^2P_{1/2})$ which is observed to emit at 13,200 A, undergoing $^2P_{1/2} \rightarrow {}^2P_{3/2}$ transition,

---

(†) Dr. A. E. Pearson is presently conducting a detailed investigation of the iodine-oxygen reaction.

can be excited by energy transfer from either $O_2(^1\Delta_g)$ or $O_2(^1\Sigma_g^+)$. Atom recombination by

$$I\ (^2P_{3/2}) + I\ (^2P_{1/2}) + M \rightarrow I_2\ (^3\pi_{ou}^+) + M \tag{105}$$

could yield the observed emitter. The increase in $O_2(^1\Sigma_g^+)$ concentration could be explained by a reaction of the form

$$O_2(^1\Delta_g) + I\ (^2P_{1/2}) \rightarrow O_2(^1\Sigma_g^+) + I\ (^2P_{3/2}) \tag{106}$$

However, further speculation along these lines is not warrented.

$O_2(^1\Sigma_g^+)$ and $O_2(^1\Delta_g)$ in the Upper Atmosphere.

Both $O_2(^1\Sigma_g^+)$ and $O_2(^1\Delta_g)$ give rise to bands which are prominent features of airglow(†). Vallance Jones, and Harrison (5) observed the (0-0) band of the a $^1\Delta_g \rightarrow X^3\Sigma_g^-$ infrared atmospheric system at 15,800 A in twilight airglow. The (0-0) band at 12,680 A is reabsorbed by the great mass of oxygen in the lower atmosphere and it consequently is not visible from the ground. The (0-0) band, however, has been observed in day airglow with an airborne spectrometer (61) and in night airglow with a balloon borne inferometer (62). The height of the emitting region was estimated by Vallance Jones and Noxon (61) as less than 120 km. with the intensity of the (0-0) band being 10×10^6 rayleights (†) in day airglow, dropping to 0.07×10^6 R in night airglow. Vallance Jones and Harrison (5) have estimated the emission of the (0-1) band to occur at an altitutde of 60 km. with an evening twilight intensity of 1.76×10^5 R.

Meinel (9) was the first to observe the (0-1) band of the $b^1\Sigma_g^+ \rightarrow X^3\Sigma_g^-$ atmospheric system at 8645 A in night airglow. The

---

(†) Airglow is defined according to Chamberlain (62) to consist of nonthermal radiation emitted by the earth's atmosphere with the exception of auroral emissions and radiation of a cataclysmic origin such as lighning and meteor trains.

(†) The brightness in rayleighs (R) as defined by Hunten, Roach and Chamberlain (64) equals $4\pi B$, where B equals the angular surface brightness of the emitting layer in units of 10^6 photons/cm.^{2} steradians sec.

(0-0) band at 7619 A, like the (0-0) band of the infrared atmospheric system, is reabsorbed by the oxygen in the lower atmosphere and is not visible from the ground. Berthier (65) has estimated that the emission occurs in the 150 - 200 km region, with the intensity of the (0-1) band being 1.5×10^3R.

Several mechanisms have been proposed to account for the formation of $O_2(^1\Delta_g)$ and $O_2(^1\Sigma_g^+)$ in the upper atmosphere. In view of the reactions of $O_2(^1\Delta_g)$ and $O_2(^1\Sigma_g^+)$ observed in the present work, some comments can be made on these proposed mechanisms. It is essential that any proposed mechanism account for the observed absolute brightness, for the altitude at which the emission occurs, for the day night variation in brightness and for the large seasonal variation in emission intensity.

Vallance Jones and Gattinger (66) have shown that the ozone dissociation mechanism where formation of $O_2(^1\Delta_g)$ is given by

$$O + O_3 \rightarrow O_2 + O_2\ (^1\Delta_g) \tag{107}$$

$$O_3 + h\nu \rightarrow O\ (^1D) + O_2\ (^1\Delta_g) \tag{108}$$

$$O\ (^1D) + O_2 \rightarrow O_2(^1\Delta_g) + O\ (^3P) \tag{109}$$

and removal of $O_2(^1\Delta_g)$ by

$$O_2(^1\Delta_g) \rightarrow O_2 + h\nu \tag{111}$$

$$O_2(^1\Delta_g) + M \rightarrow O_2 + M \text{ where } M = N_2;\ O_2 \tag{112}$$

$$O_2(^1\Delta_g) + O \rightarrow O_2 + O \tag{113}$$

is the only one of numerous mechanisms suggested(†) which is capable of giving the observed brightness and reproducing the intensity variation in twilight. It, however, does not explain the seasonal variation or the morning evening asymmetry.

In order to explain the observed rate of decay of $O_2(^1\Delta_g)$, Vallance Jones and Gattinger found that k_{112} was required to equal 10^{-19} cm^3/molecules sec. In the present work, k_{112} for $M = O_2$ was observed to have an upper limit of 6.6×10^{-19} cm^3/molecules sec. Since $O_2(^1\Delta_g)$ was observed to undergo the energy pooling process

$$2\ O_2(^1\Delta_g) \rightarrow O_2(^1\Sigma_g^+) + O_2(^3\Sigma_g^-) \qquad (29)$$

having a rate constant $k_{29} = 2 \times 10^{-18}$ cm^3/molecules sec it can be asked if this process can contribute significantly to the decay of $O_2(^1\Delta_g)$ at the 70 km. level. The rate of decay of $O_2(^1\Delta_g)$ by reaction 112 is approximate $\frac{3 \times 10^7 \text{ molecules}}{cm^3 \text{ sec.}}$ and, by reaction 113, $\sim 10^7$ $\frac{\text{molecules}}{cm^3 \text{ sec.}}$ and by reaction 29 it is 8×10^4 molecules/cm^3sec. Consequently, reaction 29 does not contribute significantly to the observed decay of $O_2(^1\Delta_g)$. However, if Young and Black's value of $k_{29} = 3 \times 10^{-14}$ cm^3/molecules sec. is used in place of the one obtained in the present work, the decay of $O_2(^1\Delta_g)$ would occur predominantly by the disproporation reaction with a rate of 1.2×10^9 molecules/cm^3 sec. Reaction 29 would have to be included in the overall ozone mechanism

---

(†) For a detailed discussion of suggested mechanisms of $O_2(^1\Delta_g)$ formation consult Vallance Jones and Gattinger (6) (66) and references quoted therein.

for the formation and removal of $O_2(^1\Delta_g)$. It is obvious that additional measurements of k_{29} are required, so that the importance of reaction 29 can be determined.

Several mechanisms have been proposed for the formation of $O_2(^1\Sigma_g^+)$. Since only the (0-1) band at 8645 A having an intensity of 1.5×10^3 R has been observed, there is some question as to how much additional emission should be assigned to the (0-0) band at 7619 A which is not observed because of absorption or scattering by O_2 below the emitting layer. Bates has suggested that the (0-0) emission would undergo resonance scattering by O_2 until it is converted to (0-1) radiation by fluorescence. If one assumes that the (0-1) emission is enhanced in this manner, the total emission in the Atmospheric system, which can be estimated from the fact that the relative photon emission in the two bands is proportional to $\frac{q(v^1\ v^{11})}{\lambda^3}$ where q is equal to the Franck-Condon factor, may be as low as 8×10^3 R. If, on the other hand, one assumes that resonance scattering and fluorescence are negligible, the total emission would approach 30×10^3 R.

Bates (67,68) has suggested that the $b^1\Sigma_g^+$ is formed by three body recombination of $O(^3P)$

$$O + O + M \rightarrow O_2(^1\Sigma_g^+) + M \quad M = N_2, O_2 \tag{4}$$

If one assumes that Young and Sharpless' (26) value of k_4 is accurate, this mechanism must be rejected because it would yield an $O_2(^1\Sigma_g^+)$ concentration which is insufficient by a factor of 10^3 to account for the observed intensity of the atmospheric bands.

Bates and Dalgarno (69) and Seaton (70) have suggested that $O_2(^1\Sigma_g^+)$ could be excited very efficiently by the deactivation of $O(^1D)$ atoms by ground state oxygen molecules.

$$O(^1D) + O_2(^3\Sigma_g^-, v=o) \rightarrow O(^3P) + O_2(^1\Sigma_g^+, v=2) \qquad (114)$$

since the reaction is nearly in exact resonance, the energy discrepency being only 0.04 ev. for v=2. The fact that no emission is observed from the v=2 level of $b\,^1\Sigma_g^+$ is explained by rapid vibrational deactivation of this state by an interchange of electronic energy between an excited molecule and one in the ground state

$$O_2(^1\Sigma_g^+, v>o) + O_2(^3\Sigma_g^-, v=o) \rightarrow O_2(^1\Sigma_g^+, v=o) + O_2(^3\Sigma_g^-, v>o) \qquad (115)$$

which Bates (71) claims will be very rapid because of an approximate equality of equilibrium internuclear distance r_e and vibrational quantum w_e in the two states.

Young and Black (50) claim that the disproporation of $O_2(^1\Delta_g)$ (reaction 29) satisfactorily accounts for the formation of $O_2(^1\Sigma_g^+)$ in the upper atmosphere. If their value of k_{29} is used the rate of formation of $O_2(^1\Sigma_g^+)$ would be $\sim 3 \times 10^3$ molecules/cm^3 which, if a ten km thick emitting layer is assumed, would yield a total intensity of 3×10^3 R. However, if the value of k_{29}, determined in the present work, is used an intensity of ~ 0.2 R is obtained. This intensity is very much less than the observed value of $(8\text{-}30) \times 10^3$ R.

Several question can be asked. Is the value of k_4 accurate? This value is at best only an approximate value which could easily be in

error by 10^3. The rate constant for reaction 114 has yet to be measured. How accurate are the concentrations of the principal species in the upper atmosphere known? Only a thorough laboratory study of the reactions of excited oxygen molecules and excited atoms, under conditions where all the experimental parameters can be accurately determined, can provide accurate values for the required rate constants. These values coupled with accurate concentration measurements would allow a proper evaluation of each of the proposed mechanisms.

CONCLUSIONS

Summary:

The following reactions of $O_2(^1\Delta_g^-)$ and $O_2(^1\Sigma_g^+)$ were observed.

reaction	rate constant	source
$O_2(^1\Delta_g) \xrightarrow{k_{56}} O_2(^3\Sigma_g^-) + h\nu$ (12680 A)	1.5×10^{-4} sec.$^{-1}$	Vallance Jones, Gattinger (6)
$O_2(^1\Delta_g) \xrightarrow{k_{nonrad.}} O_2(^3\Sigma_g^-)$	0.178 sec^{-1}.	present work
$O_2(^1\Delta_g) + O_2(^3\Sigma_g^-) \xrightarrow{k_{58}} 2\ O_2(^3\Sigma_g^-)$	$\leq 2.77 \times 10^2$ 1.moles^{-1}sec.$^{-1}$	present work
$2\ O_2(^1\Delta_g) \xrightarrow{k_{53}} 2\ O_2(^3\Sigma_g^-)$ or $\{O_2(^3\Sigma_g^-)\}_2 + h\nu$(6340 A and 7030 A)	0.28 1.mole^{-1}sec.$^{-1}$	Browne (51)
$2\ O_2(^1\Delta_g) \rightarrow O_2(^1\Sigma_g^+) + O_2(^3\Sigma_g^-)$	1.3×10^3 1.moles^{-1}sec.$^{-1}$	present work
	$1.8 \times 10^{7 \pm 0.5}$ 1.moles^{-1}sec^{-1}	Young, Black (50)
$2\ O_2(^1\Delta_g) \xrightarrow{k_{59}}$ products	$\leq 4.3 \times 10^2$ 1.moles^{-1}sec.$^{-1}$	present work
$O_2(^1\Sigma_g^+) \xrightarrow{k_{44}} O_2(^3\Sigma_g^-) + h\nu$(7619 A and 8645 A)	0.14 sec.$^{-1}$	Childs Mecke (8)
$O_2(^1\Sigma_g^+) \xrightarrow{k_{nonrad}} O_2(^3\Sigma_g^-)$	64.6 sec.$^{-1}$	present work

reaction	rate constant	source
$O_2(^1\Sigma_g^+) + Q \xrightarrow{k_{93}} O_2 + Q$	Table XXX	present work

Suggestions for Further Work:

In view of the large discrepency in the value of k_{29} as determined in the present work and as determined by Young and Black, an independent measurement of this constant is desirable. The rate constant for the three body recombination of oxygen atoms into the $^1\Sigma_g^+$ should also be reevaluated.

$$2\ O(^3P) + M \rightarrow O_2(^1\Sigma_g^+) + M \tag{4}$$

Only when these constants are known accurately, can the number of possible mechanisms for the formation of $O_2(^1\Sigma_g^+)$ in the upper atmosphere be reduced.

The reactions of $O_2(^1\Delta_g)$ with olefins should be studied in detail to determine the mechanism and the rate constants.

The energy pooling processes involving excited oxygen molecules and either iodine or nitrogen dioxide should be studied in detail to determine the detailed kinetic mechanisms for the processes. Attempts should be made to find other molecules which can undergo similar energy pooling reactions with excited molecular oxygen.

If an improved method of generating $O_2(^1\Delta_g)$, and hence $O_2(^1\Sigma_g^+)$ by reaction 29, or if an independent method of producing

sizable quantities of $O_2(^1\Sigma_g^+)$ can be found, a search for metastable molecules $[O_2(^1\Sigma_g^+)O_2(^1\Delta_g)]$ and $\{O_2(^1\Sigma_g^+)\}_2$ should be undertaken.

References

1) Kaufman, F.; Progress in Reaction Kinetics; 1 1(Pergamon Press, 1961)
Avramenko, L. I.; Kolesnikova, R. V.; Advances in Photochemistry, 2, 25 (Interscience Publishers, New York, 1964)

2) Ogryzlo, E. A.; Ph.D. Thesis McGill University 1958

3) Ellis, J. W.; Kneser, H. O.; Z. Physik 86 583 (1933)

4) Herzberg, G.; Herzberg, L.; Astrophys. J. 105 353 (1948)

5) Vallance Jones, A.; Harrison, A. W.; J. Atm. Terr. Phys. 13 45 (1958)

6) Vallance Jones, A.; Gattinger, R. L.; Planet. Space Sc. 11 961 (1963)

7) Babcock, H. D.; Herzberg, G.; Astrophys. J. 108 167 (1948)

8) Childs, W. H. J.; Mecke, R.; Z.Physik 68 344 (1931)

9) Meinel, A. B.; Astrophys. J. 112 464 (1950)

10) Meinel, A. B.; Astrophys. J. 113 583 (1951)

11) Broida, H. P.; Gaydon, R. A.; Proc. Roy. Soc. (London) A 222 181 (1954)

12) Branscomb, L. M.; Phys. Rev. 86 258 (1952)

13) Herzberg, G.; Can. J. Phys. 31 657 (1953)

14) Herzberg, G.; Can. J. Phys. 30 185 (1952)

15) Dufay, J.; Compt. rend. 213 284 (1941)
Swings, P.; Astrophys. J. 97 72 (1943)
Barbier, D.; Ann. Astrophys. 10 47 (1947)

16) Barth, C. A.; Kaplan, J.; J. Mol. Spect. 3 583 (1959)

17) Brix, P.; Herzberg, G.; Can. J. Phys. 32 110 (1954)

18) Herman, L.; Herman, R.; Rakotoarijimy, D.; J. Phys. Radium ser. 8 22 1 (1961)

19) Chamberlain, J. W.; Astrophys. J. 128 713 (1958)

20) Ingham, M. F.; Monthly Notices Roy. Astronomical Soc. 124 505 (1962)

21) Gilmore, R. F.; J. Quant. Spect. Radiative Transfer 5 369 (1965)

22) Wigner, E.; Whitmer, E. E.; Z. Physik 51 859 (1928)

23) Kaplan, J; Nature 159 673 (1947)

24) Bass, A.; Broida, H.P.; Kurzweg, H. U.; J. Mol. Spect. 1 184 (1957)

25) Young, R. A.; Sharpless, R.; J. Chem. Phys. 39 1071 (1963)

26) Young, R. A.; Sharpless, R.; J. Geophys. Res. 67 3871 (1962)

27) Clyne, M. A. A.; Thrush, B. A.; Wayne, P. R.; Nature 199 1057 (1963)

28) Barth, C. A.; Patapoff, M.; Astrophys. J. 136 1144 (1962)

29) Herron, J. T.; Schiff, H. I.; Can. J. Chem. 36 1159 (1958)

30) Forner, S. N.; Hudson, R. L.; J. Chem. Phys. 25 601 (1956)

31) Noxon, J. F.; Can. J. Phys. 39 1110 (1961)

32) Elias, L.; Ogryzlo, E. A.; Schiff, H. I.; Can. J. Chem. 37 1690 (1959)

33) Schiff, H. I.; Meyer, C. B.; Fontijn, A.; J. Chem. Phys. 40 64 (1964)

34) Baumann, W.; Mecke,R,; Z. Physik 81 445 (1933)

35) Schiff, H. I.; Fontijn, A.; Chemical Reactions in the Lower and Upper Atmosphere (Interscience Publishers, Inc.; New York, 1961) p.239

36) Tanaka, Y.; Schimazu, M.; J. Sci. Res. Inst. (Tokyo) 43 241 (1949)

37) Bayes, K. D.; Winer, A. M.; J. Phys. Chem. 70 304 (1966)

38) R. J. Browne, private communication

39) Steinfeld, J. I.; Zare, R. N.; Jones, L.; Lesk, M.; Klemperer, W.; J. Chem. Phys. 42 25 (1965)

40) Herzberg, G.; Spectra of Diatomic Molecules, 2nd edition;(D. Van Nostrand Co., Inc.; Princeton 1950)

41) Seliger, H. H.; Anal. Biochem. 1 60 (1960)

42) Salow, H.; Steiner, W.; Z. Physik 99 137 (1936)

43) Dianov-Klokov, V. I.; Opt.i.Spektr. 6 290 (1959)

7 377 (1959)

13 136 (1962)

13 200 (1962)

16 224 (1964)

44) Kasha, M.; Khan, A. U.; J. Chem. Phys. 39 2105 (1963)

45) Browne, R. J.; Ogryzlo, E. A.; Proc. Chem. Soc. 117 (1964)

46) Kasha, M.; Khan, A. U.; J. Am. Chem. Soc. 88 1574 (1966)

47) Bader, W. L.; Ogryzlo, E. A.; Disc. Faraday Soc. 37 46 (1964)

48) Finlay, F.; Whitlow, S.; Tech. Report Defence Research Board of Canada CARDE T. R. 545/66

49) Schiff, H. I.; Furnival, S. G.; March, R. E.; J. Photochem. Photobiol. 4 971 (1965)

50) Young, R. A.; Black. G.; J. Chem. Phys. 42 3740 (1965)

51) Arnold, J. S.; Browne, R. J.; Ogryzlo, E. A.; J. Photochem. Photobiol. 4 963 (1965)

52) Benson, S. W.; The Foundations of Cbemical Kinetics (McGraw-Hill Book Co., Inc., New York, 1960) p. 447

53) Parker, C. A.; Hatchard, C. G.; Proc. Chem. Soc. 147 (1962)
Parker, C. A.; Advances in Photochemistry 2 305 (1964)
(Interscience Publishers, New York

54) Hirschfelder, J. O.; Stogryn, D. F.; J. Chem. Phys. 31 1831 (1959)

55) Birks, J. B.; Moore, G. F.; Munro, I. H.; Spectrochemical Acta 22 323 (1965)

56) Russell, K. E.; Simons, J.; Proc. Roy. Soc. (London) A 217 271 (1953)

57) Turro, N. J.; Molecular Photochemistry,(W. A. Benjamin Inc.; New York, 1965)

58) Herzberg, G; Infrared and Raman Spectra(D. Van Nostrand Co.; Inc.; Princeton, 1945)

59) Kontzel, H.; Kontzel, L.; Ann Physik 2 383 (1948)

60) Hirschfelder, J. O.; Curtiss, G. F.; Bird, R. B.; (Molecular Theory of Gases and Liquids, John Wiley and Sons, Inc., New York, 1954)

61) Vallance Jones, A.; Noxon, J. F.; Nature 196 4850 (1962)

62) Chamberlain, J. W.; Physics of the Aurora and Airglow (Academic Press New York, 1961) p. 345

63) Gush, H. P.; Buijs, H. L.; Can. J. Phys. 42 1037 (1964)

64) Hunten, D. M.; Roach, F. E.; Chamberlain, J. W.; J. Atm. Terr. Phys. 8 345 (1956)

65) Berthier, P.; Compt. rend. 237 928 (1953)

66) Bates, D. R.; The Earth as a Planet (ed G. Kuiper) (Univ. of Chicago Press., Chicago, 1954) XII 576

67) Vallance Jones, A.; Gattinger, R. L.; Planet Space Sci. 14 1 (1966)

68) Bates, D. R.; The Threshold of Space (ed. M. Zelikoff) (Pergamon Press, London 1957) p. 14

69) Bates, D. R.; Dalgarno, A.; J. Atm. Terr. Phys. 4 112 (1953)

70) Seaton, H. J.; Astrophy. J. 127 67 (1958)

71) Bates, D. R.; The Airglow and Aurorae (ed. E. A. Armstrong, A. Dalgarno) (Pergamon Press, London, 1956) p. 251